C02018: Doctor of Philosophy
CRICOS Code: 036570B
Subject Code: 49986 PhD Thesis: Engineering
May 2020

Perceptive Mobile Network Based on Joint Communication and Radio Sensing

Md Lushanur Rahman

School of Electrical and Data Engineering
Faculty of Engineering and Information Technology
University of Technology Sydney (UTS)
NSW - 2007, Australia

University of Technology Sydney

Perceptive Mobile Network Based on Joint Communication and Radio Sensing

Dissertation submitted in fulfilment of the requirements for the degree of

Doctor of Philosophy in Electrical Engineering

by

Md Lushanur Rahman

Principal Supervisor:
Professor Xiaojing Huang

Co-Supervisor:
Associate Professor Dr. J. Andrew Zhang

School of Electrical and Data Engineering
Faculty of Engineering and IT
University of Technology Sydney, Australia

May 25, 2020

Certificate of Original Authorship

I, *Md Lushanur Rahman* declare that this thesis, is submitted in fulfilment of the requirements for the award of Doctor of Philosophy, in the *School of Electrical and Data Engineering*, *Faculty of Engineering and IT* at the University of Technology Sydney (UTS), Australia.

This thesis is wholly my own work unless otherwise reference or acknowledged. In addition, I certify that all information sources and literature used are indicated in the thesis.

This document has not been submitted for qualifications at any other academic institution.

This research is supported by the Australian Government Research Training Program.

SIGNATURE: Production Note: Signature removed prior to publication.

[Md Lushanur Rahman]

DATE: 25th May 2020

PLACE: Sydney, Australia

Dedication

To my beloved wife and my parents

Acknowledgments

The work for this Doctor of Philosophy in Electrical Engineering Thesis has been carried out at the School of Electrical and Data Engineering, Faculty of Engineering and IT at the University of Technology Sydney (UTS), Australia, during 2016-2019. The funding has been offered by the following scholarships: International Research Scholarships (UTS IRS) for tuition fees and UTS Presidents Scholarship (UTSP) for living allowance.

I am very much fortunate to have Professor Xiaojing Huang and Associate Professor Dr. J. Andrew Zhang as my supervisors. Firstly, I would like to express my deepest gratitude to them for enthusiastic encouragement, constant support, and precious guidance throughout this PhD journey. I am grateful to both Xiaojing and Andrew for being available whenever I needed and also for offering me the opportunity to work in their Global Big Data Technologies Centre (GBDTC) research group in UTS.

I would like to thank all panel members for their constructive feedback and helpful comments about preparation of this thesis. I would also like to acknowledge Professor Y. Jay Guo and Professor Robert W. Heath Jr. for their guidance and support from time to time. A special thanks to John Hazelton for his thorough grammatical editing and proofreading help with my English expression for my thesis. I am grateful to all my colleagues in the Department and research mates within the GBDTC group, for offering me their help whenever I needed and for sharing their technical opinions with me. I am very much pleased to find such a nice research environment and friendly colleagues within the research group in UTS.

I am deeply thankful to all my friends from Sydney, Australia, for having such a great time in travelling around Australia and parties. I am thankful to my wife for supporting me always during this PhD journey. I cannot thank you enough; without your presence I would not have travelled so far. Finally, I would like to express my love to my parents in Bangladesh, for standing by me, for supporting me, for advising me, and last but not the least for believing in me.

Sydney, Australia, May 2020
Md Lushanur Rahman

Abstract

Radio networks have been evolving from communication-only wireless connectivity to a network for services, which will enable new business models and user experiences for emerging industrial applications. Many of these applications, including automotive, industrial automation, public safety and security tasks, will require information retrieval relating to mobile devices and objects through radio sensing. Radio sensing here refers to the process of information extraction for objects of interest in the surrounding environment that is covered by radio signals. We call the evolutionary mobile network with both communication and radio sensing functions as a perceptive mobile network. Such joint functions can be promoted as one of the core components in future 5G/6G standards.

The parametric values regarding moving objects, human movement, and any change in the environment surrounding the user equipment are embedded with the wireless signal and this enables the possibility of using the cellular signal for information extraction. As both wireless communication and radar system exhibit similar receiver front-end architecture at high frequency, it triggers the concepts of joint communication and radio sensing (JCAS) operation. In that circumstance, a unified platform can introduce shared hardware between two functions, which eventually implies reduced size, cost and weight. The main purpose of this doctoral study is to analyse the radio sensing capability of a mobile network and design the framework for joint operation. The thesis aims to design advanced signals and protocols that allow communications and sensing to be better implemented jointly and benefit from each other efficiently. An additional goal is to investigate the existing sensing parameter estimation processes and their suitability in signal processing for JCAS operation.

The thesis provides a general framework for the envisioned perceptive mobile networks that enable radio sensing using downlink and uplink mobile signaling, by considering future mobile network architecture and components, practical sophisticated communication signal format, and complicated signal propagation environment. The thesis discusses the required modifications and upgrades to existing mobile networks to facilitate JCAS functionalities. One and multi-dimensional compressive sensing techniques are successfully employed for estimating the parameters of the sensed scene, following the state of the art, by applying orthogonal frequency-division multiplexing (OFDM) based multi-user multiple-input multiple-output (MIMO) signal model. The simulated results presented here demonstrate reasonable performance in radio sensing using perceptive mobile networks. The research works shown in this thesis indicate the feasibility of the perceptive mobile network and provide a way to proceed.

Table of Contents

Abstract **ix**

Table of Contents **xi**

List of Publications **xv**

List of Figures **xvii**

List of Tables **xxi**

Abbreviations **xxiii**

1 Introduction **1**
1.1 Research Description 2
1.1.1 Research Aim 2
1.1.2 Research Problems 3
1.1.3 Research Challenges 4
1.1.4 Research Objectives 6
1.2 Scope of the Research Stages 7
1.3 Thesis Contributions 9
1.4 Organisation of the Thesis 11

2 Literature Review **13**
2.1 Background 13
2.2 Related Work 15
2.2.1 JCAS by Realizing Communication in Radar Systems 17
2.2.2 JCAS by Realizing Radio Sensing in Communication Systems 19
2.2.3 JCAS by Integrated Joint Design from Scratch 21
2.3 Benefits of Joint Communication and Sensing System 22
2.4 Perceptive Mobile Network 25
2.5 Framework for a Perceptive Mobile Network 27
2.5.1 System Platform for the Perceptive Mobile Network 30
2.5.2 Three Unified Types of Supported Sensing Operations 30
2.5.3 Signals Usable From 5G for Radio Sensing 33
2.5.4 Required System Modification 35
2.6 MU-MIMO OFDM System Model 36
2.7 Channel Estimation 39
2.8 Array Signal Processing and Sensing Parameter Estimation 44

3 Direct Sensing **47**
3.1 Direct Sensing in Perceptive Mobile Networks . . . 47
3.1.1 General System and Channel Models . . . 48
3.1.2 Formulation for Downlink Sensing . . . 49
3.1.3 Formulation for Uplink Sensing . . . 51
3.1.4 Generalized Delay-Quantized On-grid Formulation . . . 51
3.1.5 Selection of Compressive Sensing Algorithms . . . 52
3.1.6 Direct Estimation of Sensing Parameters . . . 53
3.1.7 Simulation Results for Direct Sensing . . . 58
3.1.8 Summary . . . 61
3.2 Analog Antenna based Radio Sensing . . . 61
3.2.1 Problem Statement . . . 62
3.2.2 Problem Formulation . . . 62
3.2.3 Generalized Delay-Quantized On-grid Formulation . . . 63
3.2.4 Estimation of Spatial Parameters . . . 64
3.2.5 Simulation Results . . . 69
3.2.6 Summary . . . 71

4 Indirect Sensing **73**
4.1 Indirect Estimation Using Signal Stripping . . . 73
4.1.1 Signal Stripping . . . 73
4.1.2 Estimation of Sensing Parameters by Indirect Sensing . . . 75
4.1.3 Simulation Results on Indirect Sensing . . . 77
4.1.4 Summary . . . 80
4.2 Joint Communication and Radar Sensing in 5G Mobile Network . . . 81
4.2.1 5G Signal and Channel Models . . . 83
4.2.2 Sensing Parameter Estimation with DMRS . . . 86
4.2.3 Simulation Results of Indirect Sensing with DMRS . . . 90
4.2.4 Summary . . . 93

5 Radio Sensing in Cluster Channel with Clutter Estimation **99**
5.1 Clutter in Perceptive Mobile Network . . . 99
5.1.1 Recursive Moving Average based Clutter Reduction . . . 101
5.1.2 Effect of Clutter Suppression by Recursive Moving Average . . . 105
5.1.3 Gaussian-Mixture-Model based Clutter Mitigation . . . 107
5.1.4 Proposed GMM-EM-CE Method . . . 109
5.1.5 Simulation Results for GMM-EM-CE . . . 113
5.1.6 Summary . . . 116
5.2 Radio Sensing with Cluster Multipath Channels . . . 116
5.2.1 Signal and Cluster Channel Models . . . 118
5.2.2 Proposed Cluster based 2D Kron-OMP Algorithm . . . 118
5.2.3 Simulation Results for 2D Cluster Kron-OMP Algorithm . . . 122
5.2.4 Comparative Study on Computational Complexity . . . 125
5.2.5 Summary . . . 126

6 Conclusions and Future Work **131**
6.1 Conclusions . . . 131
6.2 Future Work . . . 133

A DMRS Signals **135**
A.1 **Generation of DMRS Signals** 135
A.2 **DMRS Resources within One PRB** 136

References **141**

List of Publications

Publications published and under review related to the thesis:

M. L. Rahman, J. A. Zhang, X. Huang and Y. J. Guo, Analog antenna array based sensing in perceptive mobile networks, IEEE-APS Topical Conference on Antennas and Propagation in Wireless Communications (APWC), Verona, 2017, pp. 199-202.

J. A. Zhang, X. Huang, Y. J. Guo and **M. L. Rahman**, Signal stripping based sensing parameter estimation in perceptive mobile networks, IEEE-APS Topical Conference on APWC, Verona, 2017, pp. 67-70.

M. L. Rahman, J. A. Zhang, X. Huang, Y. J. Guo, and R. W. Heath Jr, "Perceptive Mobile Network Using Joint Communication and Sensing", in IEEE Transactions on Aerospace and Electronic Systems (TAES), pp. 1-1, 2019.

M. L. Rahman, Peng-fei Cui, J. A. Zhang, X. Huang, Y. J. Guo and Z. Lu, "Joint Communication and Radar Sensing in 5G Mobile Network by Compressive Sensing", in 19th International Symposium on Communications and Information Technologies (ISCIT), Vietnam, September, 2019. **Received Best Paper Award**

J. A. Zhang, **M. L. Rahman**, X. Huang, Y. J. Guo, S. Chen, and R. W. Heath Jr, "Perceptive Mobile Network: A Cellular Network with Radio Vision via Joint Communication and Radar Sensing", submitted to IEEE Vehicular Technology Magazine, 2020.

M. L. Rahman, J. A. Zhang, X. Huang, Y. J. Guo and Z. Lu, "On Joint Communication and Radar Sensing in 5G Mobile Network by Compressive Sensing", submitted for review in the IET Communications, 2020.

M. L. Rahman, J. A. Zhang, X. Huang, Y. J. Guo and Z. Lu, "Gaussian-Mixture-Model Based Clutter Mitigation in Perceptive Mobile Networks", submitted for review in the IEEE Communication Letters, 2020.

M. L. Rahman, J. A. Zhang, K. Wu, X. Huang, Y. J. Guo, S. Chen and J. Yuan, "Enabling Joint Communication and Radio Sensing in Mobile Networks - A Survey", submitted to IEEE Communications Surveys & Tutorials, 2020.

List of Figures

Figure **Page**

1.1 Methodological approach 8

2.1 General block diagram of unified sensing and communication system. 25
2.2 CRAN architecture for 5G mobile network 26
2.3 Simplified transceiver model for joint communication and sensing . . 27
2.4 Proposed system model. 31
2.5 Multicarrier modulation based OFDM system transceiver model . . . 37
2.6 MIMO propagation channel 39
2.7 MU-MIMO communication system 40
2.8 Performance evaluation process of channel estimation in communication system 41
2.9 Basic principle of DDCE 43
2.10 Block diagram of the detailed operational procedure for DDCE 44

3.1 10 implementation results for AoA-Distance estimation in direct downlink sensing. 60
3.2 10 implementation results for AoA-Distance estimation for direct uplink sensing. 61
3.3 Parameter estimation for downlink sensing shows in (a), (b), while (c) and (d) refers to uplink sensing. Every star/circle refers to parameters for one multipath; stars and circles are for estimated and actual ones, respectively. Different colors represent multipath from different RRUs in (a), (b) and users in (c), (d). 70

4.1 10 implementation results for indirect uplink sensing with channel SIR $\eta = 15$dB, and symbol sampling interval $T = 20T_s$. 78
4.2 10 implementation results for indirect downlink sensing with $\eta = 15$dB, and $T = 20T_s$, where delay values are continuous (off-grid). Subcarriers are interleaved. 79
4.3 10 implementation results for classical 2D DFT results. System setup is the same as that in Fig. 4.2. 80
4.4 Sensing parameter estimation using the proposed 1D CS method for indirect uplink sensing, with $\eta = 15$dB. "Equivalent AOA" equals to $\pi \sin(\theta)$, and speed is relative to the static BS. All parameters have continuous values (off-grid model). 81

4.5 Sensing parameter estimation using the N-way OMP (3D CS) algorithm. Dictionaries for AoA and Doppler estimation are interpolated to size 16 and 256, respectively. Other configurations are similar to those in Fig. 4.4. 82
4.6 Proposed perceptive mobile network with 5G CRAN. 83
4.7 CIR for QuaGRiGa channel. 91
4.8 Observations in Cluster-Chl for downlink sensing. 94
4.9 Observations in uplink sensing: QuaDRiGa NLOS channel. 95
4.10 Uplink sensing with small PRB in 5G QuaDRiGa NLOS. 96
4.11 2-D DFT for uplink sensing. 97

5.1 Dynamic and static multipaths in JCAS 100
5.2 Exemplified values of $\rho(p)$, with $T_h = 20T_s$, $\max\{p\} = 30$ at approximately 2.8 ms. Curves from top to bottom correspond to Doppler frequencies from 0 to 400 Hz at an interval of 50 Hz. 103
5.3 Power ratio of the clutter to "interfering signals" after applying the recursive averaging, in the presence of approximately 10 non-clutter interfering signals over each period of $270T_s$ (assumed to be the channel stable period). Red dashed curves for $T_h = 240T_s$, blue solid curves for $T_h = 120T_s$, and black curves for $T_h = 60T_s$. 104
5.4 Difference between the reconstructed and the true clutter signals, normalized to the power of the true clutter. Learning rates α for curves from left to right are 0.9,0.94,0.97,0.99 and 0.995, respectively. 106
5.5 Estimated and true sensing parameters AoA and distance obtained using the indirect method after clutter suppression. From top to bottom, $p = 25, 50, 150$, respectively. Channel estimation $\eta = 15$ dB. 107
5.6 Processes of the proposed GMM-EM-CE method. 110
5.7 CDF of RMSE at different Υ values. 114
5.8 Clutter estimation RMSE values vs Υ at high and low values of ρ for GMM-EM-CE and RMA method. 115
5.9 Uplink sensing at $\gamma = 0.25$, $\Upsilon = 12\ dB$, $\rho = 1$, after clutter suppression by (top) GMM-EM-CE with $N_m = 10$ at $t_h = 30\ ms$ and by (bottom) RMA with $r = 10$. The estimated values for AoA are shown in star and the actual AoAs are shown in circle. Different colours correspond to different users. 117
5.10 CIR for cluster channel. 123
5.11 Two random realizations of downlink sensing using the proposed 2D cluster kron-OMP algorithm for quantized (top sub-figures) and non-quantized (bottom sub-figures) channel parameters. 127
5.12 A random realization of uplink sensing using the proposed 2D cluster kron-OMP algorithm for non-quantized channel parameters. 128
5.13 Uplink sensing using 2D kron-OMP for non-quantized channel parameters with $N_s = 28$ DMRS subcarriers (7 PRB). Black zoomed in boxes are for showing certain missed estimates incapability of preserving cluster pattern. 128
5.14 RMSE of the AoA estimates obtained by both methods with $N_s = 28$ for non-quantized channel parameters 129

A.1 DMRS subcarrier indices within one PRB 137
A.2 DMRS subcarrier allocation within one PRB (alternating subcarriers) . . 138

A.3 DMRS subcarrier allocation within one PRB (grouped subcarriers) 138
A.4 DMRS subcarrier allocation within one PRB (252 Subcarriers) 139

List of Tables

Table **Page**

2.1 Investigation on Radar, Communication and JCAS 24

Abbreviations

AoA Angle of Arrival
AoD Angle of Departure
AWGN Additive White Gaussian Noise
BSBL Block Sparse Bayesian Learning
BBU Baseband Units
CDF Cumulative Distribution Functions
CRAN Cloud Radio Access Network
CS Compressive Sensing
DDCE Decision Directed Channel Estimation
DMRS Demodulation Reference Signals
EM Expectation Maximization
GMM Gaussian Mixture Model
JCAS Joint Communication and Radio Sensing
MIMO Multiple-Input Multiple-Output
MU-MIMO Multiuser Multiple-Input Multiple-Output
MMV Multi-Measurement Vector
OFDM Orthogonal Frequency Division Multiplexing
OFDMA Orthogonal Frequency Division Multiple Access
OMP Orthogonal Matching Pursuit
PDF Probability Density Function
PDSCH Physical Downlink Shared Channel
PRB Physical Resource Block
PUSCH Physical Uplink Shared Channel
RMSE Root Mean Square Error
RRU Remote Radio Unit
SDMA Spatial Division Multiple Access
SNR Signal to Noise Power Ratio

Chapter 1

Introduction

Radio network environment is continuously changing due to human movement, moving objects, noise, interference, and weather effects. In turn, signals can experience multiple different reflections or paths before being received at the receiver. Due to this multipath propagation phenomenon, received signals experience frequency selective fading after getting passed through a channel. Intuitively, as a result, the received reflected signals at the base station of a mobile network inherently contain the information about the environment and the surroundings [1]. Effective information extraction from such signals can introduce sensing capability of the cellular network. Sensing here refers to the extraction of information from the communication signal, pertaining to the objects, users and environment in the propagation channel. Context awareness learned from channel sensing can facilitate the radio network functionality. More specifically, embedded sensing allows us to broaden the view about the radio link through obtaining detailed channel information, for example, user tracking data, speed, distance and tracking data of moving objects, angle of arrival or departure of signals, delay, attenuation from the received radio signal at the base station. Channel pattern then can be known by such parameters. Indeed, effective radio resource management deals with accurate beam steering, link adaptation and channel allocation according to channel condition and desired quality of service [2], [3].

Most of the research work found in literature, such as, [4], [5], [6], and [7] demon-

strated the possibilities and implementation of either co-existence of an actual radar system and wireless communication system or achieving communication in the radar system. However, our research proposal and aim here is to investigate the possibility of obtaining sensing functionality within the cellular network by its own radio signal. Some of the researchers have shown the potential of cellular network for sensing within its system, for example, [8] and [9] used GSM based radio signals for traffic monitoring and weather changing observation, respectively. However, these works are confined to the usage of simple mobile signals. In contrast to these previously mentioned implementations, our targeted technology is the emerging 5G cellular network to develop a perceptive mobile network where the same transmitted signal is used for both communication and sensing. The term, perceptive, means inherently sensitive to see the surroundings. Perceptive mobile network can achieve immediate benefits of reduced cost, size, and improved spectral efficiency in smart city, smart home, smart car and transportation services [1].

1.1 Research Description

My research focus is to learn about the radio channel pattern and tracking of propagation channel entities, for example, human, object, environment around the user equipment by the usage of received radio signals around the base station. In this section, I will introduce my research aim, questions or problems, challenges and objectives.

1.1.1 Research Aim

My research aims to develop innovative technologies that integrate sensing capabilities in detecting, tracking and identifying objects with the communication system. Our approaches will be able to simultaneously perform communication and sensing by sharing hardware and signal processing modules and achieve significant benefits of reduced cost, size, weight, and better spectrum efficiency.

1.1.2 Research Problems

The idea of combining radar sensing and a communication system on a single platform has long been proposed but a relevant system concept through the usage of actual mobile network has not been developed until now. Advanced techniques have been invented both in wireless communication and radar sensing individually for the past two decades. However, despite the strong potential of wireless signals usage in radar sensing, a limited intersection study is found in the literature. Moreover, emerging platforms such as unmanned aerial vehicles, smart city and smart cars are evolving towards object recognition and pattern matching. In such kinds of technology solutions where sensing of the objects is a primary requirement, the possibility of using the actual radar system is not always effective, whereas covering most of the urban and rural areas, the mobile network has the potential of becoming a ubiquitous sensor. Most existing and ongoing research works are focusing on millimeter wave (mmWave) radio and passive sensing systems. In that aspect, there is a necessity of having a further investigation on getting the sensing operation accomplished by the mobile network itself.

Therefore, there are mainly the following research problems considered in my research.

- *Problem 1.* **Potential of mobile network for radio sensing.**

  Mobile signals and mobile devices are almost everywhere today. Mobile network with its long distance signal coverage is capable of connecting everything. There is a very large amount of information associated with human behaviour, moving objects and environmental change embedded in these wireless signals. Effective information extraction techniques can eventually transform the mobile signal and network to act as a sensor system as well. In terms of applications and accessibility, no other signals and system would be as effective as the mobile network. However, very limited work has been found in literature where only simple radio signals are used to do sensing. Research work on passive radar systems and usage of Wi-Fi and TV signals are not also directly

related with this as they are constrained to the use of a third device. Hence, further exploitation is required to use the actual mobile network to do object tracking and sensing.

- *Problem 2.* **Signal processing techniques and algorithms for sensing parameter estimation by actual mobile network.**

  Signal types and processing techniques for parameter extraction are different for wireless communication and radar sensing system. Typical channel estimation algorithms in communications only estimate composited channels with limited unknown parameters, and radar systems generally use pulse width chip modulated transmitted signals. However, as the mobile signals need to be used as a sensor system, signal formulation and parameter extraction techniques need to be rearranged in line with the joint system requirements.

- *Problem 3.* **Spectrum congestion in communication and hardware cost in radar sensing.**

  Wasteful static spectrum allocations and inefficient utilization of frequency spectrum in communication system create spectral congestion. On the other hand, hardware cost, size and maintenance are common issues in a radar system. Integrating both systems in a single system to work in a wider bandwidth can increase spectrum efficiency and bring benefits over equipment cost and size.

1.1.3 Research Challenges

To solve the research problems, there are several challenges that need to be addressed.

- *Challenge 1.* **How to design single waveform, sensing protocols and sensing options in joint systems?**

  Radar sensing and communication have different requirements for signal modulation. For example, in multiple input multiple output (MIMO) communica-

tion systems, typically we use multicarrier modulation where the transmitted signal enables multiuser random access. Whereas, in MIMO-radar, sensing signals are chirp modulated and orthogonal. Such conflicting requirements can make joint design for signal propagation and sensing operation very challenging.

- *Challenge 2.* **How to set up transceivers and antennas to meet the requirements for both communications and sensing?**

  Setting up transceivers and antennas in the joint system to meet the requirements for both communications and sensing is challenging. An array with steerable beamforming and narrow beamwidth is typically required for sensing. However, communications require fixed and accurately pointed beams to achieve large beamforming gain. Hybrid antenna array architecture may provide a cost-balanced solution in such cases. Moreover, depending on used multiplexing scheme, required modification is different to do both communication and radio sensing by a single system.

- *Challenge 3.* **How to effectively extract spatial parameters from communication signals without compromising communication service?**

  Mobile radio signal is complex and connects almost everything with diverse network resources over time, frequency and space. Existing techniques for passive sensing and radar may not work efficiently in this scenario, as typical radar systems are optimized for sensing a limited number of objects in open spaces using narrow beamforming. Existing channel estimation and localisation algorithms are not directly applicable either. In particular, channel estimation in communications only requires estimation of composite channels at quantized discrete grids, and localization focuses predominantly on the line of sight path. For sensing, detailed channel composition needs to be obtained.

- *Challenge 4.* **How to preserve sensing accuracy in the proposed joint system under channel with clutter and cluster pattern?**

Complex propagation environment contains a lot of unwanted clutter signals which are largely different from the conventional radar clutter signal. Moreover, practical multipath signals arrive in clusters. Complex clustered formation of mobile channel and unwanted overhead in signal processing are obstacles in highly accurate and effective parameter extraction from mobile signals.

1.1.4 Research Objectives

- *Objective 1.* **To design a unified platform for joint communication and radio sensing.**

  This objective aims to address the research challenge 1. We will develop a single signal model for both communication and sensing, a protocol for signal transmission and address three different types of sensing schemes with available waveform options for sensing in the mobile network. Novel design of the radio sensing scheme and waveform options for sensing provides the platform for joint communication and radio sensing (JCAS) in the 5G mobile network. We also develop receiver cost optimization techniques by exploiting beamforming and introducing spatial redundancy into signal modulation.

- *Objective 2.* **To design a transceiver structure in order to integrate sensing with mobile network.**

  This objective aims to address the research challenge 2. We will develop the transceiver structure that refers to the evolution of JCAS through both low-cost near-term suboptimal and long-term integrated and optimized solutions. We will discuss the required modifications on the network and hardware of current mobile networks to support the sensing operation. Moreover, we will consider an alternative low-cost and flexible solution of using an analog antenna array for radio sensing at the base station receiver in the recently proposed perceptive mobile network.

- *Objective 3.* **To develop advanced information harvesting techniques**

  This objective aims to address the research challenge 3 and 4. We will develop efficient algorithms and apply data fusion technology to extract desired parameters with less complexity from multi-user MIMO (MU-MIMO) orthogonal frequency-division multiple access (OFDMA) signals in multipath clustered environments, which are typical in modern mobile networks. In addition, adaption of existing radar signal processing techniques and clutter suppression methods will be investigated.

- *Objective 4.* **To build a MATLAB based simulator and demonstrate applications of the results**

  This objective aims to address the research challenge 1-4. A MATLAB based simulator will be developed to demonstrate the system and main functionality of the integrated system, and showcase its potential and benefits with high accuracy. I will describe the perceptive mobile networks by referring to, not exclusively, emerging 5G networks.

1.2 Scope of the Research Stages

In this section, I will introduce my methodological approaches towards solving the research problems. In a JCAS, the single signal waveform that we have received can either be used for communication or sensing. This implies major differences between perceptive mobile networks and existing systems and technologies that combine radar and mobile communications. Specifically, usage of a single signal for both functions is different from the cases where the two separated systems share the same resource blocks in a cooperative way and the integrated system using separately transmitted signals where communication and radar are integrated on one platform but their signals use is separated. In this thesis, I will mainly deal with waveform design, transceiver modelling, and sensing solutions of the perceptive mobile network.

The signal processing for communication in the joint system will be as in the conventional orthogonal frequency-division multiplexing (OFDM) system. We can use either received signal directly or estimated channel for the sensing processing. In the case of the channel estimation matrix obtained from either pilot or interpolation in communication, that matrix can be used as a preliminary input for the sensing block. We will develop essential techniques to address the major challenges and develop a basic working system that can be validated by a software simulator to demonstrate the significant potential and benefits of such an integrated solution.

The methodological structure is illustrated in the Fig. 1.1 below, where the 4 main research stages are illustrated as Working Packages (WP; WP1-WP4).

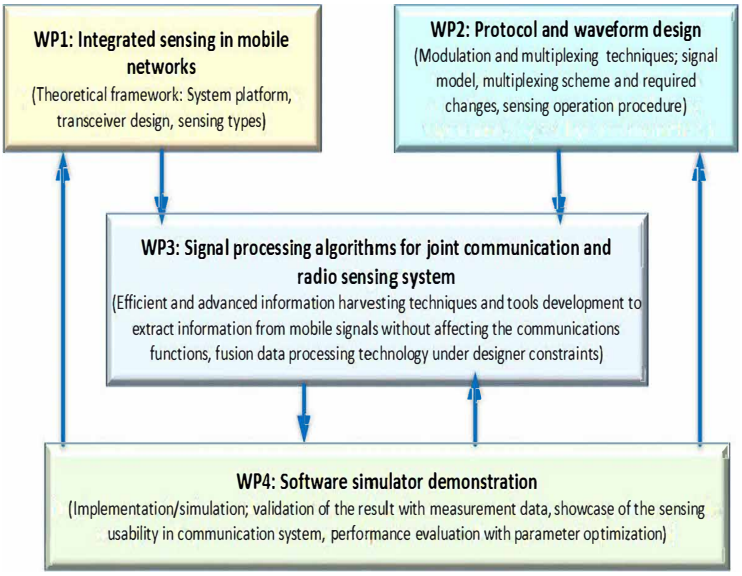

Figure 1.1: Methodological approach

WP1: In the first step, WP1 focuses on the theoretical framework design, such as, joint system transceiver design, approaches to include sensing as an integrated part of the communication base station and different types and operations of integrated sensing. Any required changes to hardware of current mobile network are also addressed and analyzed. Particular attention is given to obtain high efficiency, low power consumption, frequency flexibility, and low implementation complexity.

WP2: WP2 focuses on the protocol and waveform design, for example, selection of signal types, modulation and multiplexing techniques, parametric signal model and formation, joint signal frame structure and seamless operational procedure. Each of the solutions follows the state of the art technology where design parameters

selected need to be supported by the literature. Privacy is less an issue because sensed results are not directly linked to any user devices.

WP3: In WP3, development of digital signal processing techniques and effective sensing schemes are provided, in order to perform mobile signal based sensing. First, the generalized on-grid compressive formulation solutions can be addressed, then the work will be extended to the detailed spatial parametric estimation case, assuming that extracting information from mobile signals will not affect the communications functions. These kinds of advanced information harvesting techniques and tools development need to maintain several designer constraints, such as, multipath propagation environment, clustered multipath channels, unwanted signal exclusion, parameter estimation process error, algorithm complexity, hybrid antenna array signal processing hurdles and so on.

WP4: Then, WP4 will aim at testing the developed solutions with realistic scenarios and generated or measured data, and demonstrating overall parameter estimation simulation results. A MATLAB based simulator will be developed to demonstrate the working principle and major features of the integrated system, and showcase its potential and benefits. In our research group, a wide database of cellular channel measurement data is already available and will be used in the context of my PhD thesis work. In my thesis, I aim at a mixture of analytical and implementation work.

1.3 Thesis Contributions

Our major contributions in this work are as follows:

- We introduce a unified system platform in Chapter 2 that enables three ways of sensing from mobile signals to be integrated with mobile communications. We present the required changes for hardware and system in existing mobile networks. We also provide signals formulation for the three ways of sensing, and show that they can be represented by a common expression, which enables

the application of common sensing algorithms.

- We present two schemes for estimating sensing parameters from sophisticated communication signals with modulations of OFDMA and MU-MIMO. The first one, shown in Section 3.1 of Chapter 3, is *direct estimation* that uses the received mobile signals directly as inputs to sensing algorithms, assuming that the transmitted information data symbols are known. The second, shown in Section 4.1 of Chapter 4, is *indirect estimation* based on *signal stripping*. It simplifies the signal input to sensing algorithms by removing (demodulated) data symbols and decorrelating users using conventionally estimated channels in communications. Upon the formulated signal models based on these two methods, we demonstrate how sensing parameters can be estimated via using one-dimensional (1D) compressive sensing (CS) algorithms. The proposed 1D CS algorithms are particularly useful when there is only sufficient measurements in one dimension, which could be typical in current and near-future systems.

- We provide the low-cost option of using an analog phased antenna array in Section 3.2 of Chapter 3 dedicated to the receiver for sensing and communications, and develop sensing parameter estimation algorithms, based on the same MU-MIMO model.

- We propose an integrated solution built on a unified platform that enables estimating sensing parameters from 5G new radio (NR) standard signals in perceptive mobile networks in Section 4.2 of Chapter 4 by applying 1D to 3D CS algorithms. The communication signals used for sensing are the OFDM-type demodulation reference signals (DMRS) in the 5G specification. We use both 5G-compatible channels recommended by 3GPP and our own generated cluster channel model.

- We propose a low-complexity *background subtraction* method in Section 5.1 of Chapter 5 for reducing clutter from the input to sensing algorithms. It

reconstructs clutter using simple recursive computation and allows separation of signals with largely separated Doppler frequencies. We also provide closed-form expressions to show how the reconstruction performance and noise are related to the parameters in the recursion equation. This method is not only capable of removing clutter but also has the potential of dividing multipath signals into different groups according to their Doppler shift values.

- We demonstrate how to apply Gaussian mixture model to complicated modern mobile communication signals with MU-MIMO and OFDMA modulations and adopt an EM algorithm for clutter estimation and separation in Section 5.1 of Chapter 5. We also show how to perform clutter-free radio sensing from extracted dynamic signals.

- We propose a cluster based 2D CS algorithm in Section 5.2 of Chapter 5 that exploits the cluster structure via introducing a prior probability distribution in multipath channels for more accurate sensing parameter estimation in perceptive mobile networks.

1.4 Organisation of the Thesis

This thesis has six chapters, divided into several sections and subsections for a detailed illustration of the specific problems. A brief outline of the contents is given as follows.

In Chapter 2, we introduce the system platform for the perceptive mobile network. The chapter provides a concise review of the literature on technical fundamentals of having sensing functionalities obtained from mobile signals of a cellular network followed by a description of the MU-MIMO system and channel estimation techniques.

In Chapter 3, we provide mathematical models for the direct sensing problems. We consider both downlink and uplink sensing, to be consistent with downlink and uplink communications. The second section of this chapter provides the direct

sensing solution of receiver cost minimization through analog antenna array.

In Chapter 4, the indirect sensing schemes are presented. In the second section of this chapter, we provide indirect sensing solution of estimating sensing parameters from 5G NR standard signals in perceptive mobile networks by applying 1D to 3D CS algorithms. These CS algorithms are developed from existing ones to make them capable of estimating all the sensing parameters. We use both 5G-compatible channels recommended by 3GPP and our own generated cluster channel model which has a better control for radio propagation for the sensing purpose. We compare these CS algorithms, and demonstrate their respective advantages and disadvantages, under various channel conditions and system setup.

Chapter 5 presents the background subtraction method and Gaussian Mixture model based solution for clutter suppression. In the second section of this chapter, we exploit the cluster property in multipath channels through creating a prior probability distribution and propose a novel two-dimensional (2D) CS algorithm for sensing parameter estimation in perceptive mobile networks.

Chapter 6 concludes the thesis with a description of some interesting and challenging future work suggested by this research.

Chapter 2

Literature Review

2.1 Background

Radio science and engineering has been advancing in wireless communication and radar sensing in parallel and with limited intersections for over a century. However, as the technology advances, the gap between wireless communication and radar sensing in terms of hardware requirements and digital signal processing approaches has narrowed [5], [10], [11]. Intuitively, sensing functionality adopted from the radar system can be integrated with the wireless communication system by JCAS. Most existing research, however, is limited to passive sensing using simple TV signals [12] or small scale networks such as passive sensing in Wi-Fi [13]. The basic concept of JCAS may be traced back to 1970s [4], [5], [10], [11]. In the past few years, JCAS has been studied significantly for simple point-to-point (P2P) communications such as vehicular networks [14], [15]. An overview of the latest developments in joint vehicular communications and radar systems can be found in [16]. JCAS has the potential to integrate radio sensing into large scale mobile or cellular networks [17–19], creating what we call a perceptive mobile network. Research progression here is mainly hindered by the significant challenges caused by highly complicated mobile signals, networks, and signal propagation environment.

Traditional radar is evolving towards more general radio sensing. Radio sensing here can be widely referred to as retrieving information from received radio signals.

Radio sensing involves more diverse applications covered in internet of things (IoT) and 5G networks such as object, activity and event recognition [20]. In [21], the authors briefly described the ubiquitous use of wireless technologies such as Wi-Fi, Bluetooth, FM radio and mobile cellular networks, as signals of opportunity in the implementation of IoT. These radio signals transmitted by an already installed infrastructure and are not specifically designed for the sensing purpose. In [22], the authors showed that the Wi-Fi signal can be used for people and behavior recognition including room occupancy monitoring, activity and gesture recognition, vital signs monitoring, identity identification and localization in an indoor environment. Moreover, methods based on other radio, such as RFID and ZigBee, can be used in activity recognition [23]. These works [20–23] show the strong potential of using low bandwidth communication signals for radio sensing applications.

According to a recent research conducted in [2], beam steering can be a solution for direction estimation in JCAS. However, requirements for sensing and communication are different. Communication requires a stable and accurately pointed beam whereas sensing needs a time varying directional scanning beam. According to [24], getting the correct solutions of beam steering and beamwidth adaptation for JCAS operation are highly dependent on environmental context. Indeed, reflector position, blockage height, object speed and other environmental context factors are dominant in getting the correct solutions both for communication and sensing [24].

In literature, few articles, for example, [6], [11], [25] describe the basics of signal processing in this specific joint processing through the usage of MU-MIMO OFDM signal as a better candidate. Having mentioned all these existing works, we will base our work on a system and technology platform that aligns with those being used in evolving cellular networks. We assume the availability of (massive) antenna array and broad bandwidth (through for example channel aggregation), and the usage of MU-MIMO and multicarrier modulation techniques. The intended frequency band of operation will be the same as for the current cellular network, for example, LTE/LTE-A or future 5G.

2.2 Related Work

The JCAS (also referred to as dual-functional radar and communications (DFRC), or RadCom) technology [1–3], [11], [17–19], [26–30] is receiving increasing interest thanks to its capability in integrating communication and radar sensing into one system, using the same transmitted signals and a majority of the hardware and signal processing modules. One major potential application for the JCAS technology is in vehicular networks [14, 15], where communication signals can also be used for sensing the environment for object detection and collision avoidance. Another potentially significant application is in mobile (also referred to as cellular) networks. Having the largest broadband coverage and powerful infrastructure, JCAS-enabled mobile networks can potentially become a ubiquitous radio sensor, while providing simultaneous communication service.

The co-existence of communication and radar systems has been extensively studied in the past decade. The research articles [5, 18, 19, 31–36] illustrate that in the co-existence solutions, wireless communication and radar systems share the same resources and transmit two different signals overlapped in time and/or frequency domains. Moreover, the two systems are physically separated or co-located and perform each one's functions in a cooperative manner. The communication system generally controls its transmission power to keep the interference-to-noise ratio low at a radar. In extreme cases, the communication system can only operate under certain circumstances, for example, when the radar is not occupying the frequency or the spatial region of interest. This is because canceling mutual interference is a challenge in the co-existence of MIMO radar and multi-user communication. In [37], complicated mitigation methods were proposed for the co-existence solutions to deal with potential large mutual interference. The authors of [36] proposed a robust beamforming design to address the co-existence problem of the MIMO radar and the MU-MIMO communication system. In [32], the cooperative spectrum sharing technique jointly optimizes radar and communication system performance in the co-existence of both systems with mutual interference mitigated. In [33], opportunistic

primary-secondary spectrum sharing is introduced for JCAS with a rotating radar. The communication device in this solution is allowed to transmit as long as the resulting interference does not exceed the tolerable level of the radar. The work in [35] investigated a dynamic co-existence approach between a colocated MIMO radar system and a wireless communications system by reusing the radar's spectrum for communication. The co-existence solutions between mobile communication and radar systems required the implementation of complicated mitigation methods to suppress potential large mutual interference so that the two individually deployed systems can operate smoothly without interfering with each other. However, effective interference cancellation typically constrained the mobility of nodes and information exchange between them.

There exist major differences between perceptive mobile networks and existing systems and technologies that combine radar and mobile communications. In the perceptive mobile network ideally no spectrum needs to be separately allocated for communication and sensing, and the spectrum efficiency will be doubled. This is significantly different to existing spectrum sharing concepts such as cognitive radio and co-existence of wireless communication and radar system mentioned in [5] and [19], where two systems share the same resources in either a time-division or overlay method. Through spectrum sharing techniques, to solve the crisis of crowded spectrum, practical radar and communication systems may cohabitate at the same radio frequency bands [26]. For example, in L-band (1-2 GHz), air traffic control radar (ATR) cohabitates with 5G NR and LTE cellular systems. In mmWave band (30-300 GHz), automotive radar cohabitates with 5G and WLAN. A survey of the spectrum-sharing contributions for the co-existence between communications and radar systems can be found in [26] and [34]. More detailed descriptions on the radar-communications convergence issue in terms of co-existence, cooperation, and co-design can be found in [5], [10], [27] and [31].

There are three types of JCAS systems realization, namely: realizing communication in radar systems; realizing radio sensing in communication systems; and

joint design from scratch. In the first two categories, the design and research focus is typically on the additional function, depending on what the base systems are, with the principle of not affecting the primary functions of the base system. The last category of JCAS systems focuses on the joint system design that integrates communication and radar on one platform using a common transmitted signal jointly designed and used for both functions. The joint design is out of bias from any of the systems as the design starts from scratch to better perform both functions in one system. Perceptive mobile networks belong to the second class, where communication is already very well realized and the main challenge is how to achieve radar sensing functionality based on the cellular network by its own radio signal without degrading the performance of communications. However, the ideas and techniques related to the third class may also apply to the design of perceptive mobile networks, particularly when we target the future generation of cellular networks. We now introduce the recent research progress in each of the categories of JCAS.

2.2.1 JCAS by Realizing Communication in Radar Systems

Similar to getting sensing functionality in a communication system, communication function can be achieved within radar systems. By obtaining communication capability, as mentioned in [4] and [6], radar sensing network can improve the detection performance in military applications. In [4], authors implemented a combined radar and communication system based on a software defined radar platform, in which the radar pulses are used for communication. Further in [7], the authors specifically showed that the quasi-orthogonal multicarrier linear frequency modulation-continuous phase modulation waveform radiated by a MIMO radar can be applied for communications with multiple users. Transmit and receive beamforming design is given in [38] for full-duplex communication in joint MIMO radar and communication systems. Different from the perceptive mobile network, the JCAS proposed in [38] deployed on MIMO radar is to act as a JCAS unit. In [39] fusion of radar sensing and wireless communications solutions is presented by embedding communi-

cation signals into the radar transmit waveform. In [40], cooperative transmissions have shown for radar and communication functions in a DFRC system in which embedding of communication symbols into the MIMO radar emissions is used for the JCAS operation. A new signaling scheme for DFRC is proposed in [41], where frequency-hopped MIMO orthogonal radar waveforms are designed to carry communication symbols to utilize the waveform diversity of radar system for viable communication. In [42], random step frequency signal is used in designing a radar and communication integrated system where the carrier frequency of the radar signal is used for modulating communication information. In [43], the transmit array of a radar is partitioned into a number of subarrays that are allowed to overlap to perform spectrum sharing between an overlapped-MIMO radar and a communications system. Research work in [5] and [44] states that, communication network establishment can be possible for both static and moving radars used in the military and aviation domains. Adaptive transmit signals from airborne radar mounted unmanned vehicles can also be used to simultaneously sense a scene and communicate sensed data to a receiver at the ground base station. The joint effort is expected to have low latency and be a secure, long range communication link established by using the existing radar system. Perceptive mobile network discussed in this thesis is not referring to this form of JCAS operation.

JCAS-enabled mobile network can also be significantly different from passive bistatic and multistatic radar systems which use mobile communication signals for sensing [45–47]. In the JCAS network, receivers know the detailed structure of the transmitted signal, such as resource allocation for time, frequency and space, and the transmitted data symbols (either directly known or through demodulation). Such knowledge on the signal structure is important for coherent detection, which enables accurate estimation for sensing parameters. In a mobile network environment, without the knowledge of the signal structure, passive sensing lacks the capability of interference suppression, and cannot separate multi-user signals from different transmitters (signal sources). In addition, most passive radar sensing can only perform

non-coherent detection with the unknown signal structure, and hence only limited sensing parameters can be extracted from the received signals with degraded performance [45, 46]. Furthermore, as the clock phases between transmitter and receiver are not synchronized in passive sensing, there is always timing and therefore ranging ambiguity remains in the sensing results.

2.2.2 JCAS by Realizing Radio Sensing in Communication Systems

There have been limited JCAS results closely related to modern mobile networks. In [25], some early work on using the OFDM signal for sensing was reported. Research work in [48] performed linear interpolation on LTE downlink signal for radar target distance and velocity estimation. Research work on blockage sensing by radars deployed on towers in cellular networks found in [49]. In [50], authors implemented active radar sensing functions into a communication system with OFDM signals for vehicular applications. The presented radar sensing functions involve Fourier transform algorithms that estimate the velocity of multiple reflecting objects in IEEE 802.11.p based JCAS system. In [14], automotive radar sensing functions are performed using the single carrier (SC) physical frame of IEEE 802.11ad in an IEEE 802.11ad mmWave vehicle to vehicle (V2V) communication system. In [15], OFDM communications waveform, found in IEEE 802.11a/g/p, is used to perform radar functions in vehicular networks. More specifically, a brute-force optimization algorithm is developed based on received mean-normalized channel energy for radar range estimation. The processing of delay and Doppler information with the IEEE 802.11p OFDM waveform in vehicular networks is shown in [51] by applying ESPRIT method.

In [52], sparse array optimization was studied for MIMO JCAS systems. Sparse transmit array design and transmit beampattern synthesis for JCAS is proposed in [53] by antenna selection method where the same or different antennas are assigned to different functions. In [54], the multiple access performance bound is de-

rived for a multiple antenna JCAS system. In [55], multicarrier waveform is proposed for dual-use radar-communications, for which interleaved subcarriers or subsets of subcarriers are assigned to the radar or the communications tasks. That means each subsystem is assigned with distinct subsets of subcarriers from the total available subcarriers. In [56], mutual information for an OFDM JCAS system is studied, and power allocation for subcarriers is investigated based on maximizing the weighted sum of the mutual information for radar and communications. In [18], waveform optimization is studied for minimizing the difference between the generated signal and the desired sensing waveform under the constraints of signal-to-interference-and-noise ratio for MU-MIMO (also referred to as spatial division multiple access, SDMA) downlink communication. A multi-objective function is further applied to trade off the similarity of the generated waveform to the one desired for communication and sensing [19]. These studies involve some key signal formats in modern mobile networks, such as MIMO, MU-MIMO, and OFDM. However, there is very limited work on how JCAS can actually be realized at a system level in the mobile network, and how radar sensing can be done based on modern mobile communication signals, which is a fundamental and challenging problem.

In traditional radar, clutter is typically returned from ground, sea, rain, and atmospheric turbulence, and generally has distinct features from useful reflections [57, 58]. Most known algorithms in radar, such as space-time adaptive processing (STAP) [57], independent component analysis (ICA) [58], and Doppler focusing [59] are adapted to such scenarios. In contrast, in perceptive mobile networks, clutter can be originated from the same objects with the ones of interest for sensing. So, traditional clutter suppression methods for radars may not directly work here.

Recently, a limited number of new clutter suppression techniques that are closely related to modern mobile networks were reported. In [60], maximum-likelihood based matched filtering was proposed for clutter estimation in JCAS receivers. The sample evaluation presented in this work uses a simplistic clutter model; however, under more complicated clutter models, the clutter cancellation residual will be

larger and may adversely affect both communications and radar performance.

Moreover, the multipath signals from one cluster have similar sensing parameters values for delay, angle-of-arrival and Doppler frequency, and are typically from the same scatter(s). Complexity arises when the clusters originated in a propagation scene may have correlations among other clusters of the same user and across different users due to the same channel condition. Eventually, these create an accuracy problem when getting sensing parameters from delay or angle domain without acknowledging channel cluster structure knowledge. Moreover, there are common multipath remains among clusters. There exist research outputs on reconstructing cluster sparse signals in general, for example, through periodic compressive support [61], model based CS [62], variational Bayes approach [63], and block Bayesian method [64]. In [65] a mmWave joint radar and communication system for indoor scenarios is developed, using estimated radar channel coefficients. However, there is only very limited work on how cluster sparsity structure can be exploited in JCAS systems such as perceptive mobile networks that involve OFDMA and MU-MIMO. Therefore, cluster sparse signal reconstruction for more accurate sensing in perceptive mobile networks, employing OFDMA and MU-MIMO is our interest.

2.2.3 JCAS by Integrated Joint Design from Scratch

JCAS technologies can be developed by integrated joint design from scratch without being limited to existing communication or radar systems. In this sense, the authors, for example in [6, 26, 27], discussed how a JCAS system can be designed and optimized by considering the essential requirements for both communication and sensing.

Integrated radar-communication performs simultaneous wireless communication and remote sensing on a single platform. The joint design allows a single hardware platform to work for both functions. The integrated system uses the same transmitted signal designed for both functions. A JCAS system using separately transmitted signals suffers from lower spectrum efficiency due to the partitioning of

resources [11]. On the other hand, the integrated system using the same transmitted signals may achieve reasonable spectral efficiency without facing the problem of mutual interference. However, this particular operation of JCAS with the same signal requires full duplex or equivalent setups. A more thorough discussion can be found in [5], [10], [26], [27], and [31].

A majority of research on JCAS has demonstrated the feasibility and provided methodologies for P2P links, such as P2P mmWave links considered in works [66], [67], [68], [69] and [70]. The mmWave based JCAS can facilitate such joint design from scratch for many new exciting applications both indoor and outdoor. The implication of mmWave in joint communication and sensing network is illustrated in [66]. Beamforming design for dual functional radar-communication systems at the mmWave band is proposed in [67]. The proposed hybrid beamformers in the work [67] can give a fully digital communication beamformer, meanwhile formulating a desired radar beam to point towards targets. Research work in [68] provides an in-depth signal processing aspects of mmWave-based JCAS with an emphasis on waveform design for joint radar and communication system. The adaptive SC mmWave waveform structure designed in [69] serves as the transmitted signal at the source for both communication and radar systems. Further investigation on the selection of waveforms for the automotive application of JCAS is analyzed in [70], providing a comparison between the phase-modulated continuous-wave JCAS and OFDMA-based JCAS waveforms for V2V applications by analyzing the system model and enumerating the impact of design parameters.

2.3 Benefits of Joint Communication and Sensing System

The perceptive mobile network has more advanced infrastructure than Wi-Fi sensing, including larger antenna arrays, larger signal bandwidth, more powerful signal processing, and distributed and cooperative base-stations. In particular, with mas-

sive MIMO, the perceptive mobile network equivalently possesses a massive number of "pixels" for sensing. This enables radio devices to resolve numerous objects at a time and achieve sensing results with better resolution. Some specific application examples by JCAS on surveillance and transportation are: (1) real-time city-wide low-cost traffic monitoring and scheduling, as well as vehicle classification and tracking; (2) assisted vehicle automation (3) crowd management in big events and emergency evacuation, or population density and movement mapping; and (4) extensive on-street and open space surveillance for on-road parking space management, and pedestrian and animal detection. We can mention some key generalized benefits of joint communication and sensing system as below:

- **Spectrum efficiency:** Spectrum efficiency is improved by completely sharing the spectrum available for wireless communication and radar [11].
- **Beamforming:** Beamforming performance can be enhanced through use of sensing information [71], [72].
- **Cost/Size:** Joint system can allow reduced cost and size in transceiver implementation with an uncompromised simultaneous operation for both systems [11].
- **Smart Applications:** Sensing based application can appear in the market if we can obtain object sensing with the communication. Smart home, smart car based new application can be developed by the exciting feature of object sensing and tracking by mobile signal [1], [5], [9].
- **Network Overhead:** Sensing information may help in reducing huge network overhead by employing simply a directional beam to the user rather than having a beam in a wider area to get the same user [24], [71], [73].

Based on the study from several works, such as, [1], [4], [5], [6], [7], [10], [11] and [24] a tabular information can be given in Table 2.1 on difference and benefits of JCAS in comparison with individual radar system and communication system.

Table 2.1: Investigation on Radar, Communication and JCAS

Case	Radar	Communication	Case	Joint System
Signal Modulation	Unmodulated and orthogonal, in some cases linear frequency modulated	Mix of modulated symbols, multicarrier modulation	Coverage with multiple antenna	Digital beamforming provides wide dedicated coverage in radar while in communication, MIMO enables enhanced directivity gain and interference suppression
Transmission Power	High	Low	Powerful long distance transmission	Radar has more powerful transmitter, their transmitted signal can travel long distance which enables communication over wide area
Peak to average power ratio (PAPR)	Small	High	Antenna Pattern	Much larger antenna array with very narrow beam steering capabilities of radar system can be useful in communication.
Bandwidth	In order to achieve high resolution, a radar sensor needs large signal bandwidth	Typical communication signals bandwidth is usually less than radar	Signal spectrum	Whole frequency range can be used and increased spectrum efficiency can lead to have better communication and tracking.
Signal Band	X, S, C, Ku	ISM, RF (MHz) range	Digital signal processing platform	Gap between the hardware requirements for the radar and communication systems becomes narrower and both devices become similar as the receiver front-end becomes more digital
Transmission Capability of Modules	Only radar send signal to get the response back after reflected by object	Full or half Duplex, both BS and user can transmit and receive	Exchange of network data	Detection accuracy and probability can be improved by exchanging of network data between both system

2.4 Perceptive Mobile Network

We name the joint system as *perceptive mobile network* [1], [17], [74], [75], [76], where it involves with radio channel sensing by communication signal itself. A unified transceiver system, already mentioned in the research work of [1], could easily be used here, where communication interfaces will be directly used to sense the channel. Such a kind of sensor system can offer a wide range of radio sensing wherever radio coverage is available. Mobile network is almost everywhere and that extended range can be readily usable for obtaining detection and tracking of objects particularly, in vehicular transport network, in crowd monitoring for events, for weather sensing and many more.

A generalized transceiver block diagram for joint sensing and communication is shown in Fig. 2.1. After signal has been received at the antenna array and processed at the RF section, baseband processing handles both sensing and communication simultaneously. Sensing parameters can provide feedback in the communication section to improve the beamforming adaption. Similar kind of common baseband processing can also be applicable in the case of Wi-Fi and digital TV system.

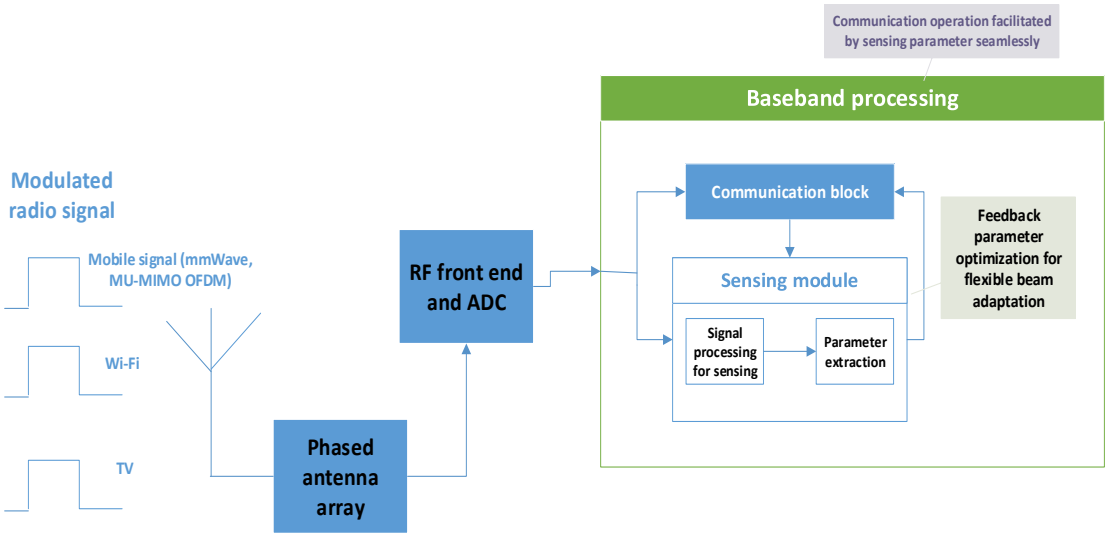

Figure 2.1: General block diagram of unified sensing and communication system.

In a typical centralized deployment for recently proposed 5G mobile network, as demonstrated in Fig. 2.2, sensing can be done in the central office where all Baseband units (BBU) are aggregated in a pool fashion. In the fronthaul, each

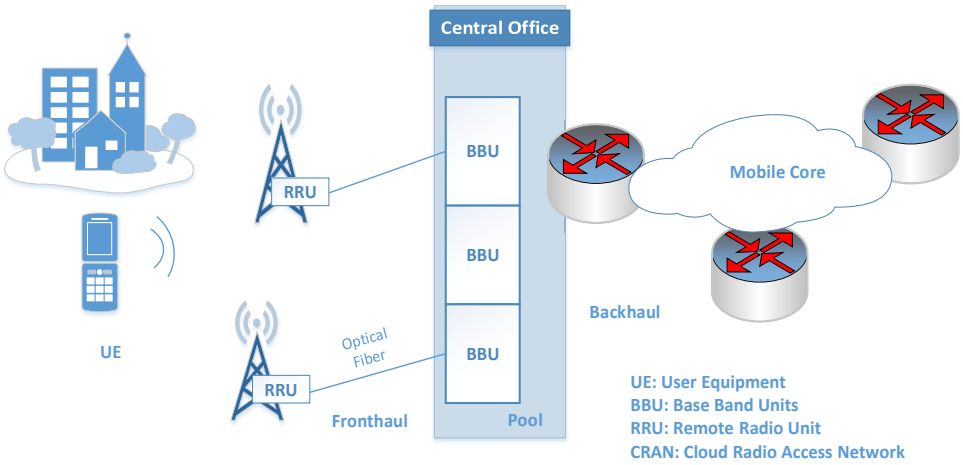

Figure 2.2: CRAN architecture for 5G mobile network

BBU can connect with the remote radio unit (RRU) through optical fibers or wireless systems. RRUs collectively operate in a co-operative manner to provide MU-MIMO service to the users. BBU performs signal processing in the digital domain. Packet based network, such as IP/MPLS is running on the mobile core in order to provide high bandwidth and low latency with proper redundancy.

Fig. 2.3 indicates cloud radio access network (CRAN) central office section, where sensing baseband performs information extraction based on signal reception at RRUs. It is a clear fact that the RRU collects signal and actual sensing processing done jointly with the communication at the CRAN central office. We define downlink and uplink sensing, as sensing performed at a RRU employing downlink transmitted signals from itself and other cooperative RRUs and uplink signals from users, respectively [1]. In order to achieve sensing using downlink signals, the transmitter and receiver at a RRU need to be able to operate simultaneously. A simple solution, as in Fig. 2.3 is to use separated antennas for transmitter and receiver.

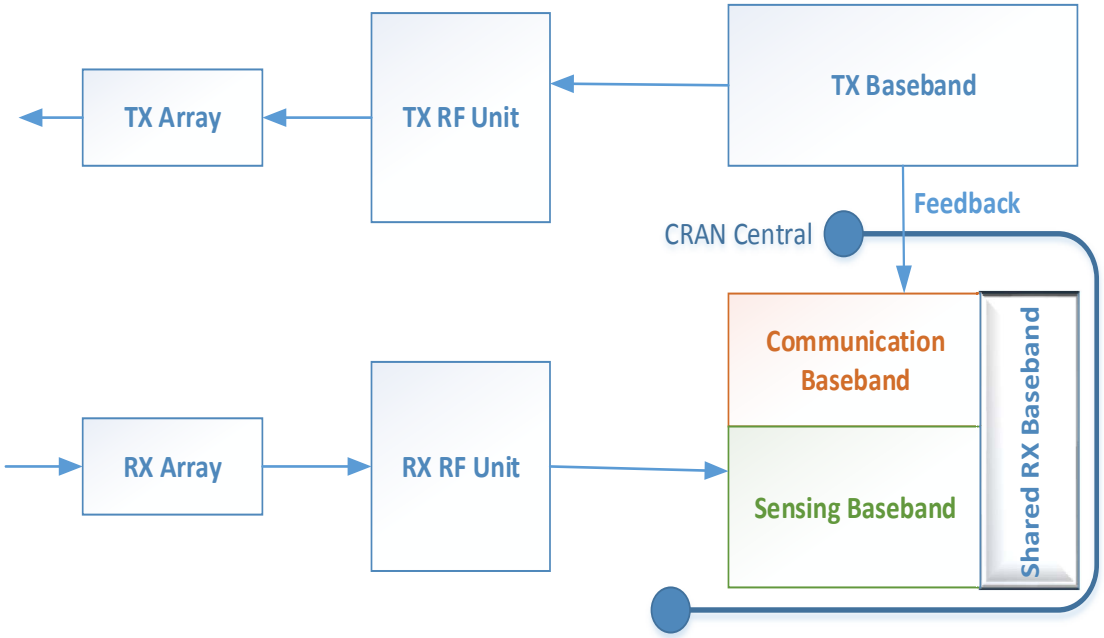

Figure 2.3: Simplified transceiver model for joint communication and sensing

2.5 Framework for a Perceptive Mobile Network

In this section, we develop a framework for integrating radar sensing into the current communication-only mobile network using JCAS technologies, by synthesizing and extending earlier work in [1, 76]. This framework includes both a *system platform* for unified radar sensing and novel *sensing solutions*. We set up the perceptive mobile network on a system platform with key components and technologies in modern mobile networks, such as antenna array, broadband through, for example, channel aggregation, MU-MIMO and OFDMA. The system platform provides system-level integration for communication and radar sensing, and unifies three types of sensing based on the communication signals. The sensing solutions address critical challenges in estimating *sensing parameters* including time delay, angle-of-arrival (AoA), angle-of-departure(AoD), Doppler shift and magnitude of multipath signals. These challenges are caused by both sophisticated signal formats and massive multipath signals due to the complicated signal propagation environment.

The first challenge for sensing parameter extraction in perceptive mobile networks is due to the sophisticated signal structure. The communication signals, which are also used for sensing, can be randomly modulated with multiple users' symbols

using MU-MIMO and OFDMA technologies and can be fragmented for each user - discontinuous over time, frequency or space. This will be detailed in Chapter 3. Such signals structure makes most existing sensing parameter estimation techniques not directly applicable. For example, active radar sensing technologies mainly deal with linear FM (LFM) chirp or pulse width modulated transmitted signals [77], [78], [79]; most passive bistatic and multistatic radars consider sources of opportunities with different carrier frequency and compare the reference signal collected from the source direction to the measurement signal collected from the target direction [45–47, 80]; and channel estimation techniques developed for modern mobile networks mainly focus on estimating channel coefficients instead of detailed channel compositions represented by the sensing parameters. In addition, conventional spectrum analysis and array signal processing techniques such as MUSIC [6] and ESPRIT [25] require continuous observations, which are not always available here. Therefore, new sensing techniques need to be developed for estimating sensing parameters from the complicated and fragmented signals. We will show in both Chapter 3 and Chapter 4 that CS is an excellent candidate technology for this problem, after proper signal formulation.

The second challenge for sensing parameter estimation comes from the rich multipath in mobile networks. Most sensing parameter estimation algorithms can only process signals containing a limited number of multipath signals. Hence we need a preprocessing method which can divide signals into different groups where each group has a significantly reduced number of multipath signals. At a minimum, it is essential to separate and reduce non-information-bearing multipath signals from the input. Such unwanted multipath is called *clutter* in the radar literature. Typical radar systems are optimized for sensing a limited number of objects in open spaces using narrow beamforming, and clutter has notably different features from useful reflections returned from ground, sea, rain etc. [6, 81]. Most known algorithms in radar systems, such as space-time adaptive processing (STAP) [82], independent component analysis (ICA) [58], and singular value decomposition (SVD) [83] are

adapted to such scenarios. In the perceptive mobile network, we define *clutter* as unwanted multipath signals that contain little new information. The clutter hence is mainly referring to the multipath signals from permanent or long-period static objects when both the transmitter and receiver of the sensing devices are static. Due to the different signal propagation environments, suppression requirements and applicable sensing algorithms, existing clutter suppression techniques developed for radar systems, e.g., those in [81, 84, 85], may not directly render the clutter reduction here. Most of them are also applied after sensing algorithms, and hence cannot achieve the goal of reducing multipath input to the sensing algorithms. In the first part of Chapter 5, we propose a background subtraction method based on simple recursive computation with a closed-form expression for performance characterization and a clutter suppression method based on the Gaussian mixture model (GMM) and expectation maximization (EM) estimation.

On a second note, in this case, we need to exploit the cluster property in multipath channels through creating a prior probability distribution for sensing parameter estimation in perceptive mobile networks. In particular, a cluster prior probability density function is introduced in the second part of Chapter 5 in the proposed 2D cluster Kronecker CS algorithm, and is shown to efficiently detect the coarse locations of the clusters, leading to more accurate sparse reconstruction performance when Kronecker CS algorithms are applied. We will also provide solutions related to this clutter reduction and sensing in cluster channel in Chapter 5.

In this research, we focus on studying system-level integration of sensing function into mobile communication networks, and investigating how to address the two critical challenges for sensing parameter estimation as described above. As an initial piece of work in this new domain, our proposed algorithms here mainly intend to demonstrate the feasibility and methodology but are yet to be optimized for complexity and performance.

2.5.1 System Platform for the Perceptive Mobile Network

Our proposed system platform aligns with the specification of the evolution of mobile networks, such as 5G. In this section, we describe the system model, the supported sensing operations and the required modifications to existing mobile communication infrastructure.

We assume a CRAN architecture using MU-MIMO and OFDMA technologies. Fig. 2.4 shows the CRAN architecture based system model of the proposed perceptive mobile network. In this model, cooperative RRU, are densely distributed and synchronized in clock. Signal processing for both cellular communication and radio sensing based on collected signals from these RRUs is done centrally in CRAN central, which includes the BBU pool for communication and the sensing processing unit. We assume that cooperative RRUs are within the signal coverage area of each other. In the fronthaul, each BBU can connect with the RRUs through optical fibers or wireless links. All RRUs' clocks are synchronized, typically via GPS. A typical communication scenario is as follows: several RRUs work cooperatively to provide connections to mobile stations (MSs), using MU-MIMO techniques over the same subcarriers. Although we consider CRAN, our proposed solution could work for a standalone base-station (BS) too. So hereafter we will use CRAN central and BS without differentiating between them.

We focus on the case where radio sensing is conducted in the BS, although MS-side sensing is also possible. Compared to MS, BS has advantages of networked connection, flexible cooperation, large antenna array, powerful computation capability, and known and fixed locations.

2.5.2 Three Unified Types of Supported Sensing Operations

There are three types of sensing that can be unified and implemented together in the mobile network. Referring to the CRAN architecture, a RRU can implement downlink active and passive sensing during downlink signal transmission, and then operate on communication and uplink sensing modes during the uplink stage.

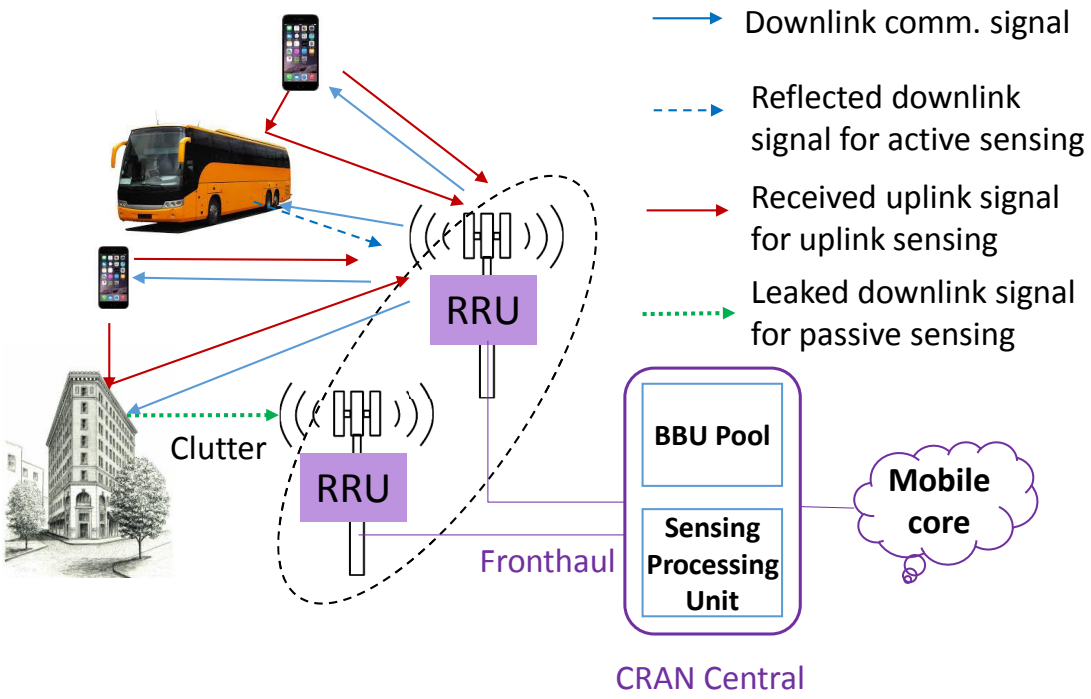

Figure 2.4: Proposed system model.

In the perceptive mobile network, the transmitted signal from base-stations (BSs) or MSs is used for both communication and sensing. The signal may be optimized jointly for the two functions, and one example is available from [18]. We define *uplink and downlink sensing*, to be consistent with uplink and downlink communications. In uplink sensing, the used sensing signal is from MSs. In downlink sensing, the sensing signals are from BSs. The downlink sensing is further classified as *Downlink Active Sensing* and *Downlink Passive Sensing*, for the cases when a RRU collects the echoes from its own and from other RRUs transmitted signals, respectively.

It is important to note that in a distributed antenna system such as CRAN, sensing is for the environment surrounding a specific transmitter and receiver, and hence it is separately done for each node (RRU in CRAN), although some joint processing is possible.

Downlink Active Sensing

We refer to *downlink active sensing* as the case that a RRU uses reflected downlink communication signals from its own transmitted signal for sensing. In this case,

similar to a mono-static radar, transmitter and receiver are co-located although they may have two independent antennas separated in space. This will enable a RRU to sense its surrounding environment.

Downlink Passive Sensing

Passive sensing typically refers to the case when a third receiver outside the communication system exploits the communication signal for sensing. Here we use downlink passive sensing for the case where a RRU uses the downlink communication signals received from other RRUs for sensing. Depending on the distance between RRUs, reflected signals from other RRUs or the RRU itself may arrive at different time segment or overlapped. Downlink passive sensing senses the environment among RRUs.

Uplink Sensing

BS uses the uplink communication signal from MS transmitters for *uplink sensing*. Uplink sensing estimates relative, instead of absolute, time delay parameters because the timing in MS transmitters and RRU receivers is typically not aligned. This timing ambiguity may be removed by using techniques developed from the triangulation techniques in localization. Uplink sensing senses MSs and the environment between MSs and RRUs.

Downlink sensing can potentially lead to more accurate sensing results than uplink sensing because RRUs exhibit more advanced transmitter capability than MS and also the transmitted data symbols are centrally known in the downlink. In addition, the privacy issue is almost not a problem in downlink sensing because the sensed results are not directly linked to any MSs.

The signals available for sensing can come from several sources, such as the DMRS and the whole data payload signals in 5G NR. The transmitted signals can also be optimized jointly for both communication and radar sensing, such as those proposed in [18, 19, 56]. In this work, we focus on using the always-available

whole data payload, as DMRS signals are random and may be insufficient for high-resolution sensing.

Downlink sensing generally has stronger capabilities than uplink sensing in terms of sensing ranges and resolution in distance, direction and speed. This difference is largely caused by the difference in transmission power, as well as the number of transmission nodes and the number of transmission antennas from each node. There are experimental results on passive radar that use signals from LTE eNodeB for detecting different types of ground-moving targets, including cars and people at a range of approximately 150 meter [47]. The simulation results presented in [17] consider practical transmission power values, also demonstrate that downlink and uplink sensing can detect objects more than 150 and 50 meters away, respectively. Other exemplified sensing capabilities shown in [17] include a distance resolution at a few meters corresponding to the signal bandwidth of 100 MHz, an angle resolution of about 10 degrees given a uniform linear array of 16 antennas, and a resolution of 5 m/s moving speed. Based on these sensing capabilities, we can foresee the following sensing applications of perceptive mobile networks: traffic monitoring and scheduling, vehicle classification and tracking, on-street and open space surveillance, parking space management, pedestrian and animal detection and so on. For downlink sensing, using directional antennas and high transmission power may extend the sensing range to one kilometer or more, particularly for detecting objects such as UAVs in the sky.

2.5.3 Signals Usable From 5G for Radio Sensing

Based on the available physical signals in 5G NR, we can categorize the most suitable candidates for performing radio sensing into three types.

Signals Used for Channel Estimation

The first option will be deterministic signals specific for channel estimations, including DMRS [86] for both uplink (PUSCH) and downlink (PDSCH), sounding

reference signals (SRS) for uplink, and channel state information – reference signals (CSI-RS) for downlink. Most of them are comb-type pilot signals, circularly shifted across OFDM symbols, and are orthogonal between different users. Among them, DMRS signal associated with the shared channel is user-specific and always transmitted with data payload. The number and position of DMRS OFDM symbols shall be available to the BSs, and they can be adjusted and optimized across the resource grid including slot and subcarriers (resource blocks). This implies good prospects for both channel estimation and sensing in different channel conditions, and maybe further optimized by considering joint optimization for communication and sensing.

With a given subcarrier spacing, the available radio resources in a sub-frame are treated as a resource grid composed of subcarriers in frequency and OFDM symbols in time. Accordingly, each resource element in the resource grid occupies one subcarrier in frequency and one OFDM symbol in time. A resource block consists of 12 consecutive subcarriers in the frequency domain. A single NR carrier in Release-15 is limited to 3300 active subcarriers as defined in Sections 7.3. and 7.4 of TS 38.211 [87]. On the other hand, signals used for beam management in connected mode, like SRS and CSI-RS can be either periodic or aperiodic, and hence they can be optimized for sensing too.

Non-Channel Estimation Signals

We may also exploit deterministic non- channel estimation signals for sensing such as the synchronization signal and broadcast blocks (SSB). Such signals typically have regular patterns, and are periodic at an interval of several to tens of milliseconds. However, they only occupy a limited number of subcarriers, which leads to limited identification of multipath delay values.

Data Payload Signals

In addition, we can also exploit the data payload signals for sensing. Since these data signals are random, they are not ideal for sensing. However, they can significantly

increase the number of available sensing signals, and hence improve the sensing performance at increased complexity.

We will mainly use DMRS for both uplink and downlink as a primary signal for sensing in this research. More details of the DMRS signal are provided here.

2.5.4 Required System Modification

We now describe potentially required modifications on hardware and systems, in order to evolve current communication only mobile networks to perceptive mobile networks. We focus on fundamental changes that enable the integration of radio sensing to current mobile networks, and do not consider low-level changes such as joint waveform optimization [18, 19, 56], joint antenna placement and sparsity optimization processing and power optimization [52].

Uplink sensing can be implemented without requiring changes to hardware and system architectures of current mobile systems, in the presence of the timing ambiguity problem. Alternatively, dedicated (static) MSs that are clock-synchronized to BSs can be used, which would be the most convenient way for achieving non-ambiguity sensing in the perceptive mobile networks.

On the other hand, downlink sensing requires changes to hardware, and the extent of changes depends on the network duplexing mode. Basically, downlink sensing requires a transceiver to work on the *full duplex* mode, where receiver and transmitter need to operate at the same time. This causes transmitted signal leakage, which can easily overwhelm the reflected echoes for downlink sensing without modifying the current hardware. The full duplex technology, which typically uses antenna separation, RF suppression and baseband suppression to mitigate the leakage, is a promising enabling technology in the long term [88]. Although it progresses well, full duplex MIMO is still challenging to realize in practice due to antenna cross-talk and coupling.

Two near-term solutions to downlink sensing are as follows:

- Using two sets of spatially well-separated antennas for transmitting and re-

ceiving. Nevertheless, this requires extra antenna installation space and can increase the overall cost.

- Deploying RRUs that only work on the receiving mode. They can be configured as working in the sensing mode only or in both communication and sensing modes.

To implement these near-term solutions, changes to the hardware are required. For time-division-duplexing (TDD) systems, the change is minor since a TDD transceiver generally uses a switch to control the connection of antennas to the transmitter or receiver. For frequency division duplexing (FDD) systems, the receivers may not be capable of working on downlink frequency bands. From this point of view, it is more cost-effective to implement downlink sensing in TDD than in FDD systems.

2.6 MU-MIMO OFDM System Model

Higher data rate and substantial gain is the point of interest in communication. OFDM, a multicarrier modulation technique, is known and suitable especially for high data rate transmissions in multipath environments. OFDM has been selected in many wireless communication systems, such as LTE/4G, Wi-Fi/WLAN, WiMAX, digital TV and many more to follow. Literature work in [89], [90], [91], and [92] mentioned details of implementation procedure and features of OFDM system in usage of today's modern communication platform.

A simplified transceiver block diagram for OFDM signal implementation is presented in Fig. 2.5. In OFDM, after channel coding and symbol mapping, the signal is being transmitted by several parallel orthogonal overlapping subcarriers. ODFM modulation is implemented on several blocks of information symbols by inverse discrete Fourier transform techniques. A guard interval of length equal to channel delay spread known as cyclic prefix (CP) is added with the information block to reduce inter-symbol interference. Next, parallel to serial conversion and RF processing tasks took place to pass the serial data stream through the channel destined

to the receiver. At the receiver after signal reception, demodulation through FFT is performed on parallel data stream. In the end, channel state information obtained from the channel estimation process is utilized in the receiver to perform accurate symbol de-mapping and signal decoding.

The continuous time domain OFDM signal at the t^{th} symbol is modeled by,

$$x(t) = \frac{\sqrt{E_b}}{N} \sum_{n=1}^{N} X(n) e^{j2\pi n f_0 t}, \tag{2.1}$$

where N is the number of used subcarriers, E_b is the symbol energy of $x(t)$, f_0 is the subcarrier frequency spacing and $X(n)$ is complex symbol on the n^{th} subcarrier.

In OFDM, multiple symbols can be transmitted in parallel. The user who is near the base transceiver station (BTS) can experience good channel quality and can be treated with a higher order modulation scheme and those at the poor channel area can be treated with a lower order modulation scheme. If CP is used, OFDM will exhibit resistance against inter-symbol interference (ISI) in a multipath propagation environment.

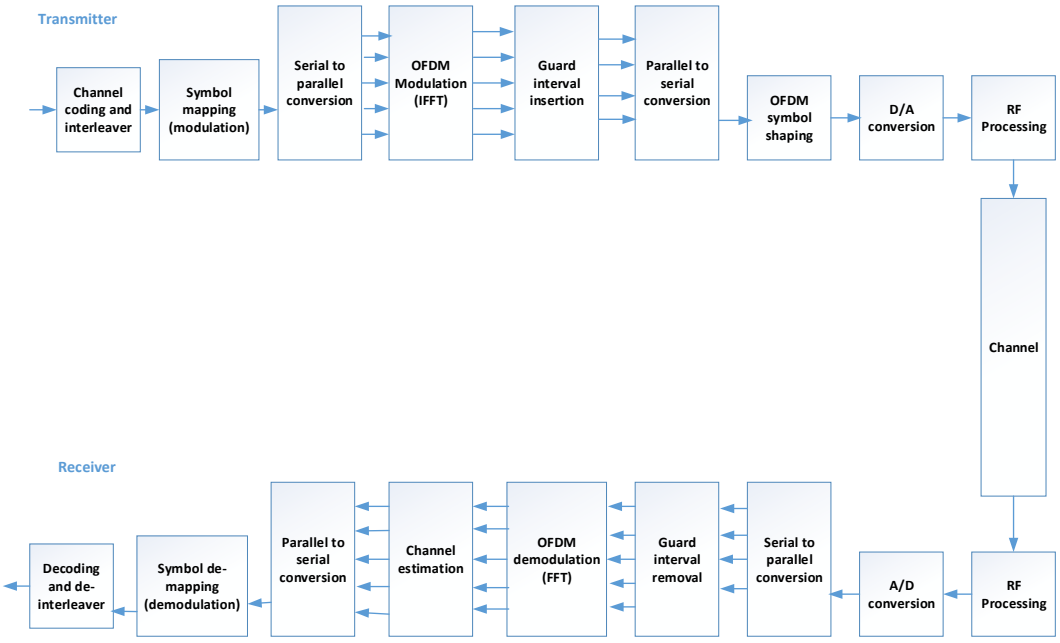

Figure 2.5: Multicarrier modulation based OFDM system transceiver model

Diversity gain and system capacity can be increased by adding an antenna array with OFDM type communication. Multiple antennas can be implemented at the transmitter and receiver to get the arrangement of the MIMO system. Three parameters can define the wireless link, namely, transmission rate, transmission range, transmission reliability. With the use of MIMO OFDM, improvement can be possible in these three sections mentioned above.

A typical MIMO channel configuration is shown in Fig. 2.6 where the OFDM system can take advantage of the spatial diversity that is obtained by spatially separated antennas. Intuitively, MIMO-OFDM system can effectively deal with multipath scattering environment to increase the diversity gain and capacity. A review is provided in [92] about the incorporation of MIMO techniques in OFDM system. Receiver and transmitter both can have multiple numbers of antennas to improve the spatial capacity and achieve better reception. A simplified MU-MIMO system is given in Fig. 2.7 where each BS and user has three antennas.

The general MIMO received signal, at the t^{th} OFDM symbol and n^{th} subcarrier, $\mathbf{y}_{n,t}$,

$$\mathbf{y}_{n,t} = \mathbf{H}_{n,t}\ \mathbf{x}_{n,t} + \mathbf{z}_{n,t}, \tag{2.2}$$

is characterized by the frequency domain $N \times M$ channel matrix $\mathbf{H}_{n,t}$, transmitted signal $\mathbf{x}_{n,t}$, and the Additive White Gaussian Noise (AWGN), $\mathbf{z}_{n,t}$. M and N are the number of antennas in transmitter and receiver, respectively.

For M transmitting and N receiving antennas, the $N \times M$ frequency domain channel matrix can then be represented as

$$\mathbf{H}(n) = \sum_{\ell=1}^{L} b_\ell e^{-j2\pi\tau_\ell n}, \tag{2.3}$$

where L is the number of total multipaths, b_ℓ is the complex amplitude of the l^{th} path and τ_ℓ is the corresponding path delay, while n usually corresponds to the frequency domain subcarrier.

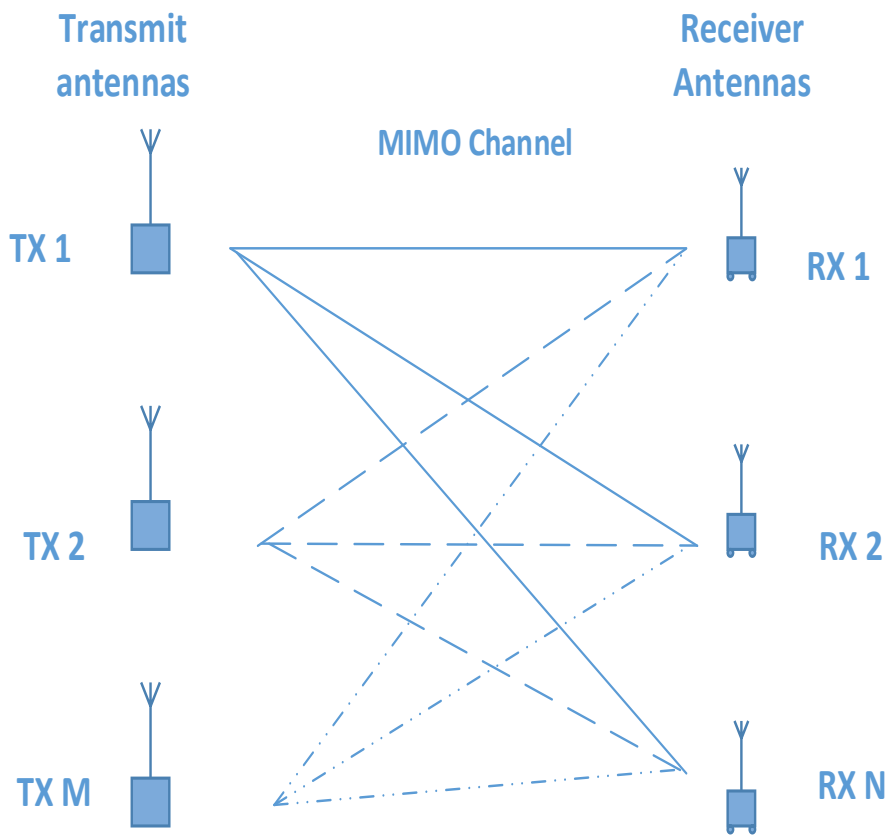

Figure 2.6: MIMO propagation channel

It is to be noted that, data rate, spectral efficiency, throughput, system capacity, transmitter and receiver diversity and spatial diversity can be improved in a MIMO enabled OFDM system without consuming more frequency resources and transmit power. Moreover, due to the increased diversity, fading effect in the channel is reduced significantly.

2.7 Channel Estimation

In JCAS, sensing and communication may share certain functionalities, such as channel estimation, beamforming, and symbol demodulation discrete Fourier transform (DFT) block. However, the required processing and outcome may be largely different for them. Existing channel estimation and localisation algorithms are not directly applicable for producing radio sensing parameter estimation. Channel estimation in communications only requires estimation of composite channels at quan-

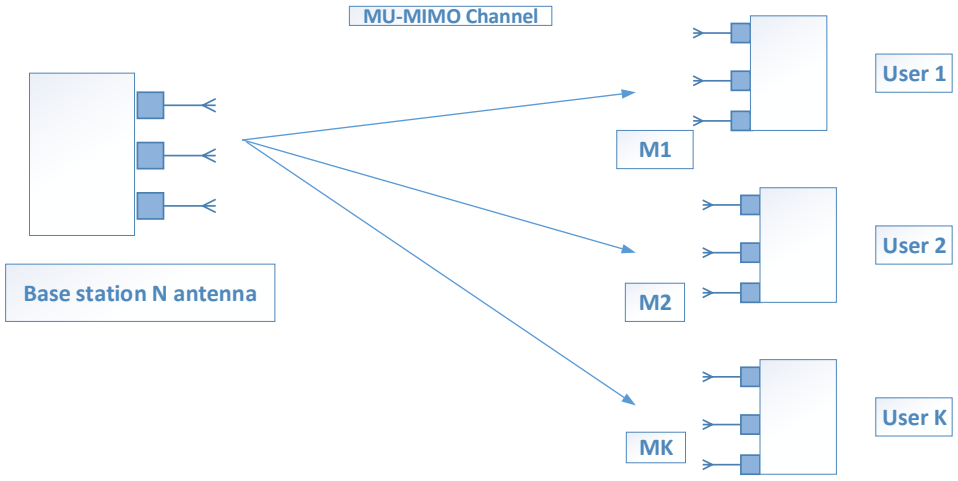

Figure 2.7: MU-MIMO communication system

tized discrete grids, and localization focuses specifically on the line of sight path. However, in radio sensing, detailed channel composition needs to be obtained for having parameters like delay, signal arrival angle and Doppler frequency.

The general idea on the channel estimation process used in communication systems can be found in [89], [93], and [94]. Channel estimation refers to the process by which we can mathematically model or describe the radio channel. Channel impairments and interference can be reduced by utilization of the channel knowledge obtained from channel estimation. Foundation work on channel estimation techniques for MIMO system can be found in articles such as, [95], [96], [97]. The general channel estimator mentioned in Fig. 2.8, works in communication with the idea of minimizing mean square error and computational complexity.

Fading occurs due to the multipath environment. Several types of scatters remain present in the radio channel environment to give rise to different types of channel effects. Mobile motion and scatter local to user give rise to Doppler spread, which causes time selective fading. Remote scatterers can be high rise buildings and

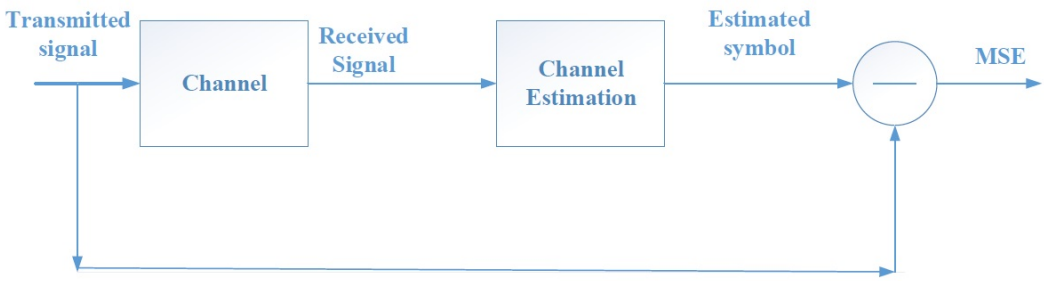

Figure 2.8: Performance evaluation process of channel estimation in communication system

can cause delay and angle spread. Delay spread causes frequency selective fading. Scatterers local to base station cause angle spread and which creates space selective fading. Due to multipath, signal experiences delay and fading which eventually creates Doppler spread, delay spread and angle spread.

Channel estimation and equalizer modelling have been a key research topic due to channel variation and non-linearity. Multipath propagation leads to ISI at the receiver which in turn leads to a high error rate in symbol detection. When the channel has less time variation, we can use training based channel estimation. However, if the channel is rapidly changing, we have to train the channel rapidly and this in fact will impact on transmission. For a varying channel, we can introduce blind channel estimation. There is one more type which is semi blind and is a method where both known and unknown symbols are being used while doing estimation. According to the study from [94], the channel estimation process in communication can be mainly divided into three categories, namely,

- Pilot assisted,
- Blind method, and
- Decision Directed Channel Estimation (DDCE).

Pilots are non-data symbols used inherently as a reference signal to estimate channel by both transmitter and receiver. Pilot based method has a disadvantage of reduction in transmission rate and an accurate estimate while minimizing the

number of pilots is still challenging. Interpolation method is being used to find channel estimation while using pilots. Blind channel estimation is not practical due to its high number of symbol requirements to get the estimated channel. Moreover, computational complexity and latency are higher in this case. Decision directed method uses both pilot and previous estimated or detected data symbol for channel estimation. Decision directed method is well studied and explained by [98], [99] in their research work. The significant benefit of DDCE is to reduce the dependency on the number of pilot subcarrier. If the channel is varying slowly, the usage of previous channel estimate is not creating an error in detection. However, if the channel is fast moving, the usage of an outdated estimate will create an error in symbol estimation. There are two conditions which need to be satisfied for getting a better estimate from DDCE, namely, channel variation needs to be slow and symbol estimation needs to be error free.

A simplified basic operational procedure of DDCE is given in Fig. 2.9. In an OFDM based system, after the FFT, we have the frequency domain received parallel symbol, $\mathbf{y}(t)$ to get into the equalizer. The equalizer gives the estimated symbol, $\tilde{\mathbf{x}}(t)$ which is then demodulated by the demodulator. This demodulated or detected symbol, $\hat{x}(t)$ can be used in the DDCE channel estimation process. The detected symbol will be divided by received symbol, $\mathbf{y}(t)$, to get the new channel transfer factor, $\hat{\mathbf{H}}_t$. The previous channel estimation can be achieved from the used preamble or pilot. The channel estimation is updated with the help of the update factor, α from the previous channel estimate $\tilde{\mathbf{H}}_{t-1}$, and current channel estimate, $\hat{\mathbf{H}}_t$ in a simple recursive filter approach to get $\tilde{\mathbf{H}}_t$ as,

$$\tilde{\mathbf{H}}_t = \alpha\hat{\mathbf{H}}_t + (1-\alpha)\tilde{\mathbf{H}}_{t-1}, \tag{2.4}$$

However, if there is any error occurring in symbol decision or detection, that error will propagate to the channel estimator section and degrade its performance. If the frequency domain symbol is not equally spaced and the channel is fast fading, then the DDCE technique cannot provide an accurate performance. Error can easily

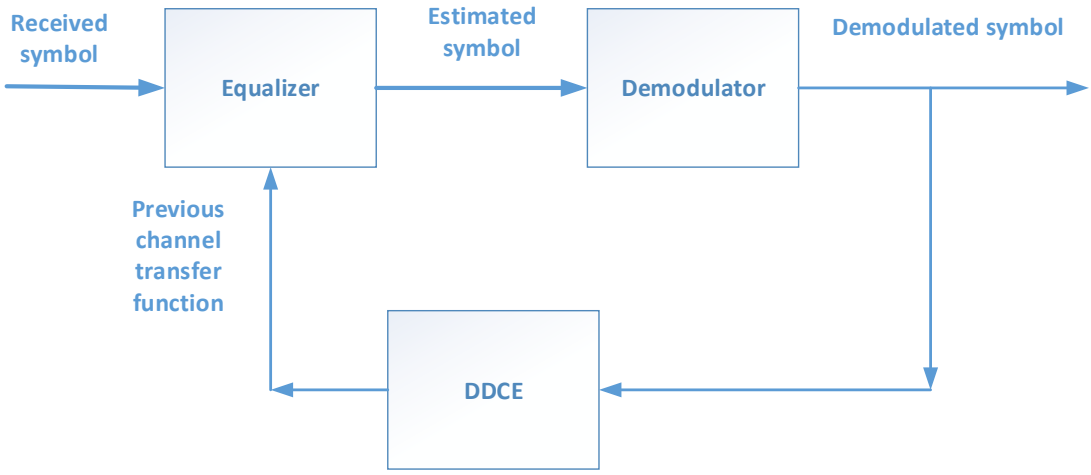

Figure 2.9: Basic principle of DDCE

propagate in further symbols in DDCE. Hence, pilot symbols are used in channel estimation for further improvement. However, the number is fewer than the actual pilot based estimation techniques. The accrued symbol decisions are re-modulated and employed as a pilot symbol for channel estimation in the DDCE algorithm.

Further, if the channel experiences fast fading in which the channel delay variation is faster in comparison with OFDM symbol duration, then more error occurs in this kind of hard decision directed channel estimation process. However, some degree of error can be reduced by taking the weighted average of channel estimation between successive symbols.

In [98], authors implemented DDCE techniques from a transform domain perspective. A simplified operational review can be given in Fig. 2.10, where subcarrier related channel transfer function (CTF), $\mathbf{H}[t, n]$ is obtained from received signal and previous demodulated signal. In order to get CTF, subcarrier related channel impulse response (CIR), $b_\ell(n)$ is obtained in the CIR estimator. Prediction is used to get updated channel matrix. However, while using this scheme for channel estimation in the sensing block, prediction is not required, as we are mainly interested in reconstructed channel matrix obtained from estimated symbol in DDCE process.

$$\mathbf{H}[t, n] = \mathbf{H}(tT_s, n\Delta f) = \delta(n\Delta f) \sum_{\ell=1}^{L} b_\ell(n) \mathbf{W}_N^{(n\tau_\ell/T)}, \tag{2.5}$$

where $b_\ell(n)$ is the frequency-variant CIR of the l^{th} path and τ_ℓ is the corresponding path delay, T_s is the total OFDM symbol duration, T is the base band signal sample duration, Δf is the sub-channel spacing, while $\delta(n\Delta f)$ usually corresponds to the pulse shaping filter. $\mathbf{W}$ is the information matrix. $\mathbf{W}$, for example, maybe consists of the eigenvectors from the covariance matrix of the channel.

CIR and information matrix is recursively transformed to frequency domain CTF and hence also updated channel matrix and in this process, in practice, due to the oversampling via subcarriers, channel coefficients are correlated in the frequency domain. If we can utilize this correlation of CIR in subcarriers, channel estimation accuracy is increased. We can exploit the subcarrier correlation in frequency, time and spatial domain to increase the channel estimation.

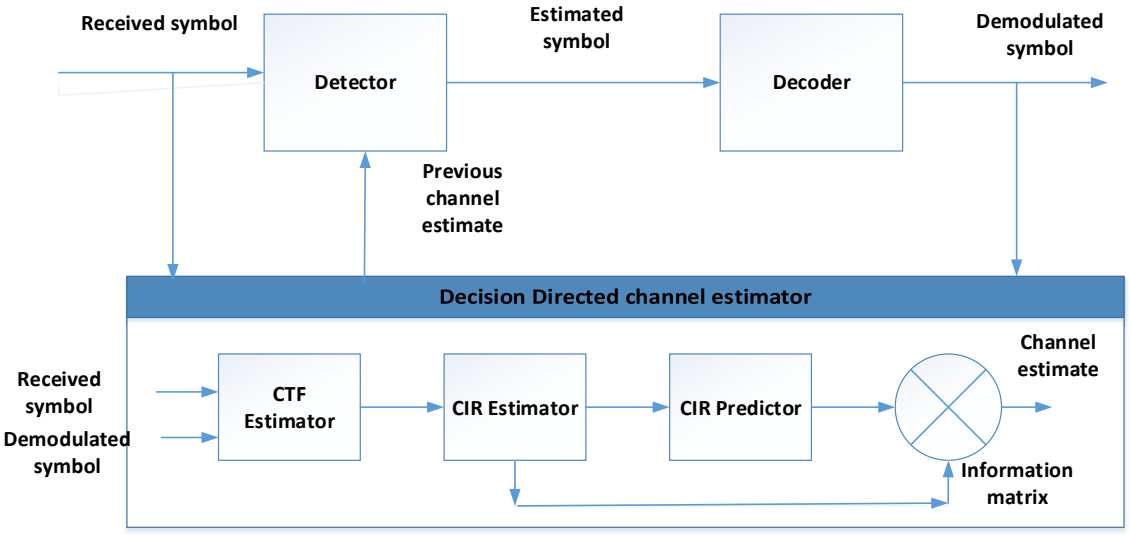

Figure 2.10: Block diagram of the detailed operational procedure for DDCE

2.8 Array Signal Processing and Sensing Parameter Estimation

Multiple antennas interconnected in space can form an antenna array architecture and generate a directional radiation pattern. Number of signal sources, their direction of arrival at the receiver and signal waveform are the point of consideration in the case of problem solving in array signal processing [100]. Different types of

implementation of radar algorithm for OFDM type signals for sensing in a mobile network can be found in [25].

According to [100], the technology related with multiple antennas is referred to as space-time processing (STP). Users are continuously moving and multipath effect creates an even more critical problem in STP. Moreover, due to the propagation range there is always a loss associated with it. Multiple antennas capture more energy and can be useful to increase signal to noise power ratio (SNR) by combining those signals. Fading and interference can be reduced by introducing multiple spatial antennas.

Antenna array signal processing deals with different spatial and temporal estimation task. Linear array is the most suitable and fundamental form of array where the centres of the antenna elements are aligned in a straight line. There can be other forms of arrays, namely, planar and conformal array. Recently, AoA estimation is playing a key role in modelling and architectural designing of multipath radio channel for mobile communication [101]. 2-D AoA estimation is a challenging task while maintaining less complexity and more accuracy. Location and number of signal generating source determination is the key concern in AoA estimation and detection techniques. Parallel implementation of AoA is an efficient way in array signal processing [102]. AoA estimation method can be divided into four categories, namely, conventional method based on beamforming, sub-space method which uses Eigenvalue of input matrix, maximum likelihood method based on optimal techniques, and integrated techniques where property restoral techniques are combined with sub-space techniques [101], [103].

Most recently, CS based AoA estimation is receiving much attention due to its robustness and accuracy in location determination [104]. Several other articles can be found in literature, for example, [105], [106], [107], which provide a theoretical review on CS techniques. In depth overview and applicability of CS can also be extracted from the research work in [108]. Application of off-grid CS in channel parameter estimation can be found in [109], [110]. Research articles, such as [104], [111]

demonstrate the validation of the sensing method, such as usage of CS techniques for channel parameters estimation like AoA, delay and Doppler shift in a multipath environment in resolving moving and static objects.

Generally, classical 2D FFT Method is simple and less complex but this provides low resolution and requires a full set of measurements in time or frequency domain. Again, in ESPRIT, reasonable resolution requires at least a large segment of consecutive samples and this is not always available in uplink sensing. On the other hand, off-grid type compressive methods do not require consecutive samples but implementation for real time operation imposes high complexity. In the case of using on-grid CS methods, the number of available observations in the selected dimension plays an important role for accuracy and resolution. Further details on the selection of CS algorithms for our problem in the perceptive mobile network are discussed in Section 3.1.5.

In this thesis, we demonstrate the feasibility by presenting two schemes, direct sensing that uses block CS and can directly work on the received signals, and indirect sensing that uses signal stripping to separate signals from different users and remove their data symbols. Both schemes are shown to work for MU-MIMO OFDMA signals, which are typical in modern mobile networks.

Chapter 3

Direct Sensing

This chapter presents the feasibility of estimating sensing parameters directly using the received signal via developing a CS based scheme and provide simulation results to validate its effectiveness. This chapter will also give an alternative low-cost and flexible solution of using an analog antenna array for radio sensing at the base station receiver in the proposed perceptive mobile networks.

3.1 Direct Sensing in Perceptive Mobile Networks

In this section, we formulate the signal models used for estimating sensing parameters. We first introduce general system and channel models, and extend them to downlink and uplink sensing, and then provide a generalized on-grid model by quantizing the delay. We show that downlink and uplink can be represented by a common model, which enables common sensing algorithms. We also provide detailed justification for the choice of this on-grid model and the corresponding CS techniques in Section 3.1.5. We then present a direct sensing scheme for sensing parameter estimation in Section 3.1.6 based on the formulated models here.

Notations: $(\cdot)^H$, $(\cdot)^T$ and $(\cdot)^c$ denote the Hermitian transpose, transpose and conjugate of a matrix/vector, respectively. $|\cdots|$ denotes the element-wise absolute value, $(\mathbf{A})_{n,m}$ denotes the (n,m)-th element of the matrix $\mathbf{A}$, $(\mathbf{A})_{\cdot,m}$ and $(\mathbf{A})_{m,\cdot}$denotes the m-th column and row of $\mathbf{A}$, respectively, $\{a_n\}$ denotes a vector

with elements a_n, diag$\{a_n\}$ denotes a diagonal matrix with diagonal elements a_n.

3.1.1 General System and Channel Models

We consider a CRAN system with Q RRUs and each RRU has a uniform linear array (ULA) with M antenna elements and antenna interval of half a wavelength. These RRUs cooperate and provide links to K users through MU-MIMO and OFDMA technologies, i.e., each user may occupy and share only part of the total subcarriers with other users through MU-MIMO. Each user has a ULA of M_T elements. For both uplink and downlink, we assume that data symbols are first spatially precoded, and an IFFT is then applied to each spatial stream. The time domain signals are then assigned to the corresponding RRUs. Let N denote the number of total subcarriers and B the total bandwidth. Then the subcarrier interval is $f_0 = B/N$ and OFDM symbol period is $T_s = N/B + T_p$ where T_p is the period of cyclic prefix.

Assume a planar wave-front in signal propagation. The array response vector of a size-M ULA is given by

$$\mathbf{a}(M, \theta) = [1, e^{j\pi \sin(\theta)}, \cdots, e^{j\pi(M-1)\sin(\theta)}]^H, \tag{3.1}$$

where θ is either AoD or AoA.

Let the AoD and AoA of a multipath be θ_ℓ and ϕ_ℓ, $\ell \in [1, L]$, respectively. For M_1 transmitting and M_2 receiving antennas, the $M_2 \times M_1$ time-domain baseband channel impulse response matrix at time t' can be represented as

$$\tilde{\mathbf{H}}(t') = \sum_{\ell=1}^{L} b_\ell \delta(t' - \tau_\ell) e^{j2\pi f_{D,\ell} t'} \mathbf{a}(M_2, \phi_\ell) \mathbf{a}^T(M_1, \theta_\ell), \tag{3.2}$$

where for the ℓ-th multipath, the sensing parameter b_ℓ is its amplitude of complex value accounting for both signal attenuation and initial phase difference, τ_ℓ is the propagation delay, and $f_{D,\ell}$ is the associated Doppler frequency, and $\otimes$ denotes the Kronecker product. Strictly speaking, the amplitude b_ℓ is frequency dependent. For typical cellular systems where the fractional bandwidth (signal bandwidth nor-

malized to carrier frequency) is small, the variation of b_ℓ across the whole bandwidth is small and hence we assume it is frequency independent here. For sensing, $\{\tau_\ell, f_{D,\ell}, \phi_\ell, \theta_\ell, b_\ell\}$ are the *sensing parameters* to be estimated from (3.2). We define a *channel static period* when all these parameters remain almost constant, which is typically a few milliseconds (equivalent to the length of hundreds of OFDM symbols).

Equation (3.2) represents the channel impulse response that can be used for both communication and sensing. Note that for communications, we generally only need to know the composited values of the matrix $\tilde{\mathbf{H}}$, which are typically obtained by directly estimating some elements in the channel matrix and obtaining the rest via interpolation. For radio sensing, however, the system needs to resolve the detailed channel structure and estimate the sensing parameters. For extended sensing primarily based on machine learning techniques [112], these parameters may not be explicitly needed, which is beyond the scope of this research.

The received signal is converted to frequency domain for processing. For the t-th OFDM block, the frequency-domain channel matrix at the n-th subcarrier corresponding to (3.2) is given by

$$\mathbf{H}_n = \sum_{\ell=1}^{L} b_\ell e^{-j2\pi n \tau_\ell f_0} e^{j2\pi t f_{D,\ell} T_s} \mathbf{a}(M_2, \phi_\ell)\mathbf{a}^T(M_1, \theta_\ell), \tag{3.3}$$

where we have approximated the Doppler phase changes over the samples in one OFDM block as a single value. We will work on several slightly varied versions of (3.3), but still denote them as $\mathbf{H}_n$ to show their connections.

3.1.2 Formulation for Downlink Sensing

As mentioned in Section 2.5.2, sensing is done for the channel environment between each transmitter and receiver, through the echoes specific to the environment. Hence for both downlink and uplink sensing, we separately formulate and use the signals received at each RRU. It is possible to jointly process the signals for sensing, but

the benefits are not obvious unless the channels are highly correlated. This could be a significant difference between communication and sensing.

For downlink sensing, each RRU sees reflected downlink signals from itself and the other $Q-1$ RRUs. Its received signal at the n-th subcarrier and the t-th OFDM block can be represented as

$$\begin{aligned}\mathbf{y}_{n,t} =& \sum_{q=1}^{Q}\sum_{\ell=1}^{L_q} b_{q,\ell} e^{-j2\pi n\tau_{q,\ell}f_0} e^{j2\pi t f_{D,q,\ell}T_s}\cdot \\ & \mathbf{a}(M,\phi_{q,\ell})\mathbf{a}^T(M,\theta_{q,\ell})\mathbf{x}_{q,n,t} + \mathbf{z}_{n,t}, \qquad (3.4)\\ =& \underbrace{\mathbf{A}(M,\boldsymbol{\phi})\mathbf{C}_n\mathbf{D}_t\mathbf{U}^T}_{\mathbf{H}_n}\mathbf{x}_{n,t} + \mathbf{z}_{n,t}, \qquad (3.5)\end{aligned}$$

where variables with subscript q are for the q-th RRU, $\mathbf{x}_{q,n,t}$ are the transmitted signals at subcarrier n from the q-th RRU,

$$\mathbf{A}(M,\boldsymbol{\phi}) = (\mathbf{A}_1(M,\boldsymbol{\phi}_1),\cdots,\mathbf{A}_Q(M,\boldsymbol{\phi}_Q)), \qquad (3.6)$$

$$\mathbf{x}_{n,t} = (\mathbf{x}_{1,n,t},\cdots,\mathbf{x}_{Q,n,t})^T, \qquad (3.7)$$

$$\mathbf{U} = \mathrm{diag}\{\mathbf{A}_1(M,\boldsymbol{\theta}_1),\mathbf{A}_2(M,\boldsymbol{\theta}_2),\cdots,\mathbf{A}_Q(M,\boldsymbol{\theta}_Q)\}, \qquad (3.8)$$

and hence $\mathbf{U}$ is a $MQ\times L$ block diagonal matrix. The ℓ-th column in $\mathbf{A}_q(M,\boldsymbol{\phi}_q)$ (or $\mathbf{A}_q(M,\boldsymbol{\theta}_q)$) is $\mathbf{a}(M,\phi_{q,\ell})$ (or $\mathbf{a}(M,\theta_{q,\ell})$), $\mathbf{D}_t$ and $\mathbf{C}_n$ are diagonal matrices with the ℓ-th diagonal element being $b_\ell e^{j2\pi t f_{D,\ell}T_s}$ and $e^{-j2\pi n\tau_\ell f_0}$, respectively, $\mathbf{z}_{n,t}$ is the noise vector. The model in (3.4) has a similar channel structure representation with the basic one in (3.2), but specifies multipath signals to different RRUs.

According to (3.5), we can see that packing $\mathbf{y}_{n,t}$ from multiple RRUs can increase its length, but the unknown parameters are similarly increased. Hence sensing does not directly benefit from jointly processing. However, due to channel reciprocity, parameters for signal propagation between RRUs could be similar. Such a property can be exploited for joint processing across RRUs.

3.1.3 Formulation for Uplink Sensing

The received signal in a RRU at the n-th subcarrier and the t-th OFDM block can be represented as

$$\mathbf{y}_{n,t} = \sum_{k=1}^{K}\sum_{\ell=1}^{L_k} b_{k,\ell} e^{-j2\pi n\tau_{k,\ell} f_0} e^{j2\pi t f_{D,k,\ell} T_s} \cdot \mathbf{a}(M,\phi_{k,\ell})\mathbf{a}^T(M_T,\theta_{k,\ell})\mathbf{x}_{k,n,t} + \mathbf{z}_{n,t}, \tag{3.9}$$

Comparing (3.9) with (3.4), we can see that they have similar expressions except for different symbols and parameter values. Hence, next we will develop a common on-grid expression for both downlink and uplink sensing.

3.1.4 Generalized Delay-Quantized On-grid Formulation

Let N_u and S be the number and index set of available subcarriers for sensing, respectively. For downlink sensing, $N_u = N$. We assume that $N \gg L$ and N is large enough such that the quantization error of τ_ℓ is small and the delay estimation can be well approximated as an on-grid estimation problem. Let the delay term $e^{-j2\pi n\tau_\ell f_0}$ be quantized to $e^{-j2\pi n\ell/(gN)}$, where g is a small integer and its value depends on the method used for estimating τ_ℓ. The minimal delay quantization is then $1/(gB)$.

Let K, M and M_T denote the total number of users/RRUs, the number of antennas for sensing, and the number of antennas in each user/RRU for transmitting, respectively, for either uplink or downlink sensing. We now convert the multipath signal models in (3.9) and (3.5) to a generalized on-grid (delay only) sparse model, by representing it using $N_p \gg L, N_p \leq gN$ multipath signals where only L signals are non-zeros. Referring to (3.5) and (3.9), the generic delay-on-grid model, applicable to further processing for either downlink sensing or uplink sensing can be represented

as,

$$\mathbf{y}_{n,t} = \underbrace{\mathbf{A}(M, \boldsymbol{\phi})\mathbf{C}_n\mathbf{D}_t\mathbf{P}\mathbf{U}^T}_{\mathbf{H}_n}\mathbf{x}_{n,t} + \mathbf{z}_{n,t}. \tag{3.10}$$

Note that to show the connection, we used similar symbols here with some of those in (3.5); however, the definitions are slightly different. Here, at this moment, $\mathbf{C}_n$ is redefined as $\mathbf{C}_n = \text{diag}\{e^{-j2\pi n/(gN)}, \cdots, e^{-j2\pi n N_p/(gN)}\}$, re-ordered according to the quantized delay values; $\mathbf{P}$ is a $N_p \times L$ rectangular permutation matrix that maps the signals from a user/RRU to its multipath signal, and has only one non-zero element of value 1 in each column; the other symbols have similar expressions with those in (3.5), with elements in $\mathbf{A}(M, \boldsymbol{\phi})$ and $\mathbf{D}_t$ being reordered according to the delay. More specifically, the columns in $\mathbf{A}(M, \boldsymbol{\phi})$ of size $M \times N_p$ and the diagonal elements in $\mathbf{D}_t$ of size $N_p \times N_p$ are now re-ordered and tied to the multipath delay values. $\mathbf{U}$ is an $M_T K \times L$ block diagonal radiation pattern matrix for M_T arrays. $\mathbf{x}_{n,t}$ is the $M_T K \times 1$ symbol vector. For the moment, we allow repeated delay values in $\mathbf{C}_n$ to account for multipath signals with the same quantized delay but different AoAs and/or AoDs.

3.1.5 Selection of Compressive Sensing Algorithms

Recently, there has been significant interest in CS techniques in radar sensing [113], [114], [115], as well as in JCAS systems [1]. The five sensing parameters in (3.3) can be estimated either individually or jointly by forming from 1D to 4D CS models. In this work, we propose to use 1D CS based on the on-grid formulation in (3.10), as will be detailed in Section 3.1.6 and 4.1, mainly for the following three reasons:

- Although high-dimensional on-grid CS algorithms such as the Tensor tool and Kronecker CS [116] could offer better performance when there are sufficient measurements in each dimension, they could face large quantization errors in the domains of Doppler frequency, AoD and AoA for our problem here, due to the limited number of measurements associated with short channel coherent

time and the small number of antennas. Comparatively, the cellular signals generally have hundreds to thousands of subcarriers, which provide numerous measurements for the delay. Therefore, quantizing delay only can potentially lead to smaller errors.

- Off-grid CS algorithms are yet to be extended to high-dimensional problems, and multi-measurement vector (MMV) and block-CS models. There exist some CS techniques dealing with off-grid models, such as the perturbation approach [117] and atomic norms [110]. However, they have high complexity and also have respective constraints on the parameter estimation range and the minimum separation of the parameter values.

- Our 1D methodology provides a solid basis for future extension. Generally, higher-dimensional CS algorithms can achieve better estimation performance, but they also involve much higher computational complexity. Our 1D methodology provides a path for many potential extensions, for example, replacing the 1D on-grid model with a 1D off-grid model, should off-grid algorithms be extended to the MMV models.

3.1.6 Direct Estimation of Sensing Parameters

We now propose a scheme based on 1D CS for estimating the spatial parameters directly using the signal $\mathbf{y}_{n,t}$ in (3.10). This scheme works for all the three sensing methods. We assume that the symbols $\mathbf{x}_{n,t}$ are known and $N \gg L$. For uplink sensing, this can be achieved by demodulating the symbols as sensing can tolerate more delay than communication, while for downlink sensing, they are centrally known. Note that, the range and indices of subcarriers in downlink and uplink sensing could be different. RRUs can see signals at more subcarriers in downlink sensing than uplink because in the uplink the total subcarriers could be shared by a different group of users and channels are specific to each user.

We first organize the received signal to a form such that from it 1D CS algorithms can be applied to get the estimates for the delay. From the associated amplitude estimates corresponding to the delay estimates, we then retrieve other sensing parameters.

Rewrite (3.10) as

$$\mathbf{y}_{n,t}^T = \mathbf{x}_{n,t}^T(\mathbf{c}_n^T \otimes \mathbf{I}_{M_T K})\mathbf{V}\mathbf{A}^T(M, \boldsymbol{\phi}). \tag{3.11}$$

where $\mathbf{c}_n = (e^{-j2\pi n/(gN)}, \cdots, e^{-j2\pi n N_p/(gN)})^T$, $\mathbf{I}_{M_T K}$ is an $M_T K \times M_T K$ identity matrix, and $\mathbf{V}$ is a $M_T K N_p \times N_p$ block diagonal matrix

$$\mathbf{V} = \text{diag}\{b_\ell e^{-j2\pi t f_{D,\ell} T_s}\mathbf{U}\mathbf{p}_\ell\}_{\ell=1,\cdots,N_p}, \tag{3.12}$$

with $\mathbf{p}_\ell$ being the ℓ-th column of $\mathbf{P}^T$.

We have now separated signals $\mathbf{x}_{n,t}^T(\mathbf{c}_n^T \otimes \mathbf{I}_{M_T K})$ that are known and dependent on n from other parameters. Then we can stack all row vectors $\mathbf{y}_{n,t}^T, n \in \mathsf{S}$ to a matrix[1], and obtain

$$\mathbf{Y}_t \triangleq (\mathbf{y}_{1,t}, \cdots, \mathbf{y}_{n,t}, \cdots)^T = \mathbf{W}\mathbf{V}\mathbf{A}^T(M, \boldsymbol{\phi}), \tag{3.13}$$

where $\mathbf{W}$ is a $N_u \times M_T K N_p$ matrix with its n-th row being $\mathbf{x}_{n,t}^T(\mathbf{c}_n^T \otimes \mathbf{I}_{M_T K})$.

Inspecting (3.13), we can see that the estimation problem in (3.13) can be treated as a MMV block sparse problem [118] with $N_u \times M$ observations $\mathbf{Y}_t$, sensing matrix $\mathbf{W}$, and block sparse signals $\mathbf{V}\mathbf{A}^T(M, \boldsymbol{\phi})$ of L-sparsity. Let $\mathbf{V} = (\mathbf{V}_1^T, \mathbf{V}_2^T, \cdots, \mathbf{V}_{N_p}^T)^T$ where $\mathbf{V}_\ell$ denotes the $M_T K \times N_p$ block signals, and L out of N_p $\mathbf{V}_\ell$s have non-zero elements. The non-zero rows and their values in $\mathbf{V}\mathbf{A}^T(M, \boldsymbol{\phi})$ can then be solved by various MMV CS algorithms, such as the fast marginalized block sparse Bayesian learning algorithm (BSBL-FM) in [118, 119] that is adopted in this work. After

[1]In uplink sensing, there may be less than N vectors available and they may be dis-continuous in index.

applying BSBL-FM in (3.13), it generate estimates for $\mathbf{V}_\ell \mathbf{A}^T(M, \boldsymbol{\phi}), \ell = 1, \cdots, N_p$. The indices of the non-zero blocks of estimated $\mathbf{V}\mathbf{A}^T(M, \boldsymbol{\phi})$ are used to extract the quantized delay values from the corresponding element of sensing matrix $\mathbf{W}$. The estimated $\mathbf{V}\mathbf{A}^T(M, \boldsymbol{\phi})$ amplitude values can be further used to estimate other sensing parameters.

The detailed estimation process based on $\mathbf{V}\mathbf{A}^T(M, \boldsymbol{\phi})$ is described for two cases next. We first consider a simple case when there is only one multipath at each delay value. In this case, a simple estimation algorithm is available for estimating all sensing parameters. We then extend the solution to the case when there are multiple multipath signals at each quantized delay bin. We will show that when these multipath signals are from different RRUs, the parameters can be similarly estimated to those in the single multipath case. Otherwise, more complex techniques need to be applied. The method for separating the two cases is yet to be developed.

Single Multipath for Each Delay

We first consider the noiseless case. Once the L nonzero blocks $\mathbf{V}_\ell \mathbf{A}^T(M, \boldsymbol{\phi})$ are obtained by BSBL-FM, we can then get the L delay estimates according to the indices of the nonzero blocks, from the corresponding element of $\mathbf{W}$.

From (3.12) we can see that only the ℓ-th column in $\mathbf{V}_\ell$ has non-zero elements $b_\ell e^{-j2\pi t f_{D,\ell} T_s} \mathbf{U}\mathbf{p}_\ell$ if $b_\ell \neq 0$. Therefore,

$$\mathbf{V}_\ell \mathbf{A}^T(M, \boldsymbol{\phi}) = b_\ell e^{-j2\pi t f_{D,\ell} T_s} \mathbf{U}\mathbf{p}_\ell \mathbf{a}^T(M, \phi_\ell). \tag{3.14}$$

Since $\mathbf{p}_\ell$ only has a single non-zero element 1, $\mathbf{U}\mathbf{p}_\ell$ will generate a column vector corresponding to one column in $\mathbf{U}$. Because $\mathbf{U}$ is a block diagonal matrix, only 1 out of K $M_T \times 1$ vectors in each column is non-zero.

Now represent $\mathbf{V}_\ell \mathbf{A}^T(M, \boldsymbol{\phi})$ as K $M_T \times M$ sub-matrices $(\mathbf{B}_{\ell,1}^T, \cdots, \mathbf{B}_{\ell,K}^T)^T$. If $\mathbf{B}_{\ell,k} \neq 0$, then this multipath is from the k-th RRU (user). We can also see that

$$\mathbf{B}_{\ell,k} = b_\ell e^{-j2\pi t f_{D,\ell} T_s} \mathbf{a}(M_T, \theta_{k,\ell}) \mathbf{a}^T(M, \phi_{k,\ell}). \tag{3.15}$$

From $\mathbf{B}_{\ell,k}$, calculating the cross-correlation between columns and rows, we can obtain AoA or AoD estimates, depending on the order of calculation. Let $(\mathbf{B}_{\ell,k})_{\cdot,p}$ and $(\mathbf{B}_{\ell,k})_{\cdot,q}$ denote the p-th column and q-th row of $(\mathbf{B}_{\ell,k})$, respectively. We then have

$$\sin(\phi_{k,\ell}) \approx \frac{1}{\pi}\angle\left(\sum_{p=1}^{M-1}((\mathbf{B}_{\ell,k})_{\cdot,p})^*(\mathbf{B}_{\ell,k})_{\cdot,p+1}\right),$$
$$\sin(\theta_{k,\ell}) \approx \frac{1}{\pi}\angle\left(\sum_{q=1}^{M_T-1}((\mathbf{B}_{\ell,k})_{q,\cdot})^*(\mathbf{B}_{\ell,k})_{q+1,\cdot}\right). \tag{3.16}$$

The Doppler frequency $f_{D,\ell}$ can be estimated across multiple OFDM blocks, based on the cross-correlation of $\mathbf{B}_{\ell,k}$ in these blocks: Let $\mathbf{B}_{\ell,k,t}$ denote the $\mathbf{B}_{\ell,k}$ obtained from the t-th OFDM block signal $\mathbf{Y}_t$, and T_d be the total OFDM blocks used for estimating the Doppler frequency, then we get

$$f_{D,\ell} \approx \frac{1}{2\pi T_s}\angle\left(\sum_{t=1}^{N_d-1}(\mathbf{B}_{\ell,k,t})(\mathbf{B}_{\ell,k,t+1})^*\right). \tag{3.17}$$

The absolute value of b_ℓ can be estimated as the mean power of all elements in $\mathbf{B}_{\ell,k}$. A better estimate is to use the cross-correlation output from estimating AoA. That is

$$|b_\ell|^2 \approx \left|\sum_{p=1}^{M-1}((\mathbf{B}_{\ell,k})_{\cdot,p})^*(\mathbf{B}_{\ell,k})_{\cdot,p+1}\right|. \tag{3.18}$$

In noisy cases, we can sort the blocks $\mathbf{V}_\ell\mathbf{A}^T(M,\boldsymbol{\phi}), \ell = 1,\cdots,N_p$ according to the estimates of $|b_\ell|$ and use a threshold to filter out blocks corresponding to multipath signals. This threshold can be set with reference to the expected received energy for that delay value, using the path loss model. We can also keep the estimated results for a subset of N_p with larger estimated b_ℓs, and then apply data fusion techniques over all measurements over a segment of space, time and frequency domains to get synthesized sensing results.

Multiple Multipath Signals with the Same Delay

We consider the case where there are two multipath signals with the same delay. The analysis below can be easily extended to more general scenarios. Let $\mathbf{c}_n = (\mathbf{c}_{n,1}^T, \mathbf{c}_{n,2}^T, \mathbf{c}_{n,2}^T)^T$, where $\mathbf{c}_{n,2}$ represents the repeated entries. We can accordingly represent $\mathbf{W} = (\mathbf{W}_1, \mathbf{W}_2, \mathbf{W}_2)$ and $\mathbf{V} = (\mathbf{V}_1^T, \mathbf{V}_2^T, \mathbf{V}_3^T)^T$ in (3.13). Then we have

$$\mathbf{WVA}^T(M, \boldsymbol{\phi}) = (\mathbf{W}_1, \mathbf{W}_2) \begin{pmatrix} \mathbf{V}_1 \mathbf{A}^T(M, \boldsymbol{\phi}) \\ (\mathbf{V}_2 + \mathbf{V}_3)\mathbf{A}^T(M, \boldsymbol{\phi}) \end{pmatrix}. \tag{3.19}$$

This shows that we can always use a $\mathbf{c}_n$ with single entry for each quantized delay, and multiple signals with different angles will show up in the MMV [120] estimates. More specifically, if $\ell \in \mathscr{S}$ multipath signals have the same delays but different AoAs or AoDs, we will then get

$$\mathbf{V}_\ell \mathbf{A}^T(M, \boldsymbol{\phi}) = \sum_{\ell \in \mathscr{S}} b_\ell e^{-j2\pi t f_{D,\ell} T_s} \mathbf{U} \mathbf{p}_\ell \mathbf{a}^T(M, \phi_\ell). \tag{3.20}$$

If these multipath signals are from different RRUs (users), multiple $\mathbf{B}_{\ell,k}$s will be non-zero. Hence in this case, sensing parameters for these multipath signals can be estimated using the algorithms similar to those for the single multipath case in Section 3.1.6.

If multipaths are from the same RRU (user), we will have

$$\hat{\mathbf{B}}_{\ell,k} = \sum_{\ell \in \mathscr{S}} b_\ell e^{-j2\pi t f_{D,\ell} T_s} \mathbf{a}(M_T, \theta_{k,\ell}) \mathbf{a}^T(M, \phi_{k,\ell}). \tag{3.21}$$

Obtaining solution from (3.21) is a complicated estimation problem. When the number of multipaths in which the specific delay value is small, which is a typical scenario, the AoAs and AoDs can be estimated by applying 2D spectrum analysis techniques to each $\hat{\mathbf{B}}_{\ell,k}$, such as by 2D-ESPRIT or 2D-MUSIC algorithms. Across multiple OFDM blocks, 3D spectrum analysis techniques could be applied to additionally get the estimate for Doppler shift too.

3.1.7 Simulation Results for Direct Sensing

We present simulation results here to validate the effectiveness of the proposed framework and parameter estimation schemes. For solving the MMV problems, we use the BSBL [118] in direct estimation and Sparse Bayesian Learning (SBL) [121] in indirect estimation.

We consider a system with 4 RRUs, providing connections to 4 users through multiuser MIMO. Each RRU has 4 antennas and each MS has 1 antenna. The carrier frequency is 2.35 GHz and the signal bandwidth is 100 MHz. Unless stated otherwise, for downlink, all $N = 512$ subcarriers are used, and for uplink, 128 subcarriers with random indices are shared by four users using MU-MIMO. We assume radar cross-section factor (RCS) is equal to 1 in the simulation and used the same value throughout the thesis. That means the presented sensing results indicate targets with cross sectional area of 1 m^2.

The multipath channels are randomly generated in cluster following a complex Gaussian distribution. We use a pathloss model with pathloss factor 4 for downlink and 2 for uplink sensing. The transmission power of the RRU and MS is 30 dBm [122] and 25 dBm [123] respectively. Throughout this work, we assume that the noise is AWGN with thermal noise power $N_0 = -174$ dBm/Hz [124]. Hence the total thermal noise in the receiver is $-174 + 10\log(10^8) = -94$ dBm and this will be used throughout the thesis.

Multipath signals for each RRU/MS are generated randomly in cluster, mimicking reflected/scattered signals from objects. Multipaths in each cluster are generated following uniform distributions of $[10, 15]$ for the total multipath number, $[0, 45]$ degrees for direction span, $[0, 45]$ m for distance, and $[0, 600]$ Hz for Doppler frequency. Across clusters there are additional offsets in direction ($[-75, 75]$ degrees), distance ($[50, 180]$ m) and moving speed ($[-40, 40]$ m/s), reflecting the different locations of the transmitter to the sensing receiver. Unless stated otherwise, delays are on grid with an interval of 10 ns, corresponding to a distance quantization of 3 m. Delays from the same RRU/MS are kept different. However, they could be the same be-

tween RRUs/MSs. Random continuous values are used for Doppler shift, AoAs and AoDs.

Note that in the simulation, the variance of the AWGN noise is determined from the product of the basic thermal noise power spectral density and the bandwidth. We can expect that downlink sensing can support a sensing range of more than 150 meters at a ground level and more towards the air, and uplink sensing can support about 50 meters, given that the transmission power of a base station and mobile phone is 30 dBm [122] and 25 dBm [123] respectively. This estimation is based on past work on, e.g., practical experimental results of passive radar using signals from LTE mobile base stations [47] and the simulation results that use practical system parameters as presented in [17] and in this thesis. While the transmission power is fixed, the multipath signals reflected from objects at different distances to the transceiver will lead to different SNRs for estimating the sensing parameters. From the pathloss factors and the multipath propagation distances, we can see that the received SNR for estimating the sensing parameters for a particular multipath could be as low as 0 dBm for the downlink sensing, while it is much higher ($\geq$ 30 dB) for uplink sensing. For the mentioned simulated sensing range, the SNR value is that much due to the pathloss factor 4 and 2 for downlink and uplink sensing respectively.

Based on these parameters, we can work out an approximate (minimum) channel stable period in which sensing parameters remain unchanged. For example, assume this period lasts when vehicles/objects move less than 5 cm, and the maximum relative moving speed is 30 m/s. This period is then $0.05/30 = 0.0017$ s, equivalent to the period of $(0.0017/(512/10^8 \times 1.25) \approx 265$ OFDM blocks.

In all the figures below, unless stated otherwise, every plus or circle represents parameters for one multipath: Pluses and circles are for estimated and actual ones, respectively. Different colors represent multipath from different RRUs/MSs. In each figure, 10 implementations are plotted. The sensing parameters are fixed in all 10 implementations, but the data symbols and noise are changed. The AoA estimates

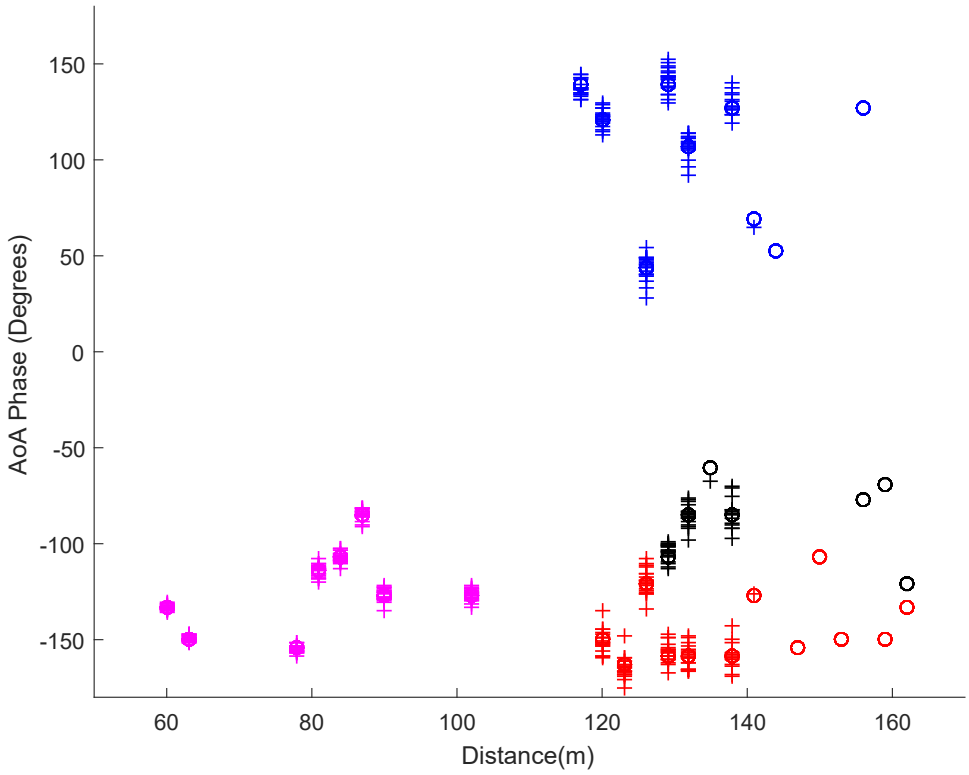

Figure 3.1: 10 implementation results for AoA-Distance estimation in direct downlink sensing.

are shown in the form of AoA phase, $\pi \sin(\phi_\ell)$, in either degrees or radian.

Figs. 3.1 and 3.2 present typical AoA-Distance results for downlink and uplink sensing respectively. Note that the depicted distance is the total signal travelling distance between a transmitter and the receiver, and does not necessarily translate to the distance of objects to the receiver directly. Complex across-RRU synthesizing is needed to achieve the translation, particularly for uplink sensing. Both figures demonstrate that the estimates are quite robust and accurate, when the received SNR is sufficiently high. Note that there are no matching estimates for some multipath at distances larger than approximately 145 meters due to the low SNR here. This is particularly obvious in the downlink sensing case where the adopted pathloss factor is 4, compared to 2 in the uplink.

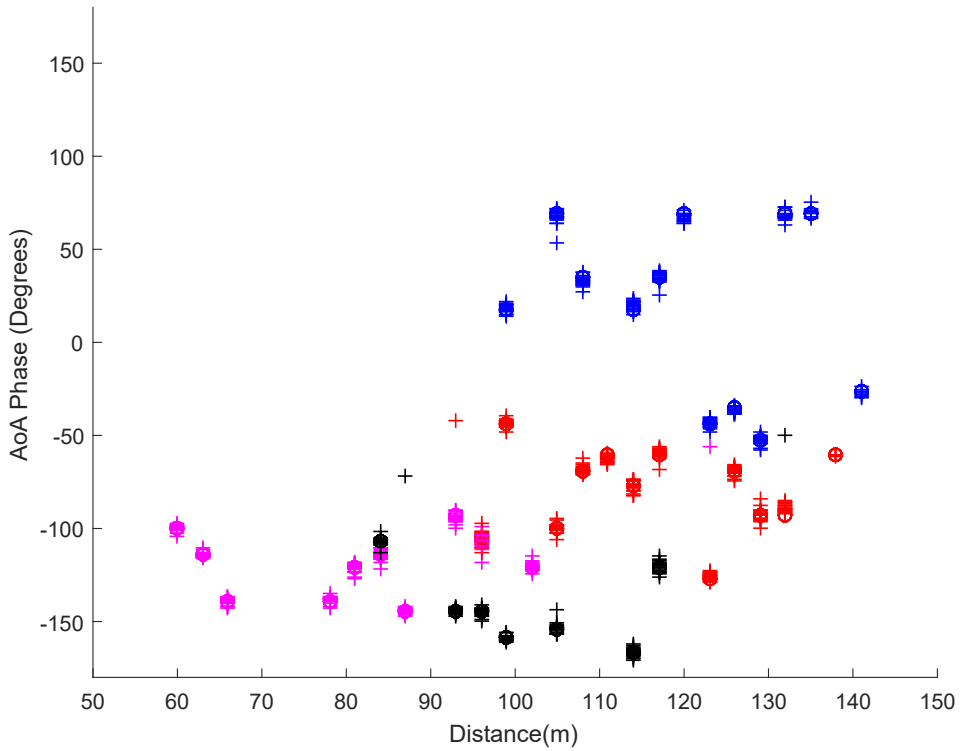

Figure 3.2: 10 implementation results for AoA-Distance estimation for direct uplink sensing.

3.1.8 Summary

We have developed a direct sensing framework for a perceptive mobile network where three types of sensing methods can be integrated with communication. A BSBL scheme is developed for estimating sensing parameters, and its effectiveness is validated by simulation results.

3.2 Analog Antenna based Radio Sensing

In this section, we consider an analog antenna array at the BS receiver as an alternative low-cost solution for radio sensing in the perceptive mobile networks. We provide receiver beamforming design, and advanced CS signal processing techniques for sensing parameter estimation in a MU-MIMO communications system. Simulation results are provided and validate the effectiveness of the proposed solution and sensing algorithms.

3.2.1 Problem Statement

The recently proposed perceptive mobile network [1] can provide integrated communication and radio sensing in one system. On a unified sensing platform, extraction of sensing parameters using both uplink and downlink signals is proposed. In order to achieve sensing using downlink signals, the transmitter and receiver at a RRU need to be able to operate simultaneously. A simple solution is to use separated antennas for transmitter and receiver. However, to obtain good estimation for sensing parameters, particularly, angle of arrivals of signals, a large number of receiving antennas, including extra antenna installation space, and RF chains are also required. In turn, these can significantly increase the cost of the receiver, although the transmitter can remain almost unchanged.

Here, we investigate the low-cost option of using an analog phased antenna array dedicated to the receiver for sensing and communications, and develop sensing parameter estimation algorithms, based on the same MU-MIMO model in [1].

We propose 1-D CS algorithm for parameter estimation in Section 3.2.4. Numerical results are provided and verify the effectiveness of the proposed scheme.

3.2.2 Problem Formulation

We here focus on estimating spatial parameters including distance, direction, and speed of objects by extracting the composition of mobile signals.

We consider a typical radio system, similar to [1], where Q RRUs collaboratively facilitate MU-MIMO service to K users. Each RRU and each user have a linear antenna array of M elements and M_T elements, respectively. We used MIMO-OFDMA type of modulation for both uplink and downlink as designed in Section 3.1.2 and Section 3.1.3, respectively.

The task for sensing is to estimate these spatial parameters $\{\tau_\ell, f_{D,\ell}, \phi_\ell, \theta_\ell, b_\ell\}, \ell = 1, \cdots, L$ from the received signals. We defined downlink and uplink sensing, as sensing performed at a RRU employing downlink transmitted signals from itself and other cooperative RRUs and uplink signals from users, respectively [1], [2].

Whereas they can have a similar mathematical formation [1]. In turn, intuitively, from the downlink perspective, processed received signal model at a RRU at the n-th subcarrier and the t-th OFDM block can be represented as (3.5).

Next we will develop a general on-grid expression for both downlink and uplink sensing. In formulating the sensing problem next, we will ignore system imperfections such as carrier frequency offsets and timing offsets between different RRUs, and between MSs and RRUs.

3.2.3 Generalized Delay-Quantized On-grid Formulation

We assume $N \gg L$ to reduce the quantization error of τ_ℓ and the delay estimation can be well approximated as an on-grid estimation problem. Let $e^{-j2\pi n\tau_{\ell'}f_0}$ be quantized to $e^{-j2\pi n\ell/(N')}$, where N' can equal to or be integer multiples of N; this implies the minimal resolvable delay as $1/N'$.

Let K and M_T denote the total number of users/RRUs and number of antennas in each user/RRU, respectively, for either uplink or downlink sensing. We now convert the multipath signal models of both uplink and downlink to a generalized on-grid (delay only) sparse model, by taking $N_p \gg L, N_p \leq N'$ multipath signals where only L signals are non-zeros. Referring to (3.5), after applying receiver beamforming with $\mathbf{Y}_{n,t}$, the delay-on-grid received signal model can be represented as

$$y_{n,t} = \mathbf{g}_t^T \mathbf{A}(M, \boldsymbol{\phi}) \mathbf{C}_n \mathbf{D}_t \mathbf{P} \mathbf{U}^T \mathbf{x}_{n,t} + \mathbf{z}_{n,t}, \tag{3.22}$$

where $\mathbf{g}_t$ is the $M \times 1$ beamforming vector applied to the t-th OFDM block, $\mathbf{C}_n$ redefined as $\mathbf{C}_n = \text{diag}\{1, e^{-j2\pi n/N'}, \cdots, e^{-j2\pi n(N_p-1)/N'}\}$, $\mathbf{P}$ is an $N_p \times L$ rectangular permutation matrix that maps the signals from a user/RRU to its multipath signal, $\mathbf{U}$ is an $M_T K \times L$ matrix while $\mathbf{x}_{n,t}$ is the $M_T K \times 1$ symbol vector; the other symbols have similar expressions with those in (3.5), with the columns in $\mathbf{A}(M, \boldsymbol{\phi})$ of size $M \times N_p$ and the diagonal elements in $\mathbf{D}_t$ of size $N_p \times N_p$ are reordered as well. Here, we allow repeated delay values in $\mathbf{C}_n$ to account for multipath signals with the same

quantized delay but different AoAs and/or AoDs.

The design of beamforming vectors $\mathbf{g}_t$ depends on factors such as energy collection and AoA estimation algorithms. Without any prior knowledge about the AoA, a simple and efficient way is to take it from equally-spaced columns of an $M \times M$ DFT matrix

$$\mathbf{F} = \{e^{-j2\pi mt'/M}\}, m, t' = 0, \cdots, M-1. \tag{3.23}$$

Assume that channel parameters are fixed during $T = M/c_1$ OFDM blocks where c_1 is an integer. Then at the phased array we repeatedly apply T $M \times 1$ beamforming vectors

$$\mathbf{g}_t = \{e^{-j2\pi m(t_0+\text{mod}(t,T)c_1)/M}\}, m = 0, \cdots, M-1,$$

where t_0 is an initial offset value, and $\text{mod}(\cdot,\cdot)$ is the modulus operator.

3.2.4 Estimation of Spatial Parameters

We now demonstrate a scheme based on 1-D CS for estimating the spatial parameters. For uplink sensing, symbols $\mathbf{x}_n$s can be achieved by demodulating them as sensing can tolerate more delay than communication. On the contrary, for downlink sensing, they are centrally known. Note, the range of subcarriers in downlink and uplink sensing could be different. RRUs can obtain signals at more subcarriers in downlink sensing than uplink, as the total subcarriers may be shared by a different group of users.

Single Multipath for Each Delay: Rewrite (3.22) as

$$y_{n,t}^T = \mathbf{x}_{n,t}^T(\mathbf{c}_n^T \otimes \mathbf{I}_{M_TK})\mathbf{V}_t\mathbf{A}^T(M, \boldsymbol{\phi})\mathbf{g}_t, \tag{3.24}$$

where $\otimes$ denotes the Kronecker product, $\mathbf{c}_n = (1, e^{-j2\pi n/N'}, \cdots, e^{-j2\pi(N_p-1)/N'})^T$, $\mathbf{I}_{M_TK}$ is an $M_TK \times M_TK$ identity matrix, and $\mathbf{V}$ is a $M_TKN_p \times N_p$ block diagonal

matrix with $\mathbf{p}_\ell$ being the ℓ-th column of $\mathbf{P}^T$. Note,

$$\mathbf{V}_t = \text{diag}\{b_\ell e^{j2\pi t f_{D,\ell} T_s} \mathbf{U}\mathbf{p}_\ell\}_{\ell=1,\cdots,N_p}. \tag{3.25}$$

We have now separated signals $\mathbf{x}_{n,t}^T(\mathbf{c}_n^T \otimes \mathbf{I}_{M_T K})$ that are known and dependent on n from others. Let $\mathscr{S}_s$ denote the set of available subcarriers for sensing and let N_s denote its size. Stacking N_s $y_{n,t}^T, n \in \mathscr{S}_s$ to a vector generates

$$\mathbf{y}_t = \mathbf{W}_t \mathbf{V}_t \mathbf{A}^T(M, \boldsymbol{\phi})\mathbf{g}_t, \tag{3.26}$$

where $\mathbf{W}_t$ is an $N_s \times M_T K N_p$ matrix with its n-th row being $\mathbf{x}_{n,t}^T(\mathbf{c}_n^T \otimes \mathbf{I}_{M_T K})$.

Inspecting (3.26), we can see that the estimation problem can be formulated as a block sparse problem [118] with $N_s \times 1$ observations $\mathbf{y}_t$, sensing matrix $\mathbf{W}_t$, and block sparse signals $\mathbf{V}_t\mathbf{A}^T(M, \boldsymbol{\phi})\mathbf{g}_t$ of L-sparsity. Let $\mathbf{V}_t = (\mathbf{V}_1^T, \mathbf{V}_2^T, \cdots, \mathbf{V}_{N_p}^T)^T$ where $\mathbf{V}_\ell$ denotes the $M_T K \times N_p$ block signals, and L out of N_p $\mathbf{V}_\ell$s have non-zero elements. A block sparse CS algorithm can solve (3.26) and generate estimates for $\mathbf{V}_\ell A^T(M, \boldsymbol{\phi})\mathbf{g}_t, \ell = 1, \cdots, N_p$.

We first consider noiseless cases. Once the L nonzero blocks $\mathbf{V}_\ell \mathbf{A}^T(M, \boldsymbol{\phi})\mathbf{g}_t$ are determined, we can then get the L delay estimates according to the indices of the nonzero blocks, from the corresponding element of sensing matrix $\mathbf{W}$.

In (3.25), only the ℓ-th column in $\mathbf{V}_\ell$ has non-zero elements $b_\ell e^{j2\pi t f_{D,\ell} T_s}\mathbf{U}\mathbf{p}_\ell$ if $b_\ell \neq 0$. Therefore,

$$\mathbf{V}_\ell \mathbf{A}^T(M, \boldsymbol{\phi})\mathbf{g}_t = b_\ell e^{j2\pi t f_{D,\ell} T_s}\mathbf{U}\mathbf{p}_\ell \mathbf{a}^T(M, \phi_\ell)\mathbf{g}_t. \tag{3.27}$$

Since $\mathbf{p}_\ell$ only has a single non-zero element 1, $\mathbf{U}\mathbf{p}_\ell$ will generate a column vector corresponding to one column in $\mathbf{U}$. As $\mathbf{U}$ is a block diagonal matrix, only 1 out of K $M_T \times 1$ vectors in each column is non-zero.

Now represent $\mathbf{V}_\ell \mathbf{A}^T(M, \boldsymbol{\phi})\mathbf{g}_t$ as K $M_T \times 1$ sub-vectors $(\mathbf{b}_{\ell,1,t}^T, \cdots, \mathbf{b}_{\ell,K,t}^T)^T$. If

$\mathbf{b}_{\ell,k,t} \neq 0$, then this multipath is from the k-th RRU (user). Hence,

$$\mathbf{b}_{\ell,k,t} = b_\ell e^{j2\pi t f_{D,\ell} T_s} \mathbf{a}(M_T, \theta_{k,\ell}) \mathbf{a}^T(M, \phi_{k,\ell}) \mathbf{g}_t. \tag{3.28}$$

From $\mathbf{b}_{\ell,k,t}$, calculating the cross-correlation between rows, we can obtain AoD estimates. The mean energy of $\mathbf{b}_{\ell,k,t}$ can also be estimated directly via the cross-correlation output.

When the channel parameters remain fixed over at least $2T$ OFDM blocks, we can calculate the cross correlation and use the following equation to estimate Doppler shift:

$$f_{D,\ell} = \angle\Big(\sum_{t=t_1}^{t_1+T-1} (\mathbf{b}_{\ell,k,t}^H \mathbf{b}_{\ell,k,t+T})\Big)/(2\pi T_s T), \tag{3.29}$$

where we have exploited the fact that $T_s T f_{D,\ell}$ is practically much smaller than 1 and hence there is no phase ambiguity here.

For the estimation of AoA, we can exploit $\mathbf{b}_{\ell,k,t}$s across T OFDM symbols. We can either ignore the phase variation caused by Doppler shift and process the signals per each transmitter antenna, or apply the estimated AoD and Doppler shift $f_{D,\ell}$ to (3.28) to improve signal energy. Consider the latter as an example. For $M - T > 1$, $\mathbf{b}_{\ell,k,t}$ can be left-multiplied with $e^{j2\pi t f_{D,\ell} T_s} \mathbf{a}^H(M_T, \theta_{k,\ell})$ to remove Doppler shift and AoD terms, and to combine signals from different transmit antennas. Stacking the resulting signals over the first T blocks into a $T \times 1$ vector, we get

$$\mathbf{q}_{\ell,k} = M_T b_\ell \mathbf{G}^T \mathbf{a}(M, \phi_{k,\ell}), \tag{3.30}$$

where $\mathbf{G}$ is an $M \times T$ matrix with the $(\mathrm{mod}(t, T) + 1)$-th column being $\mathbf{g}_t$. The signal $\mathbf{q}_{\ell,k}$ can be further averaged over the first and second T blocks.

When $T < M$, the pseudo-inverse of $\mathbf{G}^T$ does not exist, and hence $\mathbf{a}(M, \phi_{k,\ell})$ cannot be obtained directly. We propose to use the following approach to estimate $\phi_{k,\ell}$ instead.

Note that $\mathbf{g}_t^T\mathbf{a}(M,\phi_{k,\ell})$ can be computed as

$$\begin{aligned}&\mathbf{g}_t^T\mathbf{a}(M,\phi_{k,\ell})\\ =&\sum_{m=0}^{M-1} e^{j2\pi m(\alpha-(t_0+\mathrm{mod}(t,T)c_1)/M)}\\ =&\sum_{t'=0}^{T-1}\underbrace{e^{j2\pi t'(\alpha-t_0/M)}\frac{1-e^{j2\pi M(\alpha-t_0/M)}}{1-e^{j2\pi T(\alpha-t_0/M)}}}_{\rho_{t'}}\cdot R\end{aligned} \tag{3.31}$$

where $\alpha \triangleq d\sin(\phi_{k,\ell})/\lambda$ and $R = e^{-j2\pi t'\mathrm{mod}(t,T)/T}$. Note that this is a T-point DFT of $\rho_{t'}$, and in $\rho_{t'}$, only $e^{j2\pi t'(\alpha-t_0/M)}$ depends on t'.

Hence, we can apply inverse DFT to $\mathbf{q}_{\ell,k}$ in (3.30) and get $\{\rho_{t'}\}, t' = 1,\cdots,T$, and then get the AoA estimation through computing

$$\sin(\phi_{k,\ell}) = \frac{\lambda}{2\pi d}\angle(e^{j2\pi t_0/M}\sum_{t'=1}^{T-1}\rho_{t'+1}\rho_{t'}^*), \tag{3.32}$$

where $(\cdot)^*$ denotes the conjugate operator. Note that $M_t b_\ell$ in $\mathbf{q}_{\ell,k}$ is absorbed to $\rho_{t'}$ during this calculation and has no impact on the result through the angle operation.

Once all other parameters are estimated in (3.30), b_ℓ can then be obtained too.

In noisy cases, we can sort the blocks $\mathbf{V}_\ell\mathbf{A}^T(M,\boldsymbol{\phi})\mathbf{g}_t, \ell = 1,\cdots,N_p$ according to the energy of the block signals and use a threshold to pick up blocks with larger energy and corresponding to efficient multipath signals. This threshold may be determined by measuring the mean power across T OFDM blocks when beamforming completes one cycle of scanning.

The advantage of this 1-D approach is that continuous values of sensing parameters except for delay can all be estimated, in principle, at any resolution, if there is only one multipath in each delay bin. This is in contrast to many high-dimension CS algorithms which largely depend on quantization and on-grid accuracy.

This observation can be extended to any other on-grid parameter. For example, if massive MIMO is available and number of receiving antennas is much larger than the total number of multipath signals, then we can apply 1-D CS to an AoA-on-

grid model revised from (3.5), and then we can get accurate estimation for all other parameters including delay.

Multiple Multipath Signals with the Same Delay: Similar to those shown for MIMO systems in [1] and in Section 3.1.6, if $\ell \in \mathscr{S}_d$ multipath signals have the same delays but different AoAs or AoDs, we will get

$$\begin{aligned} &\mathbf{V}_\ell \mathbf{A}^T(M, \boldsymbol{\phi})\mathbf{g}_t \\ &= \sum_{\ell \in \mathscr{S}_d} b_\ell e^{-j2\pi t f_{D,\ell} T_s} \mathbf{U}\mathbf{p}_\ell \mathbf{a}^T(M, \phi_\ell)\mathbf{g}_t \end{aligned} \tag{3.33}$$

If these multipath signals are from different RRUs (users), multiple $\mathbf{b}_{\ell,k,t}$s will be non-zero. Hence, these multipath signals can be estimated straightforwardly, by applying the results from (3.28) to the end of Subsection 3.2.4 to each user separately. To determine which users' multipath signals are located in one delay bin, both the largest power of blocks in one delay bin and average powers across the delays bins for a particular user may be exploited. Detailed design remains as an open question. In simulations we use a threshold corresponding to 50% of the mean signal energy in each delay bin identified containing efficient multipath signals.

A very challenging scenario is when $L_{\ell,k} > 1$ multipath signals are from the same RRU (user). So,

$$\begin{aligned} \mathbf{b}_{\ell,k,t} &= \sum_{\ell \in \mathscr{S}_d} b_\ell e^{-j2\pi t f_{D,\ell} T_s} \mathbf{a}(M_T, \theta_{k,\ell}) \mathbf{a}^T(M, \phi_{k,\ell}) \mathbf{g}_t \\ &= \mathbf{A}_T \mathbf{D} \mathbf{A}_R^T \mathbf{g}_t, \end{aligned} \tag{3.34}$$

where $\mathbf{A}_T$ is an $M_T \times L_{\ell,k}$ matrix with columns $\mathbf{a}(M_T, \theta_{k,\ell})$, $\mathbf{A}_R$ is an $M \times L_{\ell,k}$ matrix with columns $\mathbf{a}(M, \phi_{k,\ell})$, $\mathbf{D}$ is a diagonal matrix with diagonal elements $b_\ell e^{-j2\pi t f_{D,\ell} T_s}$, all with $\ell \in \mathscr{S}_d$.

When the numbers of antennas M_T and M are large, it is possible to apply the CS technique to estimate both AoA and AoD, by working over T OFDM blocks and ignoring the change of Doppler shift between them. When M_T and M are not very

large but are larger than two times the multipath number, the AoD can be estimated using spectrum analysis techniques such as ESPRIT or MUSIC using individual $\mathbf{b}_{\ell,k,t}$ or across T $\mathbf{b}_{\ell,k,t}$s. However, there seems no efficient spectrum analysis techniques or other techniques to accurately estimating AoA for the signals in (3.34), when $T < M$. A qualitative approach is to determine a coarse AoA according to the signal energy of $\mathbf{b}_{\ell,k,t}$ and the beamforming scanning direction.

When $T \geq M$ beamforming scanning over a stable channel period is possible (phase variation due to Doppler is ignored), we can stack T $\mathbf{b}_{\ell,k,t}$s into a matrix and remove $\mathbf{g}_t$s impact via right multiplying the matrix with the (pseudo) inverse of the $M \times T$ matrix $\{\mathbf{g}_t\}$. Then, we get a standard expression for which conventional spectrum analysis techniques or 2-D DFT analysis can be applied.

3.2.5 Simulation Results

We present simulation results using the block Bayesian Sparse Learning algorithm [118] to validate the effectiveness of our parameter estimation scheme.

We consider a system with 4 RRUs, each with an 8-element antenna array, providing connection to 4 users, each with 2 antennas. The carrier frequency is 2.35 GHz, $N = 256$, $d = \lambda/2$, and $B = 100$ MHz. The total thermal noise in the receiver is -97 dBm, the transmission power is 25 dBm and the used pathloss model is the same as in [2]. Multipath signals for each RRU/MS are formed randomly in a cluster, mimicking reflected/scattered signals from objects. Each cluster is generated following uniform distributions of $[3, 5]$ for the total multipath number and $[0, 45]$ degrees for direction span, $[0, 90]$ m for distance, and $[0, 600]$ Hz for Doppler frequency. Across clusters there are additional offsets in direction, distance and Doppler frequency. AoAs, AoDs and Doppler frequencies are randomly generated within a given range. Delays, from the same RRU/MS are different while they are the same between RRUs/MSs. On-grid delay interval of 10 ns refers to a distance resolution of 3 m. Random continuous values are used for Doppler shift, AoAs and AoDs.

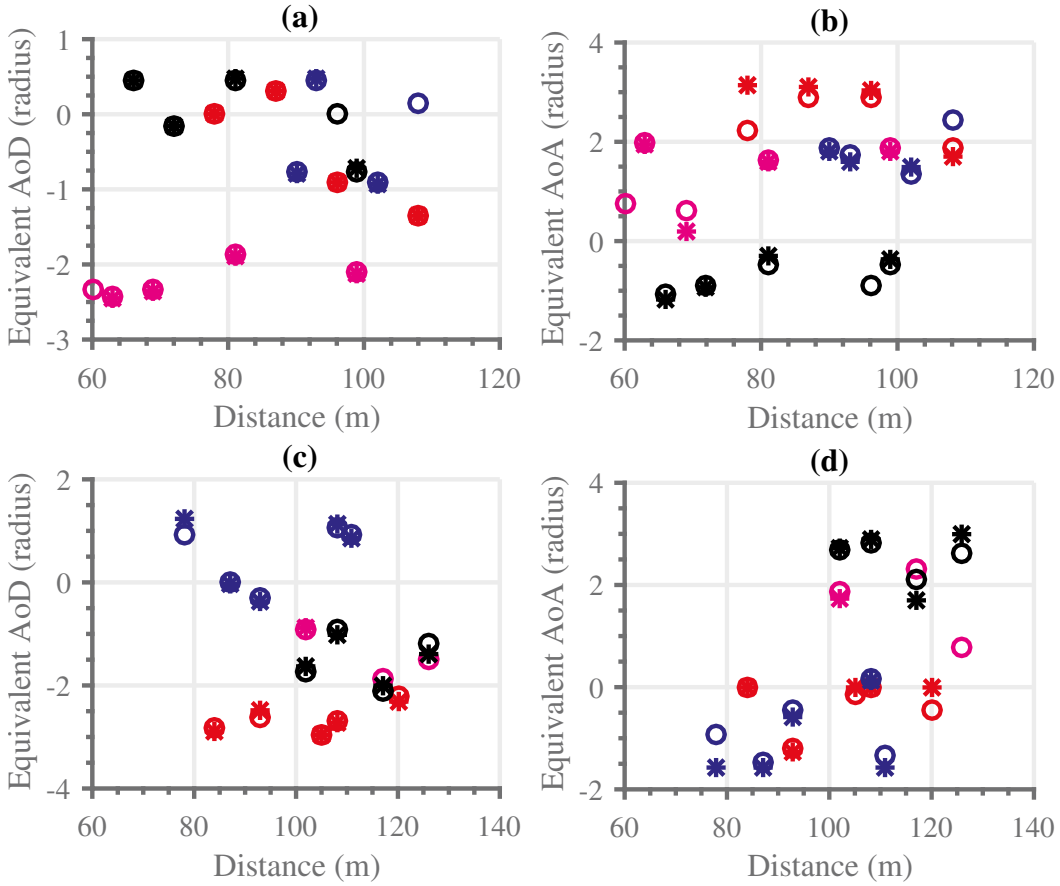

Figure 3.3: Parameter estimation for downlink sensing shows in (a), (b), while (c) and (d) refers to uplink sensing. Every star/circle refers to parameters for one multipath; stars and circles are for estimated and actual ones, respectively. Different colors represent multipath from different RRUs in (a), (b) and users in (c), (d).

Fig. 3.3 displays the simulation results for parameter estimation with $T = 4$. For downlink sensing, in (a), (b), all subcarriers are used. It shows that AoD and AoA estimates are accurately placed with the actual ones. For uplink sensing, in (c), (d), 64 randomly selected subcarriers are used by 4 users simultaneously. Estimates for this are with a few mismatched cases, especially the AoA (Figure 3.3(d)) with three circles. It reveals that, downlink sensing exploits centrally available signals at more subcarriers at static RRUs with larger arrays. However, in uplink, diverse resource allocation with random multiuser access draws an overall impact on estimation accuracy.

The depicted distance is the total signal travelling distance between a transmitter and the receiver, and does not necessarily translate to the distance of objects to the receiver directly. Complex across-RRU synthesizing is needed to achieve this

translation, particularly for uplink sensing. Both figures demonstrate that when SNR is sufficiently high, the estimated results show a very close match with the actual ones. When the SNR decreases, estimation accuracy for multipath signals with lower power degrades.

3.2.6 Summary

This research work presents a basic spatial parameter estimation method based on an analog antenna array for a sensing system unified with communication. A compressive scheme is developed for estimation, and its effectiveness is validated by simulation results. Our work here provides a step forward in demonstrating the feasibility of an analog array in receiver cost minimization for our perceptive network.

Chapter 4

Indirect Sensing

This chapter presents the indirect sensing schemes combined with CS techniques for sensing parameter estimation for both downlink and uplink sensing in the perceptive mobile networks. We propose to reconstruct the channel matrix by demodulated symbols after the channel estimation process. The reconstructed channel later will be used in sensing parameter estimation in the sensing algorithm and we called it indirect sensing.

4.1 Indirect Estimation Using Signal Stripping

We have seen in the previous chapter that due to the MU-MIMO signal, block CS is applied to estimate the sensing parameters. It has high complexity, and is sensitive to system imperfections, such as quantization errors in the delay. In this section, we propose another sensing parameter estimating scheme called *signal stripping*, which derives simpler signal models from the received signals, and then estimates parameters based on these simplified models.

4.1.1 Signal Stripping

The idea of signal stripping is to simplify the signal input to sensing algorithms by removing the modulated symbols from the signal and separating channels for different nodes (MSs for uplink sensing or RRUs for downlink sensing). More specifically,

this approach uses the estimated data symbols and channels to strip signals from different nodes, and keep as few as a single node's composited channel matrix (with estimated elements in the channel matrix) as input to sensing. This method can significantly reduce the number of sensing parameters to be estimated each time, reduce the algorithm complexity and improve its performance, should the estimated composited channel matrix for each node be accurate.

Referring to (3.5) or (3.9), the key is to get an accurate frequency-domain channel matrix estimate at subcarrier n, at time t for user k

$$\hat{\mathbf{H}}_{n,k,t} = \mathbf{H}_{n,k,t} + \mathbf{\Delta}_{n,k,t}, \tag{4.1}$$

where $\mathbf{\Delta}_{n,k,t}$ is the channel estimation error, and

$$\mathbf{H}_{n,k,t} = \sum_{\ell=1}^{L_k} b_{k,t,\ell} e^{-j2\pi n \tau_{k,t,\ell} f_0} e^{j2\pi t f_{D,k,t,\ell} T_s} \cdot \mathbf{a}(M, \phi_{k,t,\ell}) \mathbf{a}^T(M_T, \theta_{k,t,\ell}). \tag{4.2}$$

In this work, we do not provide detailed algorithms for refining the composited channel estimation, but present a general approach. The impact of channel estimation error on the performance of sensing will be evaluated in Section 4.1.3.

The composited channel matrix in (4.1) can be efficiently obtained by estimating and refining the composited channels. Channel matrices in communications are generally estimated with the assistance of interpolation techniques and hence their accuracies are insufficient for estimating sensing parameters. The typically required updating rate for sensing is no more than one kHz, and the period of a communication packet is in the order of microseconds. Therefore we can exploit demodulated signals in communication to reconstruct composited channel matrix. In other words, we can reconstruct data symbols after decoding the whole communication packet, and then use them to get multiple channel estimates during this period. This process can be implemented similar to the DDCE scheme in communication systems [99].

Different to conventional DDCE algorithms, we only need to reconstruct channels as accurately as possible, but do not need to do channel prediction.

4.1.2 Estimation of Sensing Parameters by Indirect Sensing

When the channel estimates in (4.1) are obtained, we can use them as inputs to sensing algorithms, and get the estimates for sensing parameters for each user. This is a typical mathematical model in radar signal processing [125]. Here we only consider the case when there is only one multipath signal within each quantized delay bin for each user, and propose a 1D CS based algorithm for sensing parameter estimation. The algorithm here can also be applied to the case when only the received signals at pilots such as the DMRS in 5G NR are used for sensing, since these pilots are typically orthogonal for different MSs.

We use (4.2) as a generalized channel matrix model, and drop the subscripts t and k in the parameter variables. Referring to Section 3.1.4 we consider a similar delay-on-grid model where the delays $\tau_\ell f_0$ are quantized as q_ℓ/N' with q_ℓ being an integer and $N' = gN$. Therefore $e^{-j2\pi n\tau_\ell f_0} \approx e^{-j2\pi n q_\ell/N'}$. This delay-on-grid model for reconstructed channel matrix can be written as

$$\mathbf{H}_n = \mathbf{A}_R \mathbf{D} \mathbf{C}_n \mathbf{A}_T^T, \tag{4.3}$$

where the ℓ-th column in $\mathbf{A}_R$ (or $\mathbf{A}_T$) is $\mathbf{a}(M, \phi_\ell)$ (or $\mathbf{a}(M_T, \theta_\ell)$), $\mathbf{D}$ and $\mathbf{C}_n$ are diagonal matrices with the ℓ-th diagonal element being $b_\ell e^{j2\pi t f_{D,\ell} T_s}$ and $e^{-j2\pi n q_\ell/N'}$, respectively. The m-th column of $\mathbf{H}_n$ can be represented as

$$\mathbf{h}_{n,m} = \mathbf{A}_R \mathbf{D} \mathbf{P}_m \mathbf{c}_n, \tag{4.4}$$

where $\mathbf{P}_m$ is a diagonal matrix with diagonal elements being the m-th row of $\mathbf{A}_T$, and $\mathbf{c}_n$ is an $L \times 1$ vector with the ℓ-th element $e^{-j2\pi n q_\ell/N'}$.

We may have a few options to process different columns of $\mathbf{H}_n$. For the least, we need two columns so that AoD can be estimated. Use $M_t = 2$ as a simple example.

Transpose $\mathbf{h}_{n,m}, m = 1, 2$ and stack them into a row vector

$$(\mathbf{h}_{n,1}^T,\ \mathbf{h}_{n,2}^T) = \mathbf{c}_n^T \mathbf{D}(\mathbf{P}_1 \mathbf{A}_R^T,\ \mathbf{P}_2 \mathbf{A}_R^T). \tag{4.5}$$

Now stacking similarly formulated row vectors for all usable subcarriers $n \in \mathscr{S}$ together, we can obtain

$$\widetilde{\mathbf{H}} = \mathbf{W} \underbrace{\mathbf{D}(\mathbf{P}_1 \mathbf{A}_R^T,\ \mathbf{P}_2 \mathbf{A}_R^T)}_{\boldsymbol{G}}, \tag{4.6}$$

where the ℓ-th column of the $N_u \times L$ matrix $\mathbf{W}$ is $\{e^{-j2\pi n q_\ell / N'}\}, n \in \mathscr{S}$.

We now convert the multipath signal model in (4.6) to a generalized delay-on-grid sparse model, by representing it using $N_p \gg L, N_p \leq N'$ multipath signals where only L signals are non-zeros. Without any prior knowledge of the delay, we can use $N_p = N'$; otherwise, the range of delays can be reduced. We can then treat it as a MMV CS problem and use algorithms such as orthogonal matching pursuit (OMP) or Bayesian CS to get the estimate for $\mathbf{W}$ and $\boldsymbol{G}$. The dictionary is a partial $N_u \times N_p$ DFT matrix $\mathbf{F}$. When $N_p = N'$, its q-th column is $\{e^{j2\pi n q / N'}\}, n \in \mathscr{S}$.

Let $g_{\ell,p}$ be the (ℓ, p)-th element of $\boldsymbol{G}$ in (4.6). Once the delays and $\boldsymbol{G}$ are estimated, we can get the estimates for AoA and AoD through

$$2\pi d \sin(\phi_\ell)/\lambda = \angle\big(\underbrace{\frac{1}{2M} \sum_{k=0}^{1} \sum_{p=1}^{M-1} g_{\ell,p+kM}^H g_{\ell,p+1+kM}}_{\varepsilon_\ell} \big),$$

$$2\pi d \sin(\theta_\ell)/\lambda = \angle\big(\underbrace{\frac{1}{M} \sum_{p=1}^{M} g_{\ell,p}^H g_{\ell,p+M}}_{\xi_\ell} \big),$$

respectively. The value of $|b_\ell|^2$ can also be obtained easily during the process of computing AoA and AoD, being either $|\varepsilon_\ell|^2$ or $|\xi_\ell|^2$. The estimates of $|b_\ell|^2$ can be used to find the effective multipath delay bins in noisy channels, by using a threshold determined, for example, as a fractional scalar of the maximum power of multipath signals.

The computation above can be readily extended to the case when $M_T > 2$.

This process can be repeated over multiple refined channel estimates over the channel static period. The Doppler shift can then be estimated from the cross-correlation between two or more $\boldsymbol{G}$s that are sufficiently spaced in time, when the channel still remains stable except for the Doppler phase terms. Let $\boldsymbol{G}_t$ denote the estimate of $\boldsymbol{G}$ from the t-th refined channel estimates. Using two $\boldsymbol{G}$s the estimates of Doppler phase can be obtained as

$$2\pi f_{D,\ell} T_s = \frac{T_s}{T} \angle\big((\boldsymbol{G}_{t+T})_{\ell,\cdot}\,((\boldsymbol{G}_t)_{\ell,\cdot})^H\big), \tag{4.7}$$

where $(\mathbf{X})_{\ell,\cdot}$ denotes the ℓ-th row of the matrix $\mathbf{X}$ and T is the interval of two symbols used for estimating Doppler shift.

4.1.3 Simulation Results on Indirect Sensing

Instead of implementing the DDCE algorithm to actually refine the channel estimation, we introduce channel estimation error in (4.1) as AWGN to evaluate the performance for the indirect estimation method. The *signal-to-interference ratio (SIR)* between the mean power of the channel coefficients and the reconstruction error is denoted by η.

Fig. 4.1 shows the results for uplink sensing. It can be seen that the estimates of delay and AoA are accurate and are robust to the introduced channel reconstruction error. The estimates of moving speed, through estimating the Doppler frequency $f_{D,\ell}$, have relatively large errors because the actual Doppler phase values are very small and hence sensitive to both noise and the interval T.

In Fig. 4.2, we present the results for the case when delay is generated as continuous values (off-grid model) for downlink sensing. The figures show that delays and AoAs are identified with degraded but still acceptable accuracy, but the speed estimation varies significantly across different realizations. As a comparison, we also plot the sensing results for AoA-Distance in Fig. 4.3 by applying the classical

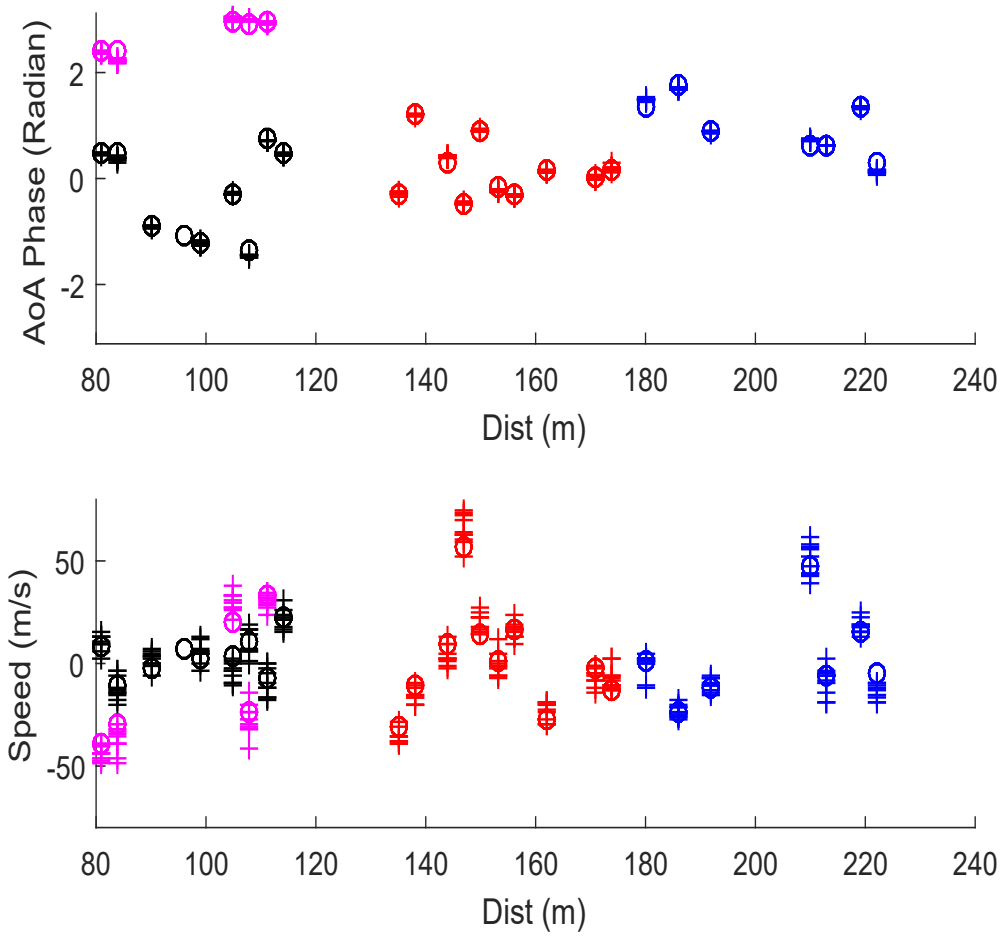

Figure 4.1: 10 implementation results for indirect uplink sensing with channel SIR $\eta = 15$dB, and symbol sampling interval $T = 20T_s$.

2D DFT method to the signal in (4.2). For AoA, a 64-point DFT is applied to the 4 signals received at four antennas. The image is cleared by setting 2D-DFT outputs with power 25 dB lower than the maximum to zeros. Comparing Fig. 4.2 with Fig. 4.3, we can see that the proposed 1D CS method achieves much better resolution than the classical 2D DFT method.

We further test our indirect uplink sensing scheme using a practical subcarrier allocation example in 5G NR with the Type B set-up and a total subcarriers of 252. Within each resource block of 12 continuous subcarriers, four subcarriers with indices 3, 4, 9 and 10 are used. Hence a total of 84 subcarriers. The sampling period $T = 35T_s$, and a total of 8 sets of observations are obtained for Doppler estimation. For comparison, the N-way OMP Tensor (NOMP) method [116], which

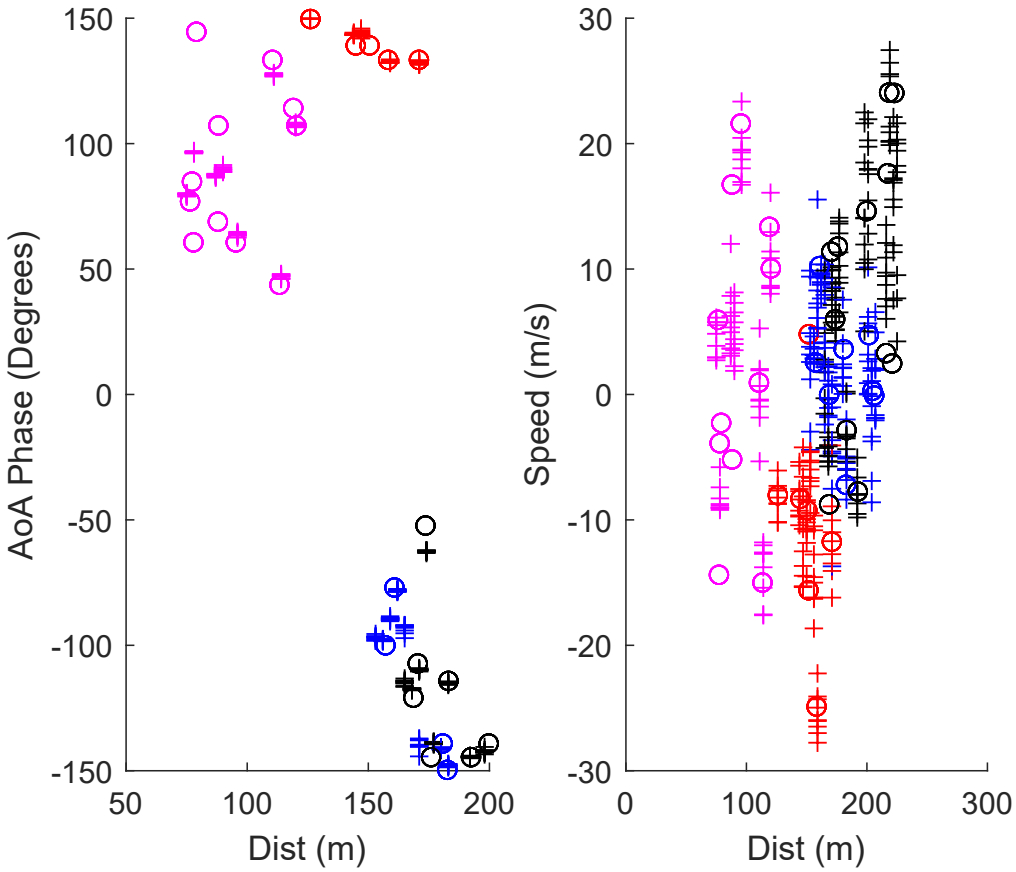

Figure 4.2: 10 implementation results for indirect downlink sensing with $\eta = 15$dB, and $T = 20T_s$, where delay values are continuous (off-grid). Subcarriers are interleaved.

is a 3D CS algorithm, is also simulated. The simulation results are presented in Fig. 4.4 and Fig. 4.5 for our scheme and the NOMP scheme, respectively. In both figures, only estimated multipath channels with power within 10 dB of the maximum are shown. Comparing these two figures, we can see that the proposed 1D CS method achieves better resolution for distance, AoA and speed for most multipath channels. This demonstrates the effectiveness of our scheme in the cases when sufficient measurements are only available in the delay domain.

Comparing the results here and those in Section 3.1.7, it is suggesting that the indirect methods can achieve better performance than the direct method when the estimation error in the channel matrix is small enough, as different users' channels/signals are efficiently separated.

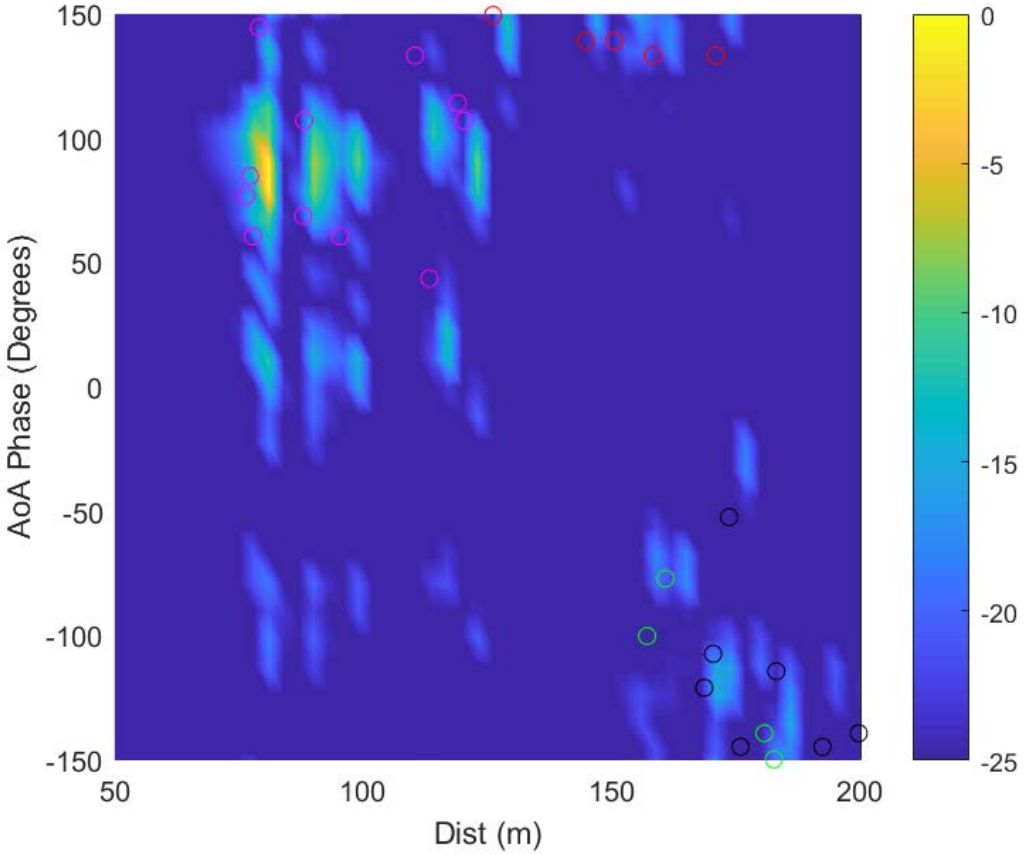

Figure 4.3: 10 implementation results for classical 2D DFT results. System setup is the same as that in Fig. 4.2.

4.1.4 Summary

We have demonstrated that by using signal stripping approaches we can simplify the signal model used for sensing parameter estimation in the recently proposed perceptive mobile networks. We also developed methods for estimating all of the other sensing parameters.

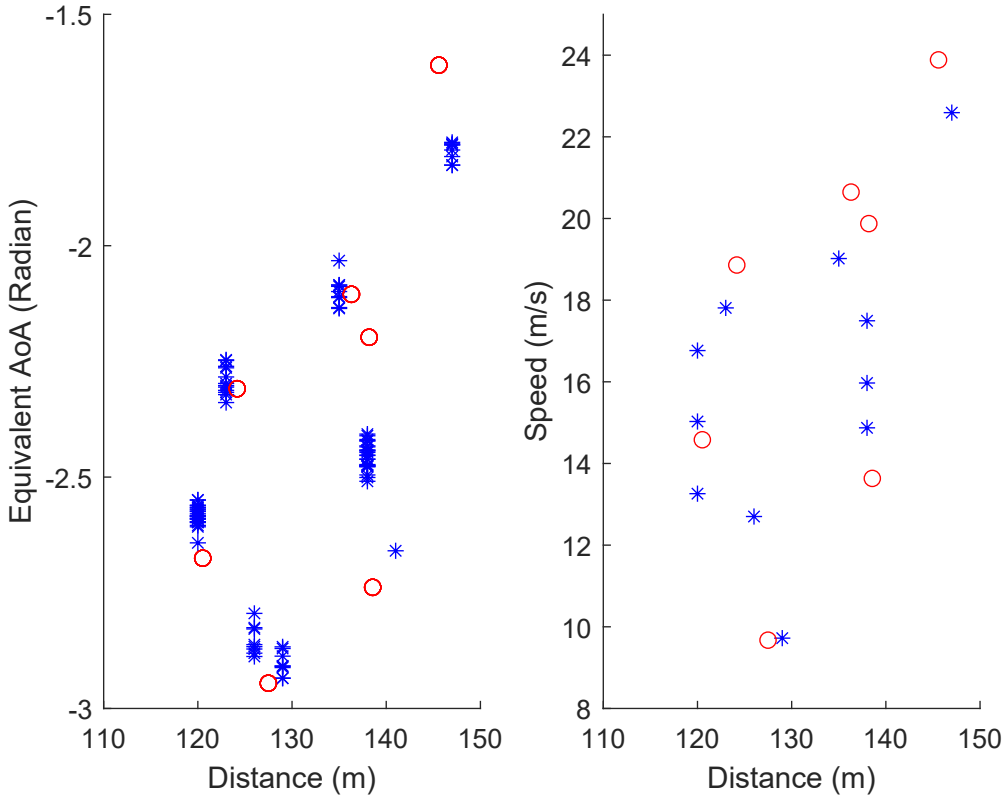

Figure 4.4: Sensing parameter estimation using the proposed 1D CS method for indirect uplink sensing, with $\eta = 15$dB. "Equivalent AOA" equals to $\pi \sin(\theta)$, and speed is relative to the static BS. All parameters have continuous values (off-grid model).

4.2 Joint Communication and Radar Sensing in 5G Mobile Network

In the perceptive mobile network with 5G CRAN, with a conceptual plot provided in Fig. 4.6, sensing parameters can be extracted from 5G communication signals via indirect sensing methods. Although existing studies demonstrate the feasibility and potential of JCAS, most of them consider general signal formats, such as simple single carrier and multicarrier modulation [6], and is limited to P2P links such as mmWave radio for vehicular networks [14]. There is only very limited work directly using modern mobile communication signals and networks in JCAS systems, involving OFDMA and MU-MIMO technologies. We will show that CS is an excellent candidate technology for this problem, after proper signal formulation.

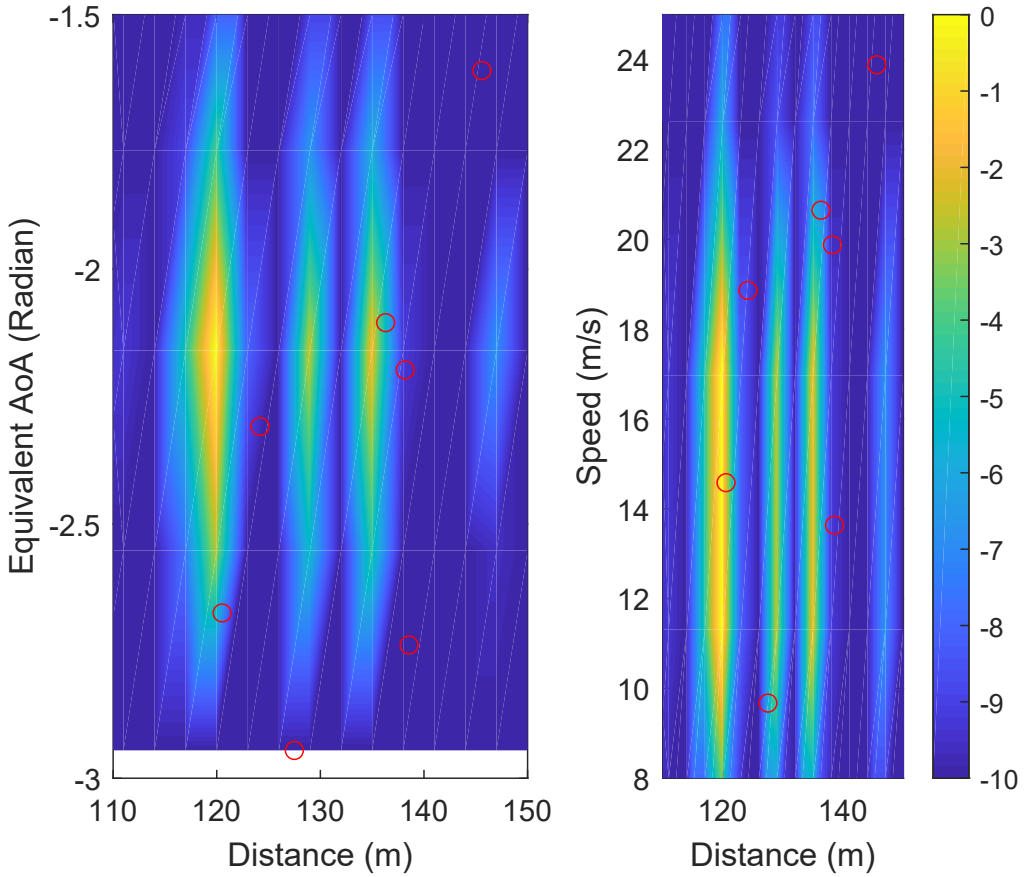

Figure 4.5: Sensing parameter estimation using the N-way OMP (3D CS) algorithm. Dictionaries for AoA and Doppler estimation are interpolated to size 16 and 256, respectively. Other configurations are similar to those in Fig. 4.4.

In this work, referring to the 5G NR standard, we study 1D to 3D CS algorithms for estimating sensing parameters in perceptive mobile networks. These CS algorithms are developed from existing ones to make them capable of estimating all the sensing parameters. We consider both downlink and uplink sensing, to be consistent with downlink and uplink communications. The communication signals used for sensing are the OFDM-type DMRS in the 5G specification [86]. We use both 5G-compatible channels recommended by 3GPP and our own generated cluster channel model which has a better control for radio propagation for sensing purposes. We compare these CS algorithms, and demonstrate their respective advantages and disadvantages, under various channel conditions and system setup.

This rest of the work is divided into three parts. The first part provides 5G usable signal and channel description. The second part describes various sensing

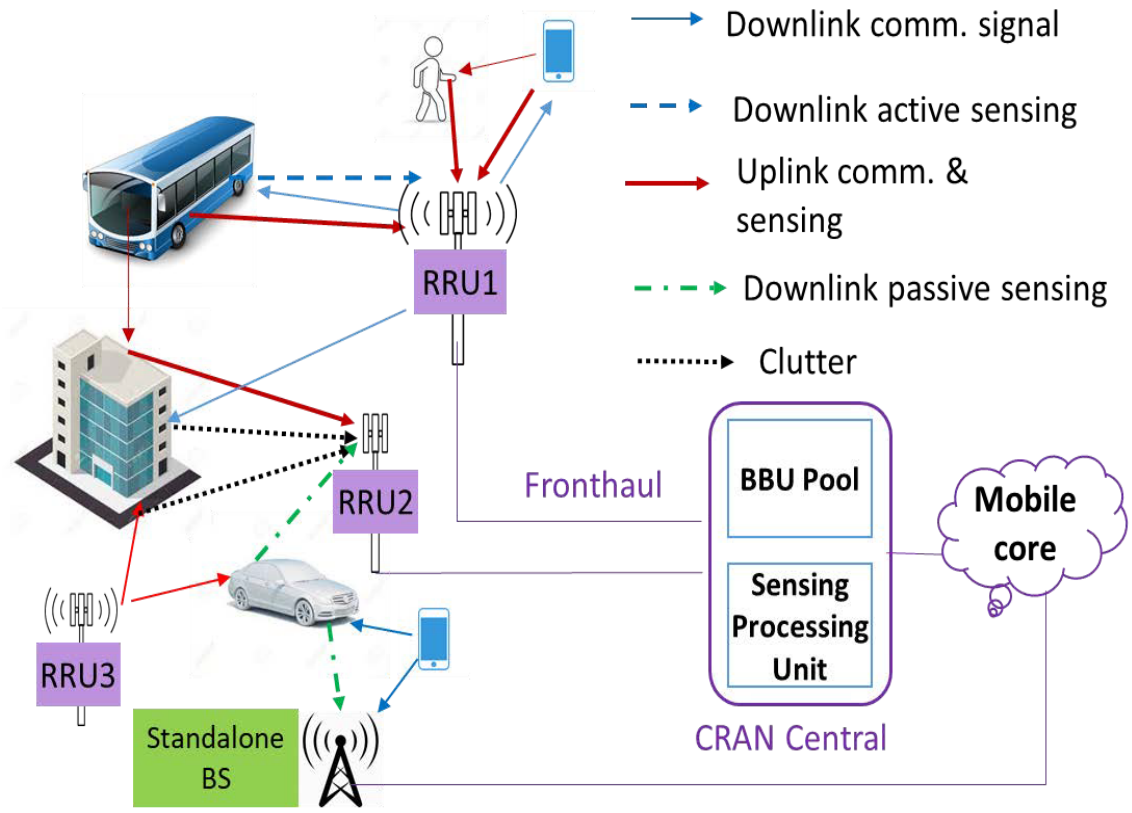

Figure 4.6: Proposed perceptive mobile network with 5G CRAN.

parameter estimation algorithms including 1D, 2D, and 3D in detail. In the third part, we discuss simulation results and outline a comparative study from these results obtained from 5G reference signals.

4.2.1 5G Signal and Channel Models

We consider 5G-compatible signals with OFDMA and SDMA (or MU-MIMO) modulations. In a typical setup, there are 4 SDMA users, each with a single antenna, and a BS with a 16 antenna uniform linear array. The signal bandwidth is assumed to be 100 MHz. DMRS [86] is used as a primary signal for sensing. Propagation channels are generated based on clustered channel models of two forms. The first one is developed by us and named *Cluster-Chl* [74], and the second one is the *QuaDRiGa* channel model [87], [126], [127], recommended by 3GPP for modelling communication channels in LTE and 5G systems.

DMRS Signal Generation

DMRS signal is generated according to the Gold sequence as defined in [86] of *3GPP TS 38.211*, both for *Physical Downlink Shared Channel-PDSCH* and *Physical Uplink Shared Channel-PUSCH*. The generated physical resource-block (PRB) indicates DMRS to a 3-D grid comprising a 14-symbol slot for the full carriers across the DMRS layers or ports. The values and indices of DMRS signals are both known to the BS, and are used as prior information when doing sensing from received signals. Here, interleaved DMRS subcarriers of PDSCH are used in downlink sensing, while groups of non-interleaved DMRS subcarriers of PUSCH are used in uplink sensing.

Channel Modelling

For radio sensing, the system needs to interpret detailed channel structure and estimate the sensing parameters. The propagation channels are generated based on clustered channel models following the 3GPP channel models for LTE and 5G systems [86]. Random continuous values are used for delay, Doppler shift, AoAs and AoDs as actual sensing parameters. The multipaths of the channels are generated in clusters, indicating reflections coming from scattering obstacles. We generate approximate scatters for simulating sensing by using both the Cluster-Chl and QuaDRiGa models.

Consider a narrowband antenna array model [1, 76]. The array response vector of a size-M array with θ of either AoD or AoA is,

$$\mathbf{a}(M,\theta) = [1, e^{j\pi\sin(\theta)}, \cdots, e^{j\pi(M-1)\sin(\theta)}]^H, \tag{4.8}$$

For M_1 transmitting and M_2 receiving antennas, the $M_2 \times M_1$ time-domain baseband channel impulse response (CIR) matrix at time t' can be represented as

$$\tilde{\mathbf{H}}(t') = \sum_{\ell=1}^{L} b_\ell \delta(t'-\tau_\ell) e^{j2\pi f_{D,\ell} t'} \mathbf{a}(M_2,\phi_\ell)\mathbf{a}^T(M_1,\theta_\ell), \tag{4.9}$$

where for the ℓ-th out of a total of L multipath signals, θ_ℓ and ϕ_ℓ denote the AoD

and AoA, respectively, b_ℓ, τ_ℓ and $f_{D,\ell}$ are the amplitude, propagation delay, and Doppler frequency, respectively.

Cluster-Chl Channel Model

In Cluster-Chl, we can have a flexible and accurate control on all the channel parameters including AoA, AoD, Doppler shift, delay, and amplitude, and then verify with sensing results. The multipath channels of Cluster-Chl are randomly generated in clusters following a complex Gaussian distribution to generate sensing parameters for moving objects around the mobile network node, which mimics the ray tracing model and are extensions of the Saleh-Valenzuela (S-V) model [128].

For the channels used in this work, we generate 3 clusters with delay centered at 29, 39 and 49 μs, corresponding to a distance of 87, 117 and 147 meters, with AoA center randomly generated between -120 to 120 degrees, and moving speed randomly generated between 0 to 40 m/s. In each of the clusters, as in [1], multipath signals for each RRU/MS are generated randomly by mimicking reflected/scattered signals from objects. In each cluster, the multipath is generated following a uniform distribution of [5, 10] for the total number, [0, 28] degrees for direction span, [0, 0.05] μs for delay (corresponding to [0, 15] m for distance). We use a pathloss model with pathloss factor 40 for downlink and 20 for uplink sensing. The transmission power of the RRU and MS is 30 dBm and 25 dBm respectively.

QuaDRiGa Channel Simulator

QuaDRiGa is a spatial geometry based 3D MIMO channel generator [87], originated from the *WINNER* series models and supports rich cluster multipath scenarios specified by the 3GPP-3D cluster-based models mentioned in *TR 36.873 and TR36.901* [87]. We generate QuaDRiGa channels equivalent to moving scatters by simulating moving transmitters and receivers from an open source simulator for sensing demonstration. Non-line of sight channels are simulated. One problem with the QuaDRiGa model is that scatters can not be accurately placed and configured. The other problem is that the Doppler frequencies for each multipath are not explicitly provided and hence we cannot verify the accuracy of estimates.

4.2.2 Sensing Parameter Estimation with DMRS

We develop and test 1D, 2D and 3D CS algorithms for sensing parameter estimation using the received signals. These algorithms are extended from the 1D-CS algorithms [121], 2D Kronecker CS [129], and 3D N-way Tensor tool [116]. The extensions formulation and processing are realized here through extracting sensing parameters from 5G received signals. We test these algorithms utilizing Cluster-Chl in downlink sensing and QuaDRiGa model in uplink sensing. We also compare our 1D to 3D results with the cases when the occupied PRB is small in uplink and with the results from 2D DFT.

Signal Model for Sensing

The received radar signal data is based on 3D observation samples, comprising of those from multiple receiving antennas, multiple DMRS subcarriers and multiple DMRS signals over time. The modulated data symbols can be removed from the received DMRS signals by applying equalization, which will be a simple one-tap multiplication if no two users are sharing the same subcarrier. In this work, we consider the case that each subcarrier is used by only one user in DMRS signals. We present the proposed scheme by referring to uplink sensing in this case. However, it can be similarly applied to downlink sensing. We will provide simulation results for both uplink and downlink sensing.

After the equalization, the processed received signal at the n-th subcarrier and the t-th DMRS signal can be represented as

$$\begin{aligned}\mathbf{Y}_{n,t} =& \sum_{\ell=1}^{L} b_\ell e^{-j2\pi n \tau_\ell f_0} e^{j2\pi t f_{D,\ell} T_s} \cdot \\ & \mathbf{a}(M_2, \phi_\ell)\mathbf{a}^T(M_1, \theta_\ell) + \mathbf{z}_{n,t}, \qquad (4.10) \\ =& \mathbf{A}_{rx}\mathbf{C}_n\mathbf{D}_t\mathbf{A}_{tx}^T + \mathbf{z}_{n,t}, \qquad (4.11)\end{aligned}$$

where the ℓ-th column in $\mathbf{A}_{rx}$ and $\mathbf{A}_{tx}^T$ are $\mathbf{a}(M_2, \phi_\ell)$ and $\mathbf{a}^T(M_1, \theta_\ell)$, respectively; if there is no two multipaths having the same delay values, $\mathbf{D}_t$ and $\mathbf{C}_n$ are diagonal

matrices with the ℓ-th diagonal element being $b_\ell e^{j2\pi t f_{D,\ell} T_s}$ and $e^{-j2\pi n \tau_\ell f_0}$, respectively; otherwise, there will be non-zero values in other entries; and $\mathbf{Z}_{n,t}$ is the noise matrix. When each user has only one transmitting antenna, $\mathbf{A}_{tx}^T$ becomes an all-one column vector, and $\mathbf{Y}_{n,t}$ and $\mathbf{Z}_{n,t}$ become column vectors too. The task for sensing parameter estimation is to estimate $\{\tau_\ell, f_{D,\ell}, \phi_\ell, \theta_\ell, b_\ell\}, \ell \in [1, L]$ from the received signals. In this work, we only consider the estimation of the first three parameters.

Estimation of Sensing Parameters

Since the signals are relatively independent in the three domains of delay, AoA and Doppler, they can be formulated in a high-dimension (3D here) vector Kronecker product form. Therefore, we can apply 1D to 3D CS techniques to estimate these sensing parameters. In a typical system, we can get a sufficient number of observations for the delay (linked to number of subcarriers), intermediate AoA observations (linked to number of antennas) and a limited number of samples in the Doppler domain (linked to DMRS signals over a portion of channel coherent period). The Doppler frequency is typically very small in a perceptive mobile network and the accumulated phase shift usable is also small due to the limited period of channel coherent time [17], [76]. This makes it inaccurate for estimating Doppler using CS algorithms. Next, we briefly review each of the three sensing algorithms based on received signal in (4.11).

1D Compressive Sensing

We assume that there is only one multipath signal within each quantized delay bin for each cluster in the 1D CS based algorithm. By stacking the signals in (4.11) from all available subcarriers to one matrix, we can get

$$\mathbf{Y}_t = \mathbf{W} \underbrace{\mathbf{D}_t \mathbf{A}_{rx}^T}_{\mathbf{G}_t} + \mathbf{Z}_t, \tag{4.12}$$

where the ℓ-th column of $\mathbf{W}$ is $\{e^{-j2\pi n \tau_{q,\ell} f_0}\}$. We can then treat (4.12) as an on-grid MMV CS problem and use algorithms such as 1D sparse Bayesian CS to get the

estimate for $\mathbf{G}_t$. The dictionary $\mathbf{\Psi}_1$ is a partial DFT delay matrix, approximating $\mathbf{W}$. Once the delays and $\mathbf{G}_t$ are estimated, we can get the AoA estimates through calculating the cross-correlation between columns from $\mathbf{G}_t$ on the indices obtained from given threshold as below,

$$\phi_\ell \approx \frac{1}{\pi}\angle\left(\sum_{p=1}^{M-1}((\mathbf{G}_t)_{\cdot,p})^*(\mathbf{G}_t)_{\cdot,p+1}\right), \tag{4.13}$$

where $(\mathbf{G}_t)_{\cdot,p}$ denote the p-th column $\mathbf{G}_t$.

The Doppler frequency $f_{D,\ell}$ can be estimated across multiple DMRS signals, based on the cross-correlation of $(\mathbf{G}_t)_{\ell,\cdot}$, where $(\mathbf{G}_t)_{\ell,\cdot}$ denotes the ℓ-th row of $\mathbf{G}_t$. Assume the interval between every two estimates of $\mathbf{G}_t$ and $\mathbf{G}_{t+1}$ is uniform and be T_s for any t, which can be relaxed easily. Let N_d be the total OFDM blocks used for estimating the Doppler frequency. Then,

$$f_{D,\ell} \approx \frac{1}{2\pi T_s}\angle\left(\sum_{t=1}^{N_d-1}((\mathbf{G}_t)_{\ell,\cdot})((\mathbf{G}_{t+1})_{\ell,\cdot})^*\right). \tag{4.14}$$

The main advantage of the 1D algorithm is that it can estimate all the parameters when each multipath is well separated in delay. Its complexity is also relatively low. It is mostly suitable for systems with a large number of subcarriers, but with a small number of antennas for AoA estimation and packets for Doppler estimation.

2D Kronecker Compressive Sensing

2D Kronecker CS can obtain direct estimation for any two parameters out of delay, AoA and Doppler. Since we can have sufficient measurements in the delay and AoA domain, the 2D CS algorithm can provide good estimates for both delay and AoA directly from $\mathbf{Y}_t$ of (4.12) using each DMRS signal of 2D observations. We construct two dictionaries for delay and AoA, $\mathbf{\Psi}_1$ and $\mathbf{\Psi}_2$, being two partial overcomplete DFT matrices, approximating $\mathbf{W}$ and $\mathbf{A}_{rx}$, respectively. Interpolated overcomplete dictionaries are used to improve resolution, given that the SNR is sufficiently large, at an increased computational complexity. We can then obtain estimates $\hat{\mathbf{D}}_t$ for the expanded matrix for $\mathbf{D}_t$ that corresponds to the two over-

complete dictionaries, using any 2D Kronecker CS algorithm, such as the 2D-OMP algorithm [129].

Note that 2D CS algorithm here can identify any pair of {delay, AoA} with at least one different values. So $\hat{\mathbf{D}}_t$ will not be a diagonal matrix anymore if one variable in the pair has two identical quantized values.

After getting the estimate $\hat{\mathbf{D}}_t$, we use a threshold to filter out very small estimates which are likely caused by noise. The threshold value is relative to the maximum amplitude of multipaths and explicitly determined to pick up "effective" estimates with significant power. We can then get the delay and AoA estimates according to the indices of the non-zero values in $\hat{\mathbf{D}}_t$, corresponding to respective columns in the two dictionaries.

The Doppler shift is estimated via calculating the angle of the cross-correlation values between the non-zero values of $\hat{\mathbf{D}}_t$ obtained over two DMRS signals. This can be represented as

$$f_{D,q,\ell} \approx \frac{1}{2\pi T_s} \angle \left(\hat{\mathbf{D}}_t \hat{\mathbf{D}}_{t+1}^{*} \right)_{\ell,\ell}. \tag{4.15}$$

Averaging can be taken over the correlation obtained from multiple DMRSs before computing the angle, to improve the accuracy of the estimates.

2D CS algorithm can achieve improved estimation accuracy when there are multipath with repeated values in any one domain, at the cost of increased complexity.

3D Tensor Compressive Sensing

The Tensor-OMP CS algorithm directly estimates parameters in a 3D domain, combining measurements $\mathbf{Y}_t$ over multiple DMRS signals. Three dictionaries, $\mathbf{\Psi}_1$, $\mathbf{\Psi}_2$, and Doppler dictionary matrix, $\mathbf{\Psi}_3$, are utilized. Since the accumulated Doppler shift is small over the coherent time period, we have to use a portion of highly overcomplete DFT matrix as $\mathbf{\Psi}_3$.

Absolute values of the estimated sparse coefficients provides the amplitude values of multipaths. After applying a threshold, each of indices in the three dimensions corresponding to non-zero estimates provides estimated values for delay, AoA and

Doppler shift.

Generally, high-order CS formulation using Tensor tools such as 3D Tensor CS provides the strongest estimation performance in resolving multipath with repeated parameter values. However, it involves much higher computational complexity than 2D and 1D, using three dictionaries $\mathbf{\Psi}_1$, $\mathbf{\Psi}_2$, and $\mathbf{\Psi}_3$, in direct estimation of parameters in 3D domain from $\mathbf{Y}_t$. In addition, as the Doppler shift value is small, 3D will not work as well as 1D and 2D.

4.2.3 Simulation Results of Indirect Sensing with DMRS

Next, we present simulation results for 1D to 3D CS using channels with continuous-value (off-grid) sensing parameters. We also show the results that are obtained by directly applying 2D-FFT over delay-AoA and delay-Doppler domains for comparison, when all subcarriers are used. Of course, most of the time, not all subcarriers are available for sensing. Estimated values (typically shown in blue star) are placed with actual ones (shown in red circle) to verify the accuracy of estimation. Fig. 4.7 shows an exemplified CIR for QuaDRiGa channels consisting of rich multipaths with 4 to 5 clusters.

Downlink Sensing

In downlink sensing, we use DMRS subcarrier configuration type-1 slot wise, with every alternating subcarriers as interleaved selection from a total of 252 subcarriers. Sub-interval is 2 for type-1, so, in total 126 subcarrier indices (for example of layer 4) are used as DMRS subcarriers.

The simulation results for downlink sensing with Cluster-Chl model are presented in Fig. 4.8 for 1D to 3D. For 1-D CS, AoA-Distance and Speed-Distance results indicate that the estimated points are well matched with three clusters with few extra points due to residuals in threshold setting. Off-grid estimation causes some missed detection. In 2D CS, AoA-Distance and Speed-Distance results give few mismatched points for both AoA and speed. In 2D, there is an important observation

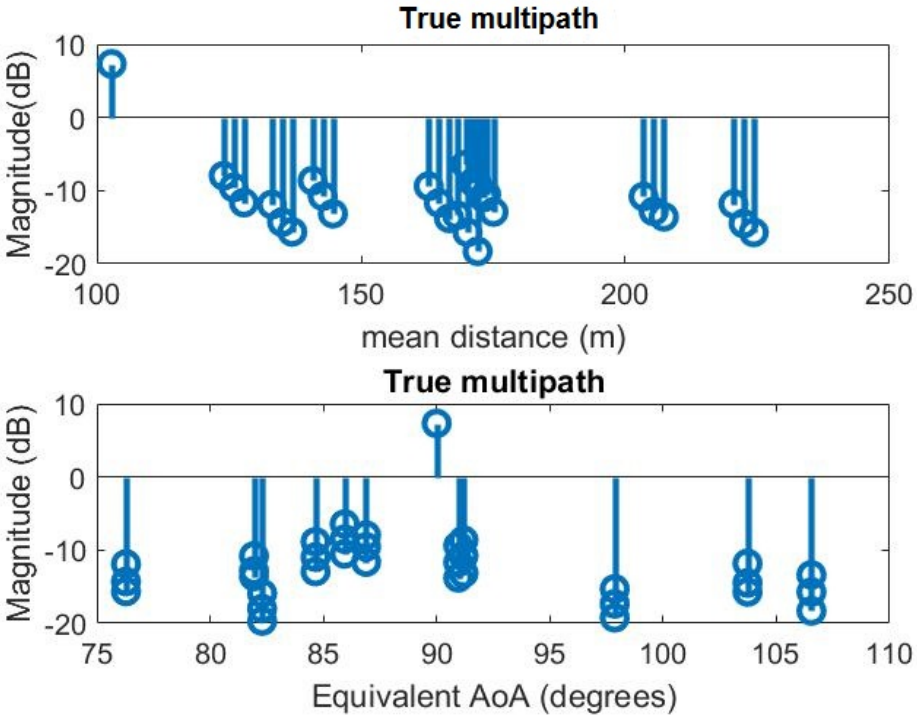

Figure 4.7: CIR for QuaGRiGa channel.

that interleaved subcarriers in this case actually cause ambiguity in estimation. 3D estimation results are not as good as for 1D and 2D CS algorithms as in 3D estimation the interleaved subcarriers cause near-singular matrix.

The ambiguity is caused by non-consecutive, but regularly spaced samples, for example, usage of comb/interleaved subcarriers [130]. In this case, the actual value can be one of the multiple integral times of a basic estimate. The simplest way is to break such regularly spaced samples; for example, we can randomly select samples from the total available ones such that the indices of these samples are not regular. This of course reduces the samples used for estimation and may degrade the estimation performance particularly when the number of samples is small. Therefore, while using DMRS, alternative methods can be based on exploiting other information to assist the selection of the right estimate, for example, the magnitude, or an integration of coarse and fine estimation methods. This is in fact part of our future work to solve ambiguity problems that may be present in all domains, but particularly for delay.

Uplink Sensing

In uplink sensing, only partial DMRS subcarriers are used. The details of obtained results from the non-line-of-sight (NLOS) QuaDRiGa channel model are given here. We use DMRS subcarrier configuration type-2 non-slot wise here, which indicates several groups of subcarriers are selected from a total of 252 subcarriers. Sub-interval is 3 for type-2, so, in total 84 subcarrier indices (of layer 4) are used as DMRS subcarriers. We use QuaDRiGa model where clusters are generated with continuous delay and AoA values for multipaths. Since the QuaDRiGa is unable to provide actual Doppler shifts, the estimates given here in all uplink sensing for speed is relative only.

Fig. 4.9 provides simulation results for uplink sensing with QuaDRiGa NLOS for 1D to 3D. In 1-D CS, AoA-distance results for the estimated points match fairly well with several clusters with few extra points due to residual in threshold setting and off-grid error.

2D CS AOA-distance results indicate that, estimated values are in closer vicinity with actual clustered multipath values (AoA) in comparison with 1D. Indeed, a higher dimensional sensing algorithm like the 2D kron CS eventually provides a better performance when there is enough measurements because it can directly identify two parameters only if one is different between any multipath channels. In both figures for 3D NOMP, only estimated multipath channels with power within -15 dB of the maximum are shown. In 3D, estimated values for AoA are coarser, but remain within the close neighbouring of actual values.

Sensing Using Small Number of PRB

Mainly in the uplink direction, allocated PRB could be limited by configuration. Therefore, we can only get a small amount of observations for the delay estimation, which could be even less than the number of multipath. We test sensing with such limited number of resources for QuaDRiGa NLOS channel here. Assume that only 28 DMRS subcarriers (7 PRB) are used in simulations for uplink sensing. Fig. 4.10

presents uplink sensing for small PRB with QuaDRiGa NLOS for 1D to 3D. In 1D CS, the resolution ambiguity problem remains in the delay domain. However, the shape is still well maintained. Reasonable estimation accuracy is found in AoA by 2D. Coarse estimation in both AoA and speed is obtained by 3D. The introduction of further approaches for increasing this accuracy in radio sensing from limited observations, especially in a clustered multipath environment is an open research problem and can be solved, for example, by designing better dictionaries and using filtering.

2D FFT Results for Uplink Sensing

2D-DFT simulation results are presented in Fig. 4.11 for QuaDRiGa channels. It can be observed that 2D-DFT provides reliable coarse estimates for uplink sensing, but the resolution is very low in comparison with all results of 1D to 3D in Fig. 4.9. It is noted that here the results are obtained by using all subcarriers. Such a 2D-FFT method only works when either all or interleaved subcarriers are available.

4.2.4 Summary

We presented three preliminary sensing algorithms using 1D, 2D and 3D CS algorithms, and provided simulation results, using channels generated from both our own cluster model and 5G QuaDRiGa channel model. These results indicate that reasonable sensing performance can be achieved, and demonstrate the respective advantages and disadvantages of these algorithms. Our work also disclosed some interesting research problems to work on as future works, such as the ambiguity problem due to interleaved subcarriers and reduced resolution in 3D CS algorithms.

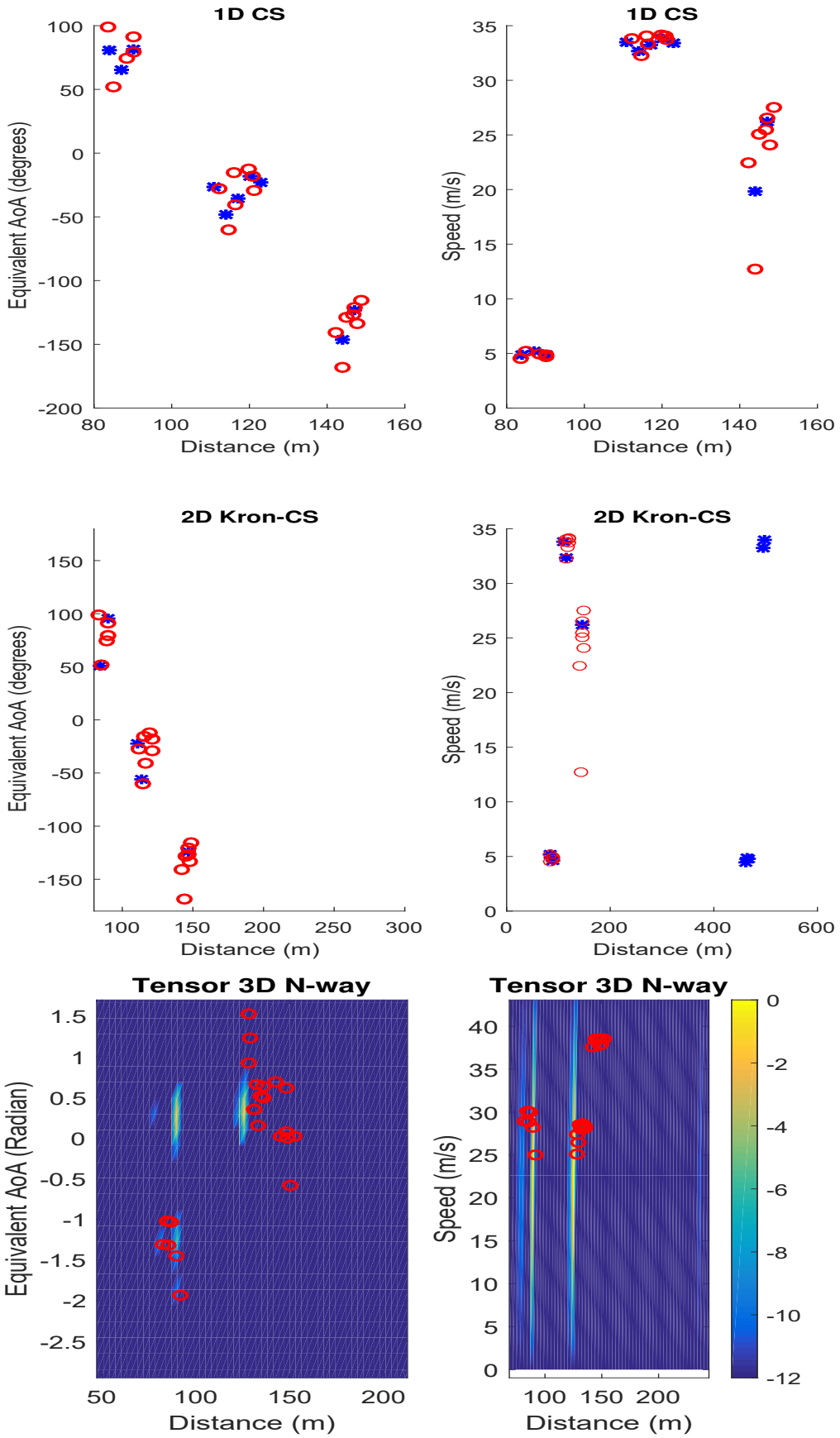

Figure 4.8: Observations in Cluster-Chl for downlink sensing.

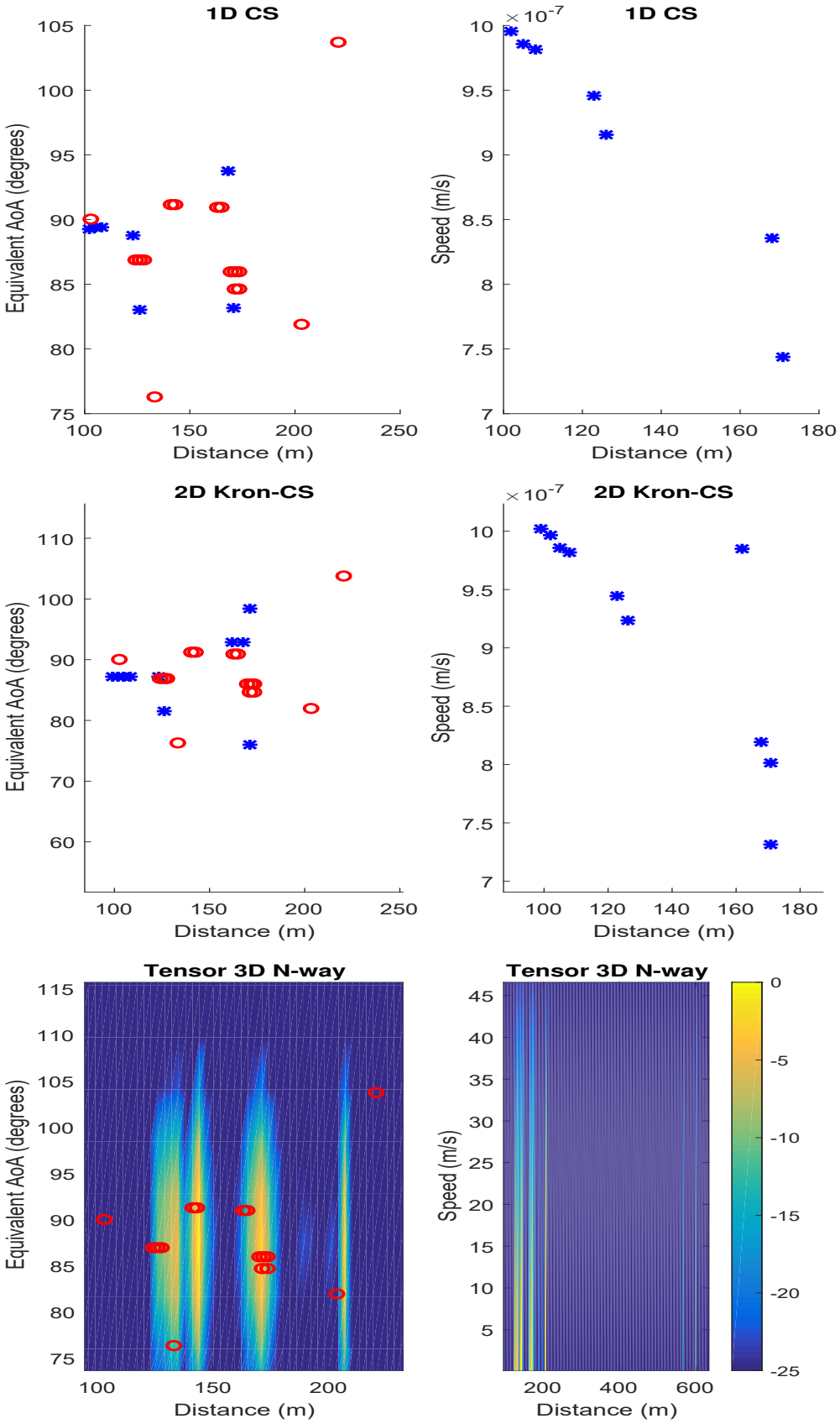

Figure 4.9: Observations in uplink sensing: QuaDRiGa NLOS channel.

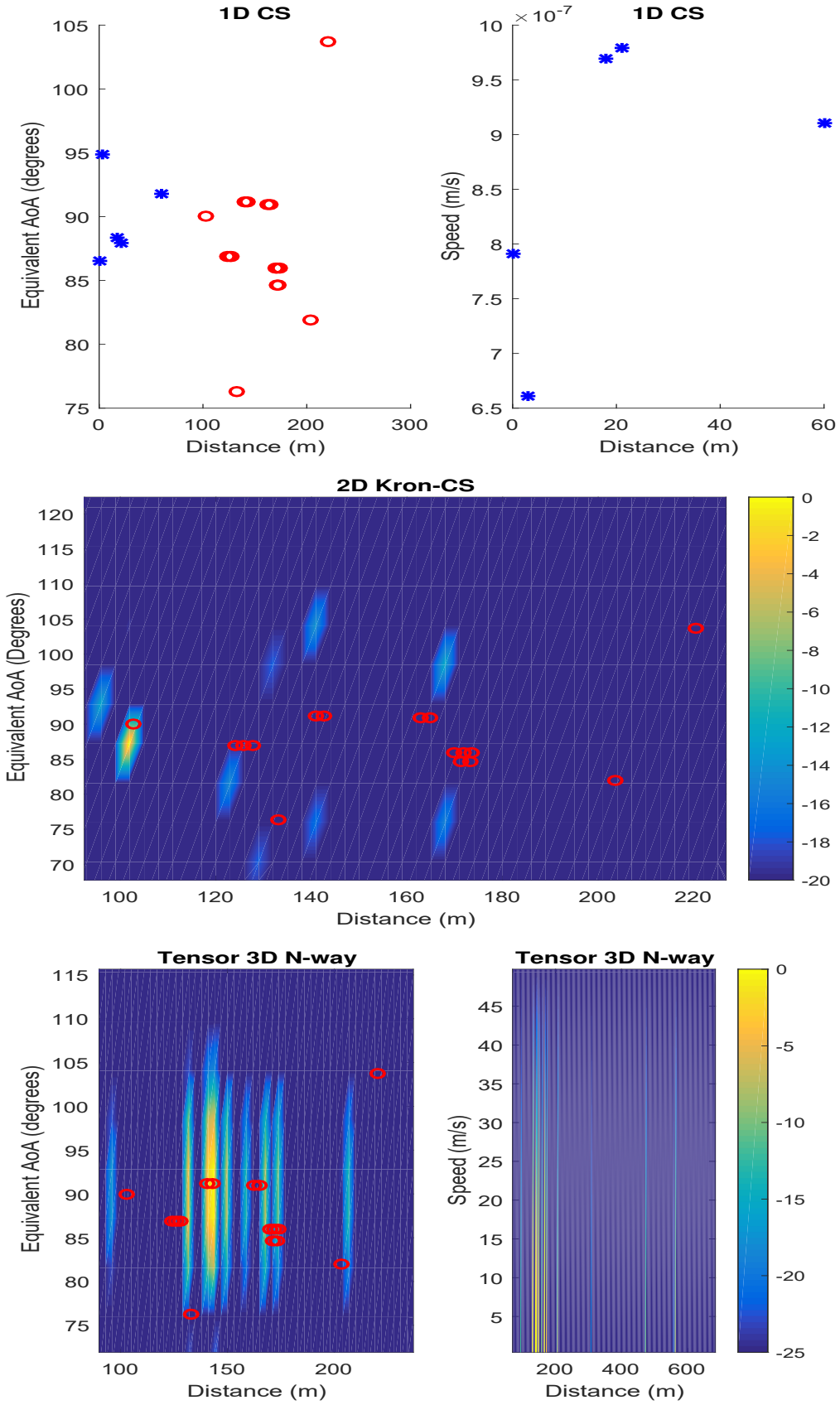

Figure 4.10: Uplink sensing with small PRB in 5G QuaDRiGa NLOS.

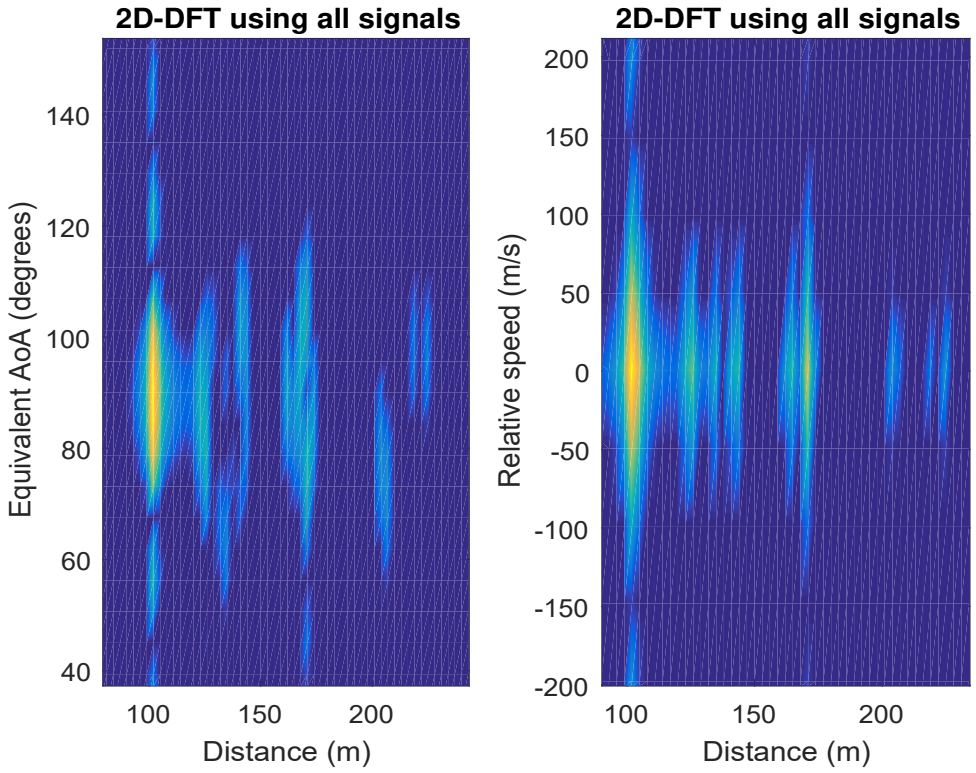

Figure 4.11: 2-D DFT for uplink sensing.

Chapter 5

Radio Sensing in Cluster Channel with Clutter Estimation

5.1 Clutter in Perceptive Mobile Network

The mitigation of static multipaths or commonly known as clutter from received signals is one of the key concerns while performing mobile signal based JCAS. In the recently proposed *perceptive mobile networks* based on JCAS techniques [17], the single transmitted signals are used for both mobile communications and sensing. In a typical environment, BSs receive many multipath signals that are originated from permanent or long-period static objects. These signals are useful for communications, but are generally not of interest for sensing and are known as *clutter* in the traditional radar literature. Clutter is better to be removed before sensing in perceptive mobile networks as it can significantly increase the number of sensing parameters to be estimated and cause sensing algorithms failure [60].

In [76], differential signal based clutter elimination is mentioned to sense moving objects by the perceptive mobile network. Differential receiver implemented by differential filter with adaptive length can be used to find the clutter reduced signal. Differential signal can be taken by only getting the difference between two channel estimation values. However, the OFDM symbol separation over which the differen-

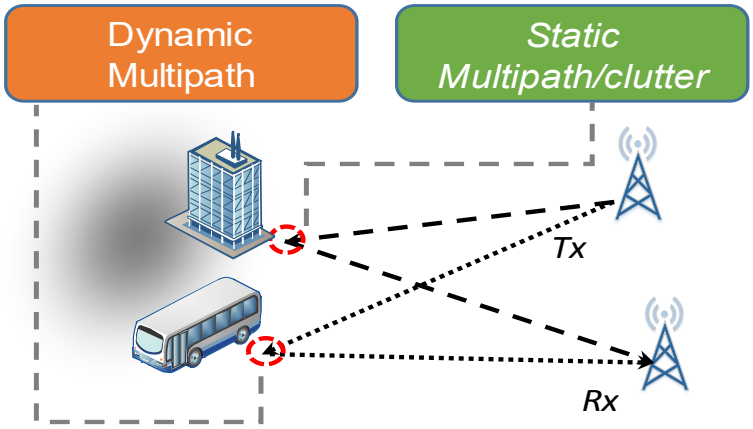

Figure 5.1: Dynamic and static multipaths in JCAS

tiation is taking place needs to be large enough in order to get a sufficient amount of signal amplitude from the subtracted signal output. However, we may miss the parameters containing information of slow moving objects in the environment.

Alternatively, as another solution, background subtraction method, mentioned in [131], [132], can be applied to overcome the problem of differential approach. In order to realize the background subtraction method here to reduce the clutter signal, the average of the all the previous estimated channel values can be subtracted from the instantaneous current estimated channel value. Current estimated channel value contains both dynamic and static multipath components. In the averaged term, only static multipath component values remain. As a result, after this background estimation process, sensing stage can only handle varying multipath components. Fig. 5.1 shows both types of multipaths appearing in a JCAS system.

More specifically, in the process of averaging all of the previous time estimated channel values, all dynamic multipaths will cancel out each other. The cancellation of dynamic terms happens due to Doppler frequency changing during the averaging process. The Doppler frequency changes due to object movement. The changing Doppler induces phase shift. The phase shift term is how related to object movement. For instance, in static multipath, Doppler frequency is zero and then no phase shift changes occur. If the object is moving, then the Doppler frequency is a non zero value where the phase shift value changes with time depending on the behaviour of

object motion. Such multipath with non- zero Doppler frequency is called dynamic or varying multipath. In radio sensing, we are focusing in particular in parameter estimation from those multipaths.

Therefore, dynamic channel component of current OFDM symbol can be expressed as,

$$\Delta \mathbf{H}_{n,t} = \underbrace{\mathbf{H}_t(\text{Dynamic+Static})}_{\text{Instantaneous value}} - \frac{1}{m}\sum_{i=0}^{m-1} \mathbf{H}_{t-i} = \mathbf{H}_t - \mathbf{H}_{\text{average}} \tag{5.1}$$

where, $\mathbf{H}_t$ can be from equation (4.1).

The averaging process can be set up by having a moving smoothing averaging filter with an adaptive window. Window can be taken in the form of a few OFDM symbols. If we decide the window length, then we automatically fix that the averaging will be within that window length. We may not need to move over every symbols for tracking moving channel. The Doppler phase compensation will also be exactly updated for that time period.

Clutter echoes remain stable for long duration, and as a result, while averaging estimated channel values for the previous m OFDM samples, $\mathbf{H}_{\text{average}}$, indicates strong energy value. $\mathbf{H}_{\text{average}}$, only contain static multipath values of previous m samples. Hence, $\Delta \mathbf{H}_{n,t}$ provides dynamic multipath components at t OFDM symbols. This $\Delta \mathbf{H}_{n,t}$ can be taken as an input to the sensing block to reduce the computational complexity. Our next target is to get such improvement in this perceptive mobile network framework development.

5.1.1 Recursive Moving Average based Clutter Reduction

As discussed in Section 5.1, we treat echoes with near-zero Doppler frequencies as clutter. Relatively, we call other echoes with non-zero Doppler frequencies as *dynamic multipath*.

We propose a low-complexity and efficient *Background Subtraction* solution for clutter reduction, which is inspired from the background subtraction method in

image processing [133]. The basic idea is to construct an estimate for clutter by averaging over a long period, and then subtract it from the input to the sensing algorithms. This requires static sensing parameters for clutter, and signals that are unmodulated or modulated with the same data. Hence it is suitable for the indirect sensing scheme, and can also be applied to the direct sensing scheme, but only when the received signals corresponding to the training signals in each frame are used. In the following, we will present the solution by referring to the indirect sensing method.

The proposed processing will be applied to the channel matrix at each subcarrier for each user. From the refined channel matrix estimates, we pick up estimates at an interval of T_h seconds, and denote them as

$$\cdots, \mathbf{H}(i-1), \mathbf{H}(i), \mathbf{H}(i+1), \cdots, \tag{5.2}$$

where the expression of $\mathbf{H}(i)$ is similar to (4.3), but $\mathbf{H}(i_1)$ and $\mathbf{H}(i_2)$, $i_1 \neq i_2$ may have different sensing parameters.

We define a recursive equation for estimating the clutter matrix as $\bar{\mathbf{H}}$

$$\bar{\mathbf{H}}(i) = \alpha \bar{\mathbf{H}}(i-1) + (1-\alpha)\mathbf{H}(i), \tag{5.3}$$

where α is the learning rate (forgetting factor) and the initial one $\bar{\mathbf{H}}(1)$ can be either 0 or computed as the average of several initial $\mathbf{H}(i)$s.

There is a major difference for background subtraction between radio sensing and image processing. In image processing, the image difference corresponds to pixel variation. However, in radio sensing, both Doppler shifts and variation in sensing parameters cause a difference in two channel matrices. This makes the choice of T_h critical in radio sensing.

Consider a Doppler frequency f_D. Its corresponding phase shift at iT_h is given by $\exp(j2\pi f_D T_h i)$. When this multipath's other parameters remain unchanged, applying the recursive equation (5.3) to the whole channel is equivalent to the Doppler

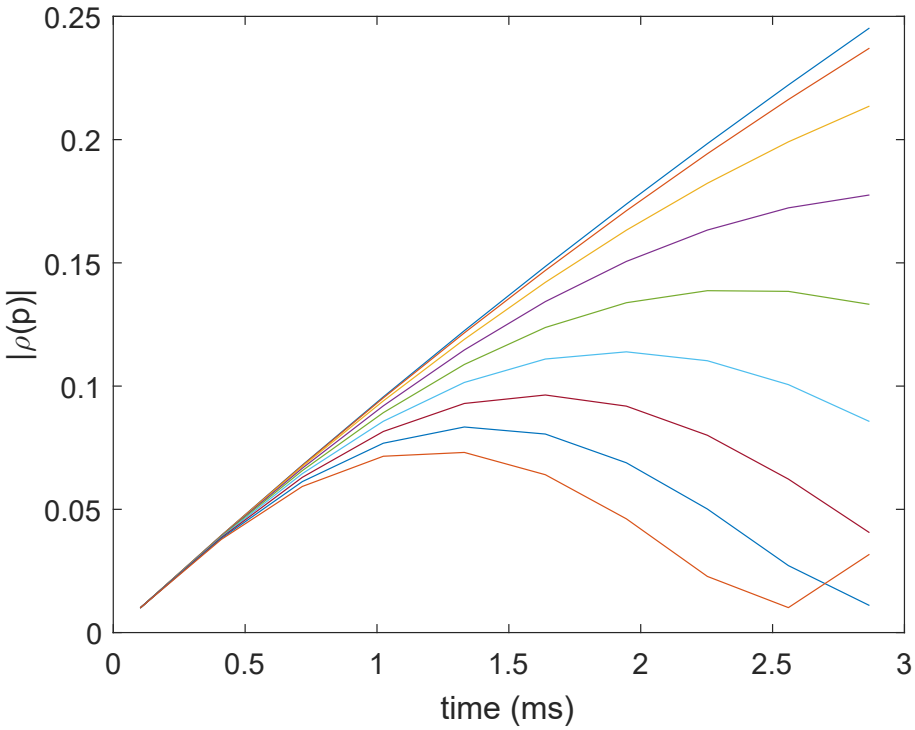

Figure 5.2: Exemplified values of $\rho(p)$, with $T_h = 20T_s$, $\max\{p\} = 30$ at approximately 2.8 ms. Curves from top to bottom correspond to Doppler frequencies from 0 to 400 Hz at an interval of 50 Hz.

phase only. Let $\rho(i)$ and $\exp(j2\pi f_D T_h i)$ replace $\bar{\mathbf{H}}(i)$ and $\mathbf{H}(i)$ in (5.3), respectively. Starting from $i = 1$, after p recursions we can get

$$\rho(p) = e^{j2\pi f_D T_h} \frac{(1-\alpha)(1-\alpha^p e^{j2\pi f_D T_h p})}{1-\alpha e^{j2\pi f_D T_h}}. \tag{5.4}$$

For example, in (5.4), when $f_D = 0, \rho(p) = 1-\alpha^p$. To make $\rho(p)$ approach to 1 with $\alpha = 0.99$ for $f_D = 0$, $p = 500$ is approximately needed.

For typical applications in perceptive mobile networks, the maximum f_D is about 400 Hz, and the channel stable period is in the order of a few milliseconds. Due to the small Doppler frequency value, the Doppler phases typically change slowly over the channel stable period, unless the vehicle moving speed is very large. This makes averaging at small T_h useless in terms of reducing "interfering" dynamic multipath signals from the clutter estimation. An example is shown in Fig. 5.2, which indicates that much larger T_h must be used to get a clear clutter estimate.

Since the slowly changing Doppler phases over the channel stable period generally

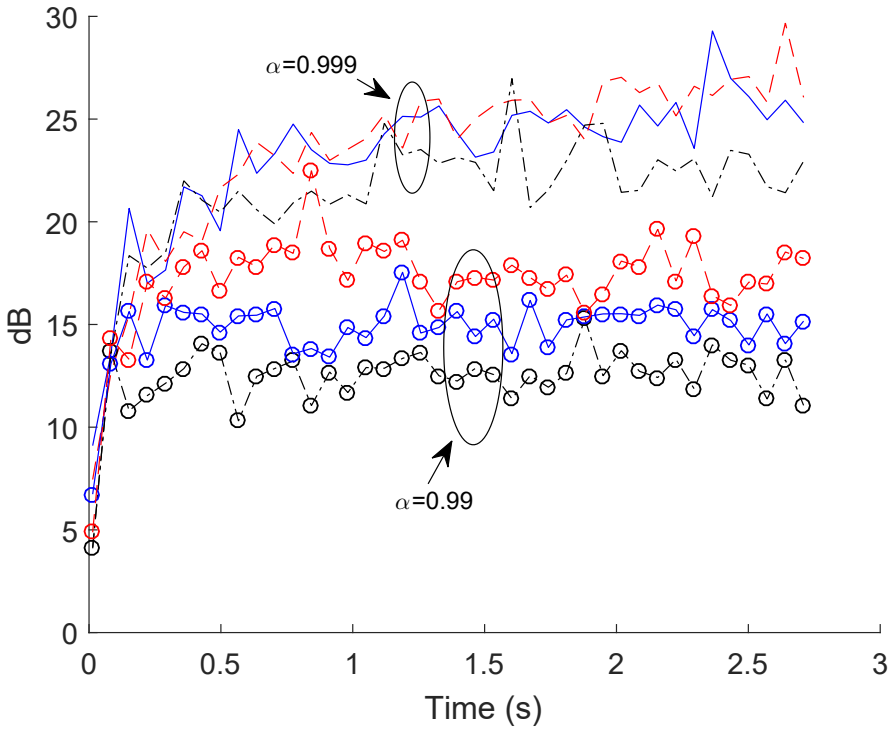

Figure 5.3: Power ratio of the clutter to "interfering signals" after applying the recursive averaging, in the presence of approximately 10 non-clutter interfering signals over each period of $270T_s$ (assumed to be the channel stable period). Red dashed curves for $T_h = 240T_s$, blue solid curves for $T_h = 120T_s$, and black curves for $T_h = 60T_s$.

do not cause cancellation for dynamic multipath signals, we want to minimize the number of samples obtained from each channel stable period. However, smaller sampling rate causes slower collection of the clutter signals. Hence a trade-off is needed here, and the reasonable value is found to be 1 or 2 samples per medium channel stable period. A more optimal value may be determined through statistical analysis over a distribution of the Doppler frequency and the channel stable period. On the other hand, the learning rate α also has an important impact on the averaging operation. These effects are demonstrated in Fig. 5.3. We can see that the power ratio becomes almost stable after 0.5 and 2 seconds of recursive averaging operation for $\alpha = 0.99$ and 0.999 respectively. The stabilization of this power ratio is the convergence in clutter estimation. Larger α achieves better performance.

The clutter estimate is always updated every T_h seconds using (5.3). Once a stable estimate is obtained, it is subtracted from the current and future refined

channel estimates during the interval T_h.

For noisy channel estimates, we can work out the distribution parameters of the combined noise output after the recursion. Assuming the noise in different channel estimates is uncorrelated and each follows the same Gaussian distribution with mean zero and variance σ^2. Then the output noise matrix will still have zero mean, and covariance matrix $\sigma_c^2\mathbf{I}$, with

$$\begin{aligned}\sigma_c^2 &= \sigma^2(1-\alpha^{-1})^2\sum_{i=1}^{p}(\alpha^2)^i \\ &= \sigma^2(1-\alpha)^2\frac{1-\alpha^{2p}}{1-\alpha^2},\end{aligned} \tag{5.5}$$

It can be seen that when p is large, σ_c^2 approaches to $\sigma^2(1-\alpha)^2/(1-\alpha^2)$. When $\alpha = 0.99$, it becomes $0.005\sigma^2$. Hence noise is suppressed in the recursive operation. Our simulation shows that it converges approximately at $p = 150$.

Therefore when subtracting the clutter from the current channel estimate, the noise is almost not increased. This is an advantage of the background subtraction method. In addition, the clutter channel matrix output from the recursive algorithm also allows us to efficiently estimate the clutter. Comparing two estimates obtained at different times, we can also efficiently identify the changes in static objects in the radio image.

Note that by adjusting the parameters in the recursion equation, we can actually obtain signals with different Doppler frequencies. Hence this method can be extended for separating multipath signals with different Doppler frequencies into different groups.

5.1.2 Effect of Clutter Suppression by Recursive Moving Average

We only present the simulation results for the background subtraction method here, as for the differential method, in the simple form, it is almost a repeat of the simulation in Section 4.1.3 with increased number of multipath and noise. The clutter

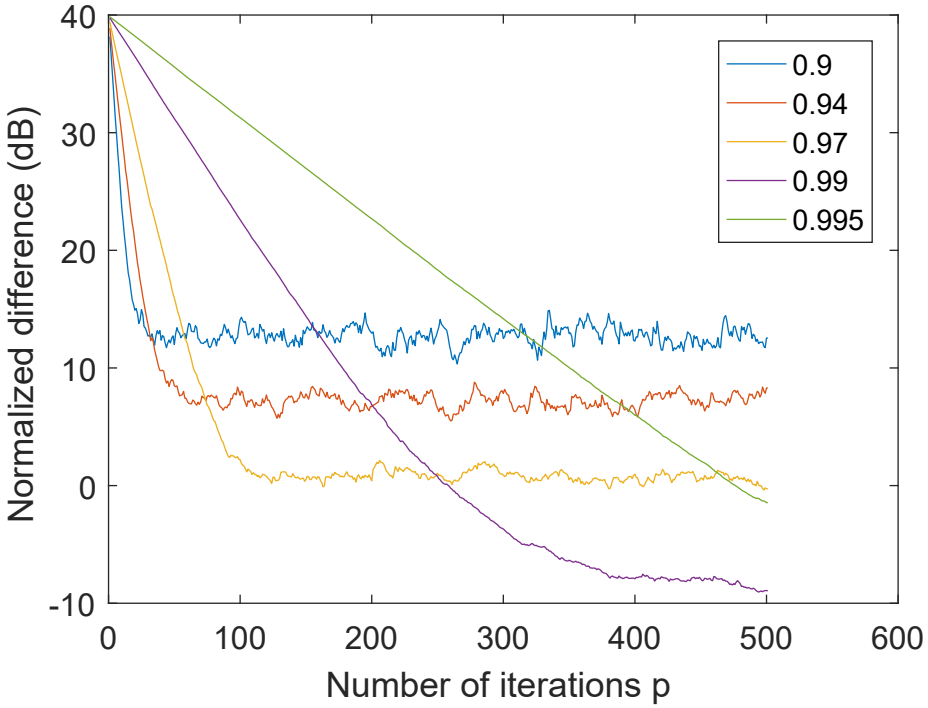

Figure 5.4: Difference between the reconstructed and the true clutter signals, normalized to the power of the true clutter. Learning rates α for curves from left to right are 0.9,0.94,0.97,0.99 and 0.995, respectively.

signals are generated similarly to other multipath signals, with Doppler frequencies set to be zero. Simulation settings and system parameter values described in 3.1.7 are applicable here for simulation.

In Fig. 5.4, we plot the normalized difference between the output from the recursive reconstruction algorithm and the actual clutter. We use one sampled channel estimate within each channel stable period of 2 ms. The figure indicates that $\alpha > 0.99$ is a good option that balance the difference and convergence time. The curve for $\alpha = 0.99$ is also consistent with the analytical one in Fig. 5.3.

In Fig. 5.5, we show three random implementations with different values of p used in estimating the clutter. From the top figure we can see both missed estimation for the current dynamic multipath and the estimate for the clutter and some residual dynamic multipath, which still have a strong presence in the subtracted signal. The middle one shows improved performance, and the bottom one achieves excellent estimation with clutter completely removed. This figure demonstrates the effectiveness of the proposed background subtraction algorithm.

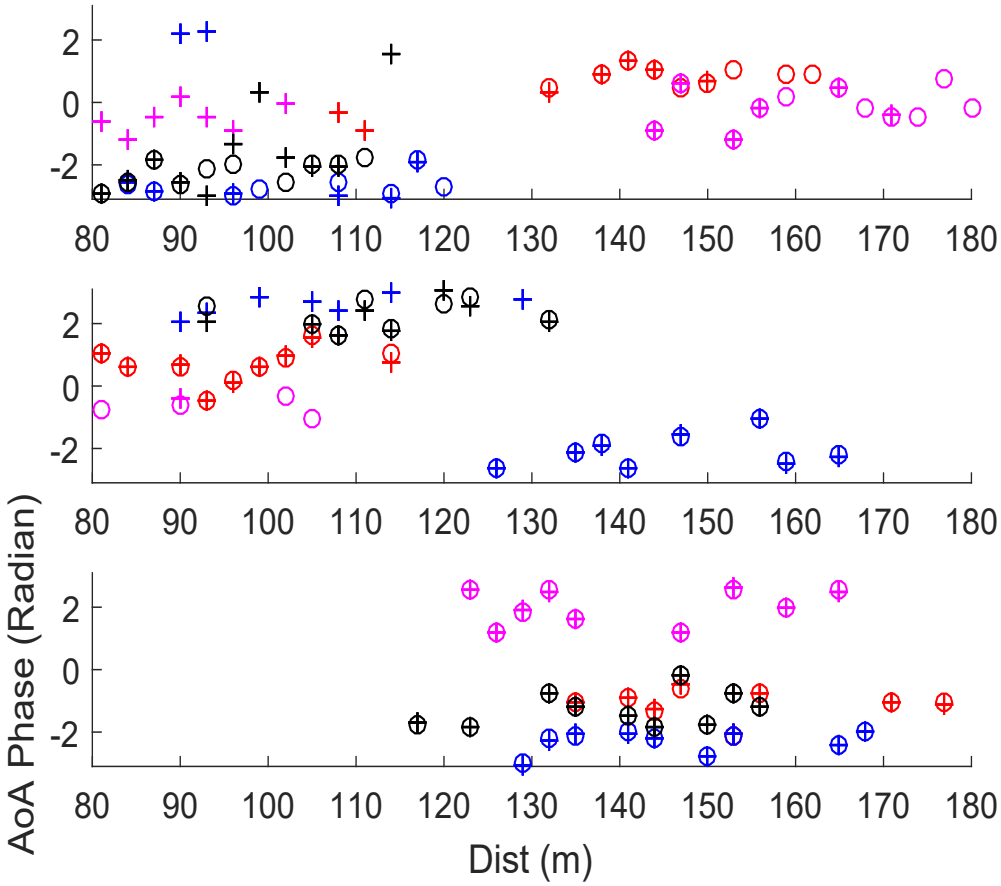

Figure 5.5: Estimated and true sensing parameters AoA and distance obtained using the indirect method after clutter suppression. From top to bottom, $p = 25, 50, 150$, respectively. Channel estimation $\eta = 15$ dB.

5.1.3 Gaussian-Mixture-Model based Clutter Mitigation

Suppression of undesired non-information bearing multipaths from received signals is a key process for sensing parameter estimation in perceptive mobile network, which is proposed as a cellular network with integrated radar sensing. This section proposes a clutter suppression method based on the GMM and EM estimation. We then apply a 1D CS based sensing algorithm to extract useful channel information after removing the estimated clutter. Simulation results are provided and validate the effectiveness of the proposed scheme.

In [17], and Section 5.1.1, we proposed a recursive method based on background subtraction. This method is simple and effective, but its performance highly depends on the assumption of unchanged signal phases across packets which may not always

be met in practice.

In this section, we propose a novel clutter estimation and suppression method, called *GMM-EM-CE*, based on GMM and EM for perceptive mobile networks. GMM has been widely used for analyzing and separating moving objects from the background in image and video analysis [133] and speech processing [134]. It has also been applied recently to extract static channel state information from channel measurement in [135], using estimated signal parameters. Different to GMM in video analysis where background and foreground cover each other, clutter and multipath of interest in perceptive mobile networks are additive and can coexist. Different to [135], we apply GMM directly to the received signals rather than to the estimated channel parameters. For the first time, we demonstrate how to apply GMM to complicated modern mobile communication signals with MU-MIMO and OFDMA modulations and adopt an EM algorithm for clutter estimation and separation. We also show how to perform clutter-free radio sensing from extracted dynamic signals.

We consider 5G-compatible DMRS [86] for sensing, which are comb-type training signals at non-equally-spaced interleaved subcarriers. The values and indices of interleaved DMRS subcarriers of received signals are known to the BS when doing sensing from the received signals.

After removing the DMRS signals, the estimated frequency-domain channel matrix $\hat{\mathbf{H}}$ at the n-th subcarrier in the t-th OFDM block between the $k-th$ transmitter and the BS receiver is given by (4.1). The channel estimation error is approximated as AWGN. The SIR between the mean power of the channel coefficients and AWGN is denoted by Υ.

The true channel matrix $\mathbf{H}_{n,k,t}$ can be represented as (4.2). In this case, we consider clutter as propagation paths with near-zero Doppler-frequencies. Now, $\mathbf{H}_{n,k,t}$ can be written as,

$$\mathbf{H}_{n,k,t} = \mathbf{H}^{dy}_{n,k,t} + \mathbf{H}^{st}_{n,k,t}, \tag{5.6}$$

where $\mathbf{H}^{st}_{n,k,t}$ and $\mathbf{H}^{dy}_{n,k,t}$ refer to (static) clutter matrix and dynamic channel matrix,

respectively. Both $\mathbf{H}^{st}_{n,k,t}$ and $\mathbf{H}^{dy}_{n,k,t}$ have a size of $M \times M_T$.

Note, the total number of multipaths $L = L_1 + L_2$, where L_1 is the number of paths from moving scatters and L_2 is the number of paths from static scatters.

Our clutter reduction method focuses on separating $\mathbf{H}^{st}_{n,k,t}$ from $\mathbf{H}_{n,k,t}$. Once the clutter $\mathbf{H}^{st}_{n,k,t}$ is estimated, it can be removed from $\mathbf{H}_{n,k,t}$ to reduce the unknown parameters to be estimated and improve the accuracy of target sensing parameter estimation.

5.1.4 Proposed GMM-EM-CE Method

Fig. 5.6 highlights the major processes in the GMM-EM-CE method. Firstly, estimated channel matrix is obtained from the received signal and then GMM-EM is used to estimate the clutter. The clutter estimate is then subtracted from the channel estimate to obtain the dynamic channel, and 1D CS technique is finally applied to accomplish radio sensing.

Signal Modelling Using GMM

Wireless channels can be modeled and estimated by a mixture of Gaussian distributions since each density represents multipaths in the channel [136]. Static and dynamic paths can be represented by Gaussian distributions with very different parameters over the time domain. This is because over a short time period, $\mathbf{H}^{st}_{n,k,t}$ changes little and $\mathbf{H}^{dy}_{n,k,t}$ could vary significantly. It is also quite common that static paths typically have larger mean power than dynamic ones. Hence, their distributions at least have very different variance values: static paths have near zero variances, which is much smaller than those of the dynamic ones. Therefore, by learning the mean values of the distribution, static paths can be identified and separated via comparing the variance. GMM on the repeated prior received channel distribution of (4.1) for each user can provide the approximate distribution of the static multipaths with the EM principle.

We define ρ as a measure of clutter to dynamic signal ratio for all users K at

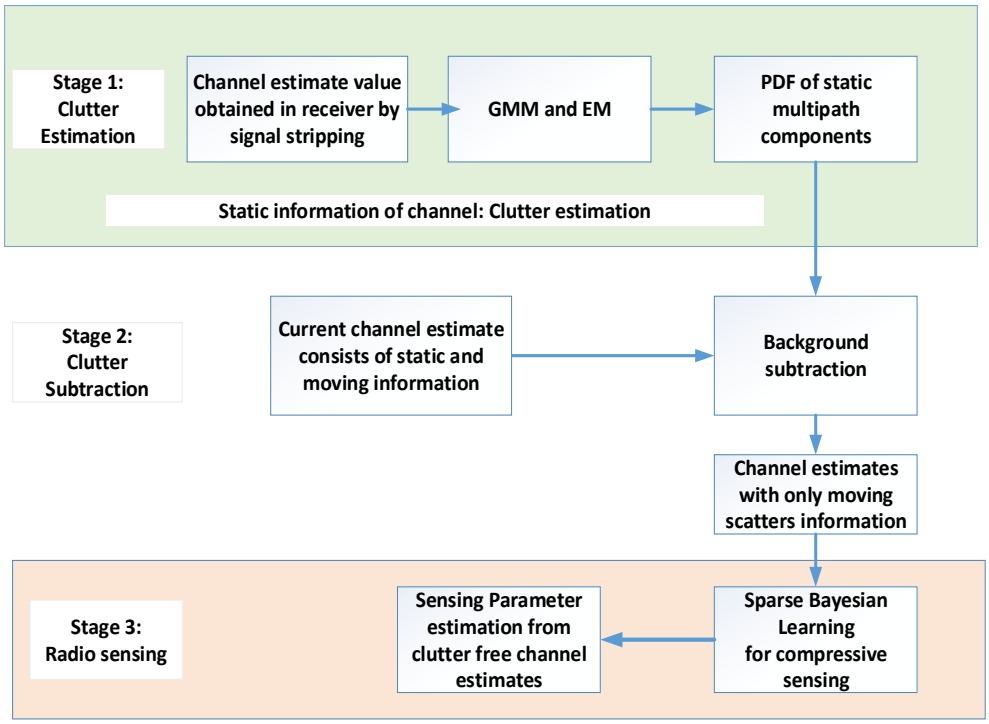

Figure 5.6: Processes of the proposed GMM-EM-CE method.

the t-th OFDM block, which is given by

$$\rho = \frac{1}{NMK} \sum^{N} \sum^{M} \sum^{K} \left| \frac{\mathbf{H}^{st}_{n,k,t}}{\mathbf{H}^{dy}_{n,k,t}} \right|. \tag{5.7}$$

The GMM consists of L multivariate Gaussian distributions known as mixture components [135]. The probability density function (PDF) of multipath channel is obtained based on the estimated channel data, $\hat{\mathbf{H}}_{n,k,t}$ in (4.1). The PDF for GMM for the estimated channel is expressed as,

$$P(\mathbf{\Theta}_{t_h}) = \sum_{l=1}^{L} \omega_l . \eta(\mathbf{\Theta}_{t_h} | \mu_l, \Sigma_l). \tag{5.8}$$

where $\eta(\mathbf{\Theta}_{t_h} | \mu_l, \Sigma_l)$, each component of the multivariate Gaussian mixture $l = 1, .., L$ has its mean value μ_l, covariance matrix Σ_l and non-negative mixing weight ω_l. Here the value of $\mathbf{\Theta}_{t_h}$ in (5.8) is taken the same as $\hat{\mathbf{H}}_{n,k,t}$ in (4.1) for over a time t_h and d is the dimension of $\hat{\mathbf{H}}_{n,k,t}$.

Assuming moving scatters move a short distance over the period of t_h and the individual Gaussian distribution $\eta(\mathbf{\Theta}_{t_h}|\mu_l, \Sigma_l)$ is given by

$$\eta(\mathbf{\Theta}_{t_h}|\mu_l, \Sigma_l) = \frac{1}{(2\pi)^{\frac{d}{2}} |\Sigma_l|^{\frac{1}{2}}} e^{-\frac{1}{2}(\hat{\mathbf{H}}_{n,k,t}-\mu_l)^T \Sigma_l^{-1} (\hat{\mathbf{H}}_{n,k,t}-\mu_l)}. \tag{5.9}$$

The Expectation Maximization Algorithm

Here, we estimate $\omega_l, \mu_l, \Sigma_l$ to maximize the log-likelihood function $\sum_{i=1}^{N_s} P((\mathbf{\Theta}_{t_h})_i)$, where $(\mathbf{\Theta}_{t_h})$ denotes the set of samples and $(\mathbf{\Theta}_{t_h})_i$ denotes its $i-th$ element. Note, N_s is the number of samples taken within the period of t_h. EM starts from some initial estimate of $\omega_l, \mu_l, \Sigma_l$ and then proceeds to iteratively updating them until convergence is detected. The detailed operations in each EM iteration are described next.

In the *expectation* step, we estimate the probability matrix of $(\mathbf{\Theta}_{t_h})_i$ generated by the l^{th} Gaussian mixture component from dividing the weighted probabilities by the sum of weighted probabilities as

$$\Omega(i,l) = \frac{\omega_l.\eta((\mathbf{\Theta}_{t_h})_i|\mu_l, \Sigma_l)}{\sum_{j=1}^{L} \omega_j.\eta((\mathbf{\Theta}_{t_h})_i|\mu_j, \Sigma_j)}. \tag{5.10}$$

We take initial mean μ_l as a randomly selected data point from the set $(\mathbf{\Theta}_{t_h})$. We use the overall covariance of the dataset $(\mathbf{\Theta}_{t_h})$ as the initial variance Σ_l and assign unit prior probability as initial mixing weight ω_l. EM algorithm is then used to derive the parameters of the GMM.

In the *maximization* step, we estimate the updated $\omega_l, \mu_l, \Sigma_l$. The updating equations are given by

$$\mu_l = \frac{1}{N_l} \sum_{i=1}^{N_s} \Omega(i,l)(\mathbf{\Theta}_{t_h})_i. \tag{5.11a}$$

$$\Sigma_l = \frac{1}{N_l} \sum_{i=1}^{N_s} \Omega(i,l)((\Theta_{t_h})_i - \mu_l)((\mathbf{\Theta}_{t_h})_i - \mu_l)^T. \tag{5.11b}$$

$$\omega_l = \frac{N_l}{N_s}. \tag{5.11c}$$

where $N_l = \sum_{i=1}^{N_s} \Omega(i,l)$. The final $\{\omega_l, \mu_l, \Sigma_l\}$ are obtained when the results either converge or the maximal number of iterations N_m is reached. Then we obtain the clutter estimate as $\hat{\mathbf{H}}^{st}_{n,k,t}$ from the finalized values of $\{\omega_l, \mu_l, \Sigma_l\}$. That means, clutter estimation is actually the estimate of the mean with covariance matrix near zero.

Clutter Free Sensing Parameter Estimation

Now, we get the clutter free channel estimate, $\hat{\mathbf{H}}^{dy}_{n,k,t}$, as

$$\hat{\mathbf{H}}^{dy}_{n,k,t} = \hat{\mathbf{H}}_{n,k,t} - \hat{\mathbf{H}}^{st}_{n,k,t}, \tag{5.12}$$

Referring to (4.2), we consider delay-on-grid signal model where the delays $\tau_\ell f_0$ are quantized as q_ℓ/N' with q_ℓ being an integer and $N' = gN$. Therefore $e^{-j2\pi n\tau_\ell f_0} \approx e^{-j2\pi n q_\ell/N'}$. Then, the dynamic channel matrix part of (5.6) can be written as,

$$\mathbf{H}^{dy}_{n,k,t} = \sum_{\ell=1}^{L_1} b_\ell e^{-j2\pi n q_\ell/N'} e^{j2\pi t f_{D,\ell} T_s}.$$

$$\mathbf{a}(M,\phi_\ell)\mathbf{a}^T(M_T,\theta_\ell) = \mathbf{A}_R \mathbf{D}\mathbf{C}_n \mathbf{A}_T^T, \tag{5.13}$$

where the ℓ-th column in $\mathbf{A}_R$ (or $\mathbf{A}_T$) is $\mathbf{a}(M,\phi_\ell)$ (or $\mathbf{a}(M_T,\theta_\ell)$), $\mathbf{D}$ and $\mathbf{C}_n$ are diagonal matrices with the ℓ-th diagonal element as $b_\ell e^{j2\pi t f_{D,\ell} T_s}$ and $e^{-j2\pi n q_\ell/N'}$, respectively.

By stacking similarly formulated row vectors for all usable subcarriers together, we obtain

$$\hat{\mathbf{H}}^{dy}_{n,k,t} = \mathbf{W} \underbrace{\mathbf{D}\mathbf{A}_R^T \mathbf{A}_T^T}_{\boldsymbol{G}}, \tag{5.14}$$

where the ℓ-th column of the $N_u \times L$ matrix $\mathbf{W}$ is $\{e^{-j2\pi n q_\ell/N'}\}$.

Now, we do sensing parameter estimation for each user using $\hat{\mathbf{H}}^{dy}_{n,k,t}$ of (5.14) by the same developed indirect method in our earlier work in [17] by extending 1D CS algorithms [121]. Here we consider only one multipath signal stays within each

quantized delay bin for each user.

$\mathbf{\Psi}_1$ with N_A number of columns is used as dictionary for delay, being a partial overcomplete DFT matrix, approximating $\mathbf{W}$. After treating (5.14) as an on-grid MMV CS problem, we get the estimate for $\boldsymbol{G}$. Once the delays and $\boldsymbol{G}$ are estimated, we get the AoA estimates through calculating the cross-correlation between columns from $\boldsymbol{G}$ on the indices obtained from a given threshold as below,

$$\hat{\phi}_\ell \approx \frac{1}{\pi}\angle\big(\underbrace{\sum_{p=1}^{M-1}((\boldsymbol{G})_{\cdot,p})^*(\boldsymbol{G})_{\cdot,p+1}}_{\varepsilon_\ell}\big), \tag{5.15}$$

where $(\boldsymbol{G})_{\cdot,p}$ denote the p-th column of $\boldsymbol{G}$.

The value of $|b_\ell|^2$ can also be obtained easily during the process of computing AoA, being $|\varepsilon_\ell|^2$. The estimates of $|b_\ell|^2$ can be used to find the effective multipath delay bins in noisy channels from the MMV CS estimation output by using a threshold of $\gamma \cdot \max(\text{abs}(\varepsilon_\ell))$ determined, e.g., as a fractional scalar of the maximum power of multipath signals.

5.1.5 Simulation Results for GMM-EM-CE

We consider a system setup with 4 SDMA users, each with a single antenna, and a BS with a 4 antenna uniform linear array. The signal bandwidth is assumed to be 100 MHz and the carrier frequency is 2.35 GHz. Propagation channels are generated based on clustered channel model following a complex Gaussian distribution, which mimics the ray tracing model. Multipaths in each cluster are generated following uniform distributions of $[5, 10]$ for the total multipath number. Random continuous values are generated within a given range as actual values for AoAs, AoDs, Doppler shift, delay, and amplitude. We use a pathloss model with pathloss factor 40 for downlink and 20 for uplink sensing. The transmission power of the RRU and MS is 30 dBm and 25 dBm respectively.

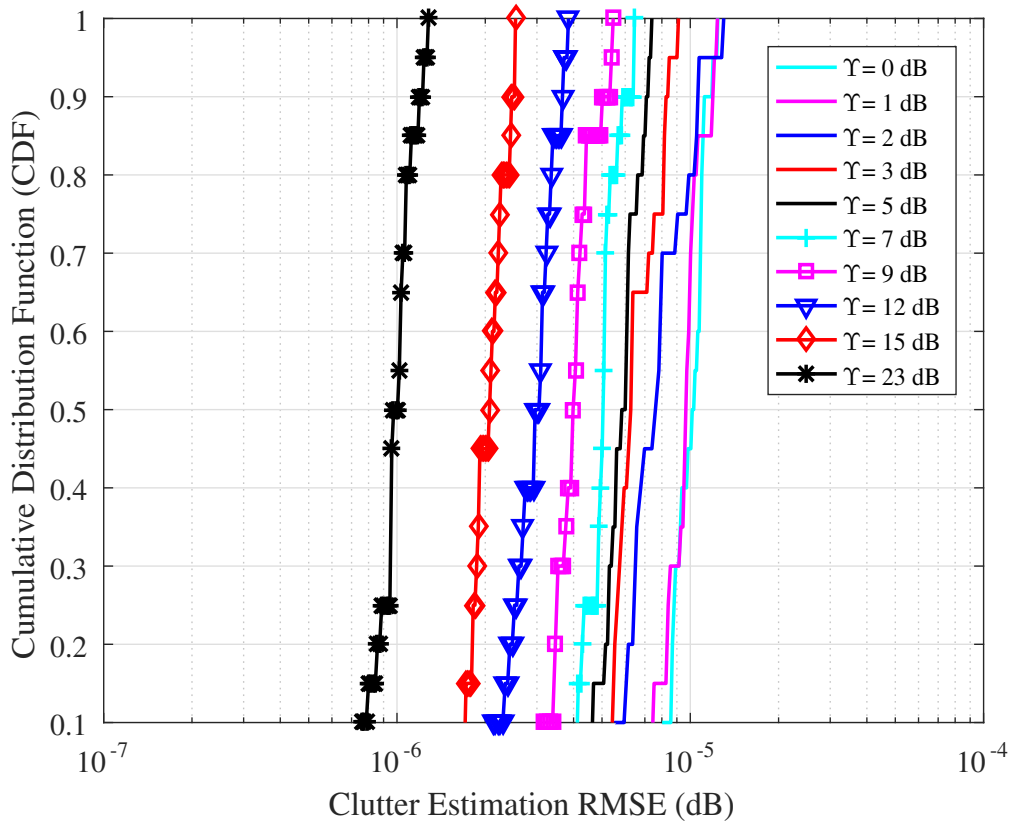

Figure 5.7: CDF of RMSE at different Υ values.

Performance Evaluation of GMM-EM-CE

GMM-EM is applied to obtain the clutter channel estimation, $\hat{\mathbf{H}}^{dy}_{n,k.t}$. Then we calculate root mean square error (RMSE) of clutter estimation as

$$RMSE = \sqrt{\frac{1}{(\Psi * NMK)} \sum_{j=1}^{\Psi} \left| \hat{\mathbf{H}}^{st}_{n,k,t} - \mathbf{H}^{st}_{n,k,t} \right|^2}. \tag{5.16}$$

We take histogram-based PDF from the correct window of 40 bins while $\Psi = 20$. Then, interpolated cumulative distribution functions (CDF) are derived from the PDFs of RMSE to present clutter estimation results.

Fig. 5.7 provides CDF results for RMSE of clutter estimation obtained at different values of SIR, Υ with $N_m = 10$. The figure shows that the RMSE is quite small at a high probability and it also decreases with Υ increases.

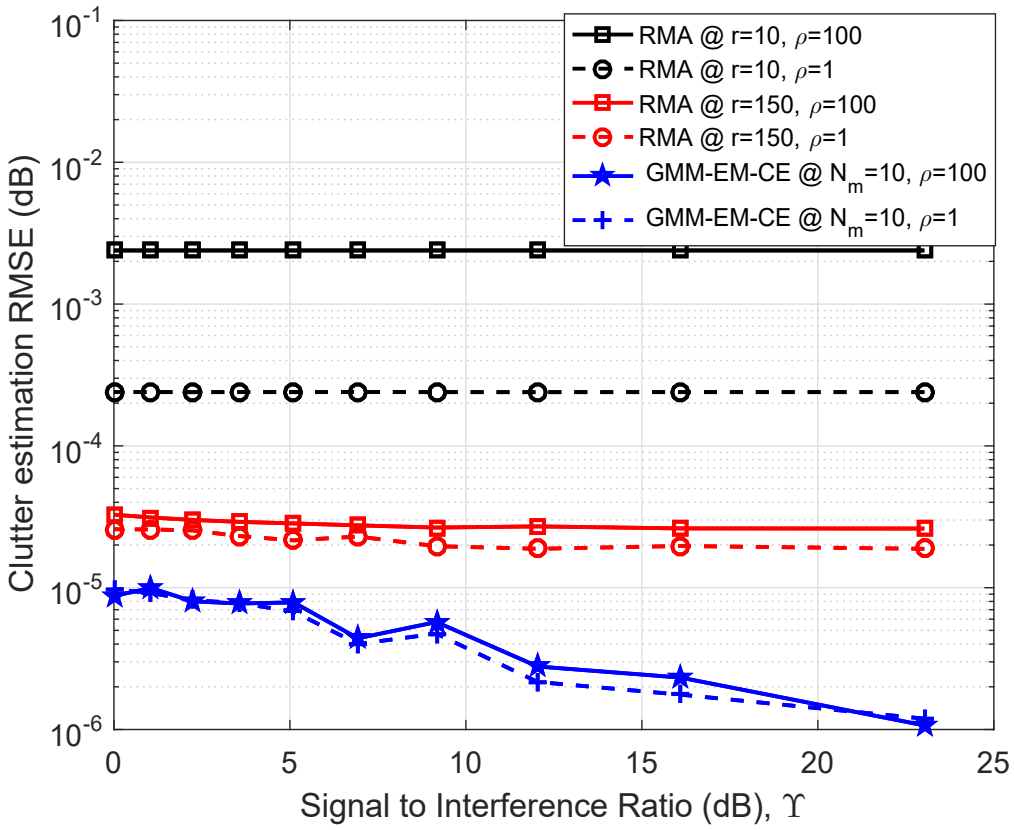

Figure 5.8: Clutter estimation RMSE values vs Υ at high and low values of ρ for GMM-EM-CE and RMA method.

Comparison of GMM-EM-CE and Recursive Averaging

Next we compare GMM-EM-CE with the simple recursive moving average (RMA) method [17], which estimates the clutter via averaging over channels at different measurements using a forgetting factor.

Fig. 5.8 provides clutter estimation RMSE results vs Υ values obtained at high and low ranges of ρ for both GMM-EM-CE and RMA. The RMSE of clutter estimation with GMM-EM-CE is obtained at $N_m = 10$. Whereas, the RMSE of RMA is obtained with the forgetting factor of 0.95 over both $r = 10$ and 150 iterations. For both cases of $\rho = 1$ and 100, the GMM-EM-CE method with $N_m = 10$ outperforms RMA with both $r = 10$ and 150 iterations, achieving significant lower RMSE for clutter estimation.

Radio Sensing Results

Fig. 5.9 demonstrates the results of AoA estimation in the uplink sensing, for the cases with (in the top plot) GMM-EM-CE and with (in the bottom plot) RMA. A total of $N_u = 128$ interleaved subcarriers are used. The estimates with clutter reduction by GMM-EM-CE with $N_m = 10$ are shown to be much more accurate compared to those by RMA with the same 10 iterations. Moreover, different from the bottom plot, the top plot results show no presence of residual clutter in AoA estimation. Note that, with the increment of iterations r and simulation complexity, the RMA method can also provide more accurate AoA estimation with complete clutter removal as seen in our earlier work in [17]. Hence, GMM-EM-CE indicates its usefulness by providing more accurate results at much lower complexity and iterations in comparison with the RMA method.

5.1.6 Summary

We showed the background subtraction method for clutter suppression and provided indirect CS results. After that, we presented Gaussian mixture model based clutter estimation algorithms for joint communication and sensing and provided 1D CS based cluster channel parameter estimation results using estimated dynamic channels. These results indicate that reasonable radio sensing performance can be achieved with clutter free channel estimation.

5.2 Radio Sensing with Cluster Multipath Channels

In earlier proposed JCAS solutions, as shown in Fig. 2.4, for example, in [1], and in [76], we cast the radio sensing problem as a block sparse/sparse reconstruction problem. In practice, multipath signals always arrive in clusters [128], and paths from one cluster typically come from the same scatter(s) and have close parameter values.

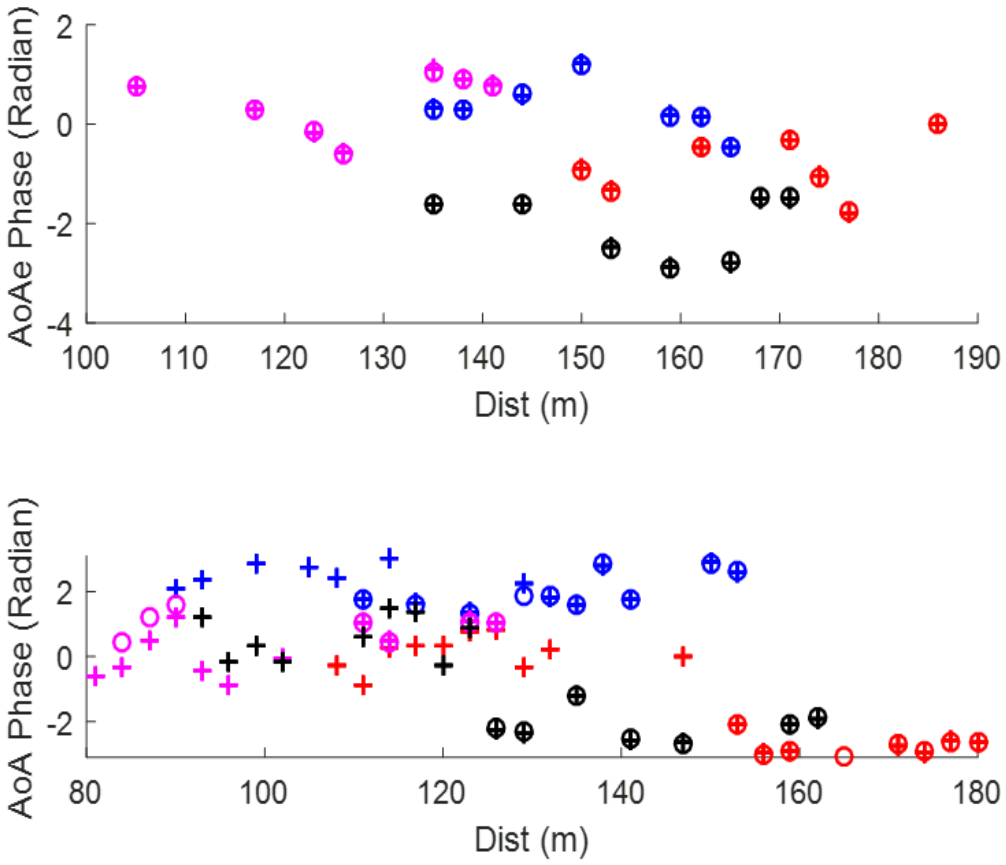

Figure 5.9: Uplink sensing at $\gamma = 0.25$, $\Upsilon = 12\ dB$, $\rho = 1$, after clutter suppression by (top) GMM-EM-CE with $N_m = 10$ at $t_h = 30\ ms$ and by (bottom) RMA with $r = 10$. The estimated values for AoA are shown in star and the actual AoAs are shown in circle. Different colours correspond to different users.

As explained earlier in Chapter 2, there exist research outputs on reconstructing cluster sparse signals in general, for example, through periodic compressive support [61], model based CS [62], variational Bayes approach [63], and block Bayesian method [64]. In [65] a millimetre-Wave joint radar and communication system for indoor scenarios is developed, using estimated radar channel coefficients. However, there is only very limited work on how cluster sparsity can be exploited in JCAS systems such as perceptive mobile networks that involve OFDMA and MU-MIMO. Due to the complicated signal structure in perceptive mobile networks, significant modification and adaptation are needed for exploiting existing cluster sparse signal reconstruction algorithms.

In this section we exploit the cluster property in multipath channels and propose

a novel 2D CS algorithm for sensing parameter estimation in perceptive mobile networks. In particular, we introduce a method for characterizing the prior probability density function and propose a 2D cluster Kronecker (kron) CS algorithm. Referring to the 5G NR standard, we use the OFDM-type DMRS in the 5G specification [87] for sensing. We consider both downlink and uplink sensing, where downlink and uplink communication signals are used for sensing, respectively.

The rest of the work is as follows. In Section 5.2.1, we introduce 5G usable signal and clustered channel description. In Section 5.2.2, we present the proposed algorithm based on a 2D kron-OMP method. In Section 5.2.3, we provide simulation results.

5.2.1 Signal and Cluster Channel Models

Referring to the 5G NR standard signals with OFDMA and SDMA (or MU-MIMO) modulations and channel described in Section 4.2.1, we use the OFDM-type DMRS 5G usable signals and Cluster-Chl channel [74] for sensing using the proposed algorithm based on 2D kron-OMP techniques. We consider both downlink and uplink sensing, where downlink and uplink communication signals are used for sensing, respectively.

5.2.2 Proposed Cluster based 2D Kron-OMP Algorithm

Since the signals are relatively independent in the three domains of delay, AoA and Doppler, they can be formulated as a 3D cluster sparse signal. Then, we can apply cluster based greedy method equipped with cluster prior probability to estimate these sensing parameters. In a typical system, we can get a sufficient number of observations for the delay (linked to the number of subcarriers), AoA (linked to the number of antennas) and a limited number of samples in the Doppler domain (linked to DMRS signals over a portion of channel coherent period). Next, we present the proposed cluster-based sensing algorithm referring to the received signal in (4.11).

2D Cluster Kron-OMP Algorithm

We assume that there is only one multipath signal within each quantized delay bin. Let M_r and M_T denote the number of antennas for receiving in BS and in each user for transmitting, respectively. Let $\mathscr{S}_s$ denote the set of available subcarriers for sensing and let N_s denote its size. Referring to (4.11), we can stack signals $\mathbf{Y}_{n,t}, n \in \mathsf{S}$ from all available subcarriers to a matrix and obtain

$$\mathbf{Y}_t = \mathbf{W} \underbrace{\mathbf{D}_t \mathbf{A}_{tx}}_{\mathbf{G}_t} \mathbf{A}_{rx}^T + \mathbf{Z}_t, \tag{5.17}$$

where $\mathbf{W}$ is a $N_s \times L$ matrix with its ℓ-th column being $\{e^{-j2\pi n \tau_{q,\ell} f_0}\}$. Note that N_s is typically smaller than N and the indices of subcarriers are often dis-continuous.

We construct two dictionaries for AoA and delay, $\mathbf{\Psi}_1$ and $\mathbf{\Psi}_2$, being two partial overcomplete DFT matrices, approximating $\mathbf{A}_{rx}$ and $\mathbf{W}$, respectively. Let N_A and N_D be the number of codes, i.e., the number of columns, in $\mathbf{\Psi}_1$ and $\mathbf{\Psi}_2$. In practical applications, the non-zero entries of the sparse signals appear in clusters over each column of the matrix $\mathbf{G}_t$ in $\mathbf{Y}_t$. We can then treat (5.17) as an on-grid 2D cluster sparse CS problem with a $M_r \times N_s$ observation matrix $\mathbf{Y}_t$, two dictionaries $\mathbf{\Psi}_1$ and $\mathbf{\Psi}_2$, and block sparse signals $\mathbf{G}_t$ of k- sparsity that appears in clusters. Such a problem can be solved by using, for example, the 2D block sparse Bayesian CS in [64] and 2D kron-OMP in [129]. However, no prior information on the cluster structure is properly applied in these solutions.

Our proposed novel 2D cluster kron-OMP algorithm incorporates a cluster prior Δ to the sparse probability of each entry in the support set, ξ. Such an incorporation exploits both cluster structure and sparsity in the solution than conventional 2D kron-OMP algorithms.

For producing the cluster prior Δ, at each iteration, inspired from the neighborhood model [137], we can compute the cluster pattern through measuring the changes in the values of ξ. We first compute the absolute sum of the differences in

the support set ξ via

$$\Delta(\xi) = \sum_{i=1}^{k} |\ \xi_i - \xi_{i-1}|\ . \tag{5.18}$$

The cluster prior for the support learning vector ξ is dependent on the term $e^{-\alpha(\Delta(\xi))}$ for $\alpha > 0$. We model the behavior of the function $e^{-\alpha(\Delta(\xi))}$ via the Gamma distribution,

$$(\Delta|\beta, \alpha) \sim \Gamma(\beta, \alpha), \tag{5.19}$$

where β and α are the shape and rate parameters of the Gamma distribution, respectively. We also assume that $\beta = 1$ and as a result,

$$(\Delta|\beta, \alpha) \propto e^{-\alpha\Delta}. \tag{5.20}$$

The conditional joint probability density function of $\mathbf{Y}_t$ and Δ can be written as

$$\begin{aligned} &P(\mathbf{Y}_t, \Delta|\alpha, \mathbf{\Psi}_1, \mathbf{\Psi}_2, \mathbf{G}_t, \xi) \sim \\ &P(\mathbf{Y}_t|\mathbf{\Psi}_1, \mathbf{\Psi}_2, \mathbf{G}_t, \xi, \alpha, \Delta)P(\Delta|\beta, \alpha). \end{aligned} \tag{5.21}$$

With the constructed prior probabilities, we can then extend conventional 2D kron-OMP algorithms to incorporate such prior information. The proposed 2D cluster kron-OMP algorithm is detailed in Algorithm 1.

Initially at iteration $i = 0$, the residual value $\boldsymbol{R}^{(0)}$ is set as $\mathbf{Y}_t$ and the initial non-zero index locations are set as $J_0 = \emptyset$. As the iteration progresses, we find the updated indices J at step 4 by $\max \left|\mathbf{\Xi}^{\boldsymbol{i}}\right|$, corresponding to the case where the dictionary $\mathbf{\Psi}$ has maximum correlation with the residual $\boldsymbol{R}^{(i)}$. After computing Δ in step 5, the support set ξ is updated at step 6 with the extracted index locations J by utilizing the joint probability density function in (5.21). The prior on the parameter α in (5.19) is assumed to have Gamma distribution, $\alpha|\eta, \theta \sim \Gamma(\eta, \theta)$, and

Algorithm 1 2D Cluster Kron-OMP Algorithm

Input: Estimation of $\boldsymbol{G}_t$.

Input: Observation matrix $\mathbf{Y}_t \in \mathbb{R}^{M_r \times N_s}$, combined dictionary $\boldsymbol{\Psi} = (\boldsymbol{\Psi}_1 \in \mathbb{R}^{M_r \times N_A}, \boldsymbol{\Psi}_2 \in \mathbb{R}^{N_s \times N_D})$,
iteration control threshold ρ, sparsity k, initial cluster sparse estimate $\hat{\mathbf{G}}_t = \emptyset$, initial index $J_0 = \emptyset$

Output: Reconstructed signal $\hat{\mathbf{G}}_t$ after k iteration, non-zero positions J, residual $\boldsymbol{R}^{(k)}$

1: **Initialization** $\boldsymbol{R}^{(0)} = \mathbf{Y}_t$
2: **while** $i \leq k$ **do**
3: Compute $\boldsymbol{\Xi} = \boldsymbol{\Psi} * \boldsymbol{R}^{(i)}$
4: Compute index J so that $\max |\boldsymbol{\Xi}^i|$
{finding the atom and indices J in cases where
$\boldsymbol{\Psi}$ is with maximum correlation with residual}
5: Compute Δ
6: Update ξ with extracted J now at with probability proportional to $\max \left| e^{((c^2/2(\sigma)^2 * \boldsymbol{\Xi}^i) - \alpha\Delta)} \right|$
and update the support ξ as $\xi^i = \xi^{i-1} \cup J$
7: Update α from $\Gamma(\eta, \theta + \Delta)$
8: Compute $\boldsymbol{\Omega} = \text{pinv}(\boldsymbol{\Psi}_2{}^* \bigotimes \boldsymbol{\Psi}_1)\mathbf{Y}_t$
9: Update $\boldsymbol{R}^{(i)} = \mathbf{Y}_t - \boldsymbol{\Psi}_1 \text{diag}(\boldsymbol{\Omega})\boldsymbol{\Psi}_2{}'$
10: If $\boldsymbol{R}^{(i)} < \rho$, $i = i + 1$
11: Compute $\hat{\mathbf{G}}_t = \text{sptensor}(J_i, \boldsymbol{\Omega}, M_r)$

we experimentally set $\eta = \epsilon$ and $\theta = 1$, where ϵ denotes the length of the support learning vector ξ. With the progression of measurements, at step 7, the posterior density on α is updated. This posterior distribution can be described as,

$$P(\alpha|\eta, \theta, \Delta) \sim \Gamma(\eta, \theta + \Delta), \tag{5.22}$$

where $P(\alpha|\eta, \theta, \Delta)$ denotes the conditional posterior density on α given the related parameters. We estimate this via $E[\alpha|\eta, \theta, \Delta] = \eta/(\theta + \Delta)$. Then, we compute $\boldsymbol{\Omega}$ as the multiplication product of $\mathbf{Y}_t$ and Moore-Penrose pseudoinverse of kronecker product of $\boldsymbol{\Psi}_1$ and $\boldsymbol{\Psi}_2$ in step 8. Finally the estimate $\hat{\mathbf{G}}_t$ is computed as a sparse matrix of size $N_A \times N_D$ derived from open MATLAB sparse tensor (sptensor) toolbox [138] with J_i and $\boldsymbol{\Omega}$ for M_r. The algorithm usually stops when the iteration i reaches the desired sparsity level of k for $\hat{\mathbf{G}}_t$.

Estimation of Sensing Parameters

The proposed 2D cluster kron-OMP algorithm can obtain direct estimation for any two parameters out of delay, AoA and Doppler. Since we can have sufficient measurements in the delay and AoA domain, the algorithm can provide good estimates for both delay and AoA directly from $\mathbf{Y}_t$ of (5.17) using each DMRS signal of 2D observations. Note, in step 6 of Algorithm 1, $c = 1/(1+\sigma^2)$, where σ^2 is the thermal noise variance. We can obtain efficient estimates $\hat{\mathbf{G}}_t$ and non-zero indexes J for the expanded matrix of $\mathbf{G}_t$ that corresponds to $\mathbf{\Psi}$, using the prior cluster structure knowledge.

Note that the proposed algorithm can identify any pair of {delay, AoA} with at least one different value. So $\hat{\mathbf{G}}_t$ will not be a diagonal matrix anymore if one variable in the pair has two identical quantized values.

After getting the estimate $\hat{\mathbf{G}}_t$, we can then get the delay and AoA estimates according to the J indices of the non-zero values in $\hat{\mathbf{G}}_t$, corresponding to respective columns in the two dictionaries.

The Doppler shift is estimated via calculating the angle of the cross-correlation values between the non-zero values of $\hat{\mathbf{G}}_t$ obtained at J indices over two DMRS signals. Assume the interval between every two estimates of $\mathbf{G}_t$ and $\mathbf{G}_{t+1}$ is uniform and be T_s for any t, which can be relaxed easily. This can be represented as

$$f_{D,q,\ell} \approx \frac{1}{2\pi T_s} \angle \left(\hat{\mathbf{G}}_t \hat{\mathbf{G}}_{t+1}^* \right)_{\ell,\ell}. \tag{5.23}$$

Averaging can be taken over the correlation obtained from multiple DMRSs before computing the angle, to improve the accuracy of the estimates.

5.2.3 Simulation Results for 2D Cluster Kron-OMP Algorithm

We present simulation results for direct estimation over delay-AoA and delay-Doppler domains using quantized and continuous-value sensing parameters. In the simula-

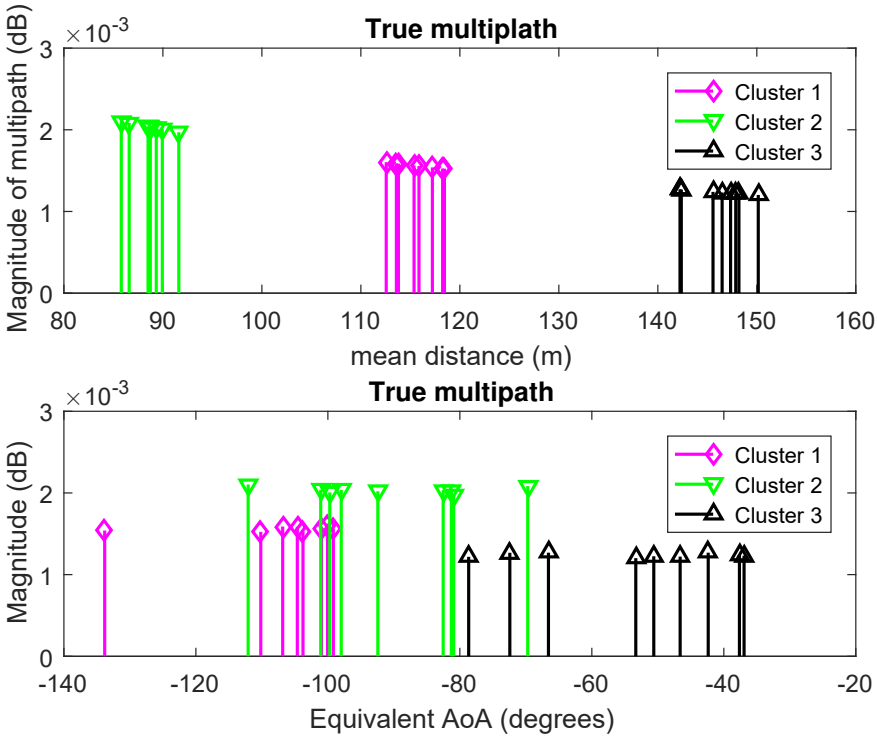

Figure 5.10: CIR for cluster channel.

tion, we consider a system with 4 SDMA users, each with a single antenna, and a BS with a 16 antenna uniform linear array. Estimated values (typically shown in blue star) are placed with actual ones (shown in red circle) to verify the accuracy.

Fig. 5.10 shows an exemplified CIR for 3-cluster multipath channels consisting of rich multipaths. Propagation paths in each cluster have close parameter values particularly in the distance (delay) domain, and different clusters are distinguished by different colors.

Downlink Sensing

In downlink sensing, we use DMRS subcarrier configuration type-1 slot-wise, with every alternating subcarriers selected from a total of $N = 252$ subcarriers. So, in total $N_s = 126$ DMRS subcarriers are used. Total 8 OFDM packets are used for estimating the Doppler frequency.

The simulation results are presented in Fig. 5.11 for the case when the proposed 2D cluster kron-OMP algorithm is applied to delay-AoA and delay-Doppler

domains, respectively. For quantized on-grid parameters, as shown in the top two sub-figures, we can obtain nearly perfect estimation of delay, AoA and Doppler. For continuous off-grid parameters, as shown in the bottom two sub-figures, performance degradation can be observed with reduced accuracy and missed estimates. However, the estimates preserve the cluster structure, and convey correct information for determining the location and moving speed of the scatters.

Uplink sensing

For uplink sensing, the allocated subcarriers are limited by configuration. The results in this case can particularly show the usefulness of the proposed algorithm. In the simulation, clusters are generated with continuous delay and AoA values. We take configuration of type-2 with non-slot-wise subcarrier, where only $N_s = 28$ DMRS subcarriers (7 PRB) of layer 4 are used.

Fig. 5.12 provides the simulation results for the proposed algorithm. Both AoA-Distance and Speed-Distance results for the estimated points are well matched with all clusters. However there are a few missed estimates for speed.

For comparison, we present the simulation results in Fig. 5.13 for the conventional 2D kron-OMP method [129] that does not consider cluster prior so that we can directly compare the actual accuracy of estimates obtained in Fig. 5.12. There are some major problems with this method, compared to the proposed one. Firstly, we note that there exists the estimation accuracy problem and hence missed estimation occurs in cluster channels, which is overcome by the cluster prior in the proposed algorithm. Secondly, we have to use a threshold of $T_h = -15\ dB$ to pick up "effective" estimates with significant power. Comparatively, in the proposed algorithm, the indices are generated automatically without using any explicit threshold. Thirdly, even when we relax the accuracy requirement of the estimates and observe the zoomed box section of estimates, we see that the estimates are hardly following the cluster pattern of the actual ones in Fig. 5.13.

Moreover, we do Monte-Carlo trials for both our proposed 2D cluster kron-OMP

and conventional 2D kron-OMP for same non-quantized channel parameters with $N_s = 28$ DMRS subcarriers. Uplink sensing simulated for N_{iter} trails each time and we compute the RMSE for AoA estimates at each N_{iter} as,

$$RMSE_{AoA} = \sqrt{\frac{1}{(N_{iter}L)} \sum_{j=1}^{N_{iter}} \sum_{\ell=1}^{L} \left| \hat{\phi}_{\ell,j} - \phi_{\ell,j} \right|^2}. \tag{5.24}$$

AoA estimation performance is evaluated versus all N_{iter} iterations considered in top figure and versus number of clusters in channels with $N_{iter} = 100$ in bottom figure of Fig. 5.14 respectively. The proposed 2D cluster kron-OMP algorithm achieves the best performance for all iterations in comparison with its cluster-less peer 2D kron-OMP. In addition, as we increase the number of clusters in Cluster-Chl, we can also observe relatively better estimation in the proposed algorithm.

5.2.4 Comparative Study on Computational Complexity

Existing algorithms have respective shortcomings for sensing parameter estimation in perceptive mobile networks, as compared with the simulation results obtained from the proposed methods. Generally, the classical 2D DFT method is simple and less complex but this provides low resolution in comparison with all the results of proposed 1D-3D CS and requires a full set of measurements in time or frequency domain. Again, in ESPRIT and MUSIC, the reasonable resolution requires at least a large segment of consecutive samples and this is not always available in uplink sensing. In contrast, off-grid type compressive methods do not require consecutive samples but implementation for real time operation imposes high complexity. Moreover, off-grid CS contain respective constraints on the parameter estimation range and the minimum separation of the parameter values [17]. We rather establish the received signals to an arrangement such that from it any of the methods in 1D-3D CS algorithms can be functional to acquire the estimates for the sensing param-

eters from the linked sparse reconstructed estimates corresponding to the utilized dictionaries.

Normally, higher-dimensional CS algorithms achieve better estimation performance with the price of much higher computational complexity. The sensing problem becomes more critical when the number of measurements is limited because of the short channel coherent time and a small number of antennas in the perceptive mobile network. In the case of using on-grid CS methods, the number of available observations in the selected dimension plays an important role in dominating the estimation accuracy and resolution. The lack of sufficient measurements in each dimension could likely create large quantization errors even using high-dimensional on-grid CS algorithms such as the Tensor tool and Kronecker CS in the domains of Doppler frequency, AoD and AoA. Fortunately, the cellular signals usually have hundreds to thousands of subcarriers, which provide numerous measurements for the delay. Therefore, quantizing the only delay can hypothetically lead to reduced errors. In particular in the 2D cluster kron-OMP, the cluster prior probability density function that introduced with the CS reconstruction algorithm, efficiently detect the coarse locations of the clusters, leading to more accurate sparse reconstruction performance when 2D Kron CS algorithms are applied.

5.2.5 Summary

We have proposed a 2D cluster Kronecker OMP algorithm for sensing parameter estimation in perceptive mobile networks, which can exploit the cluster structure in multipath channels. By introducing a cluster prior, our algorithm can efficiently detect the coarse locations of the clusters, leading to more accurate sparse reconstruction performance when block CS algorithms are applied. Simulation results demonstrate better parameter estimation accuracy, for both on-grid and off-grid channel models, compared to the scheme without using prior knowledge.

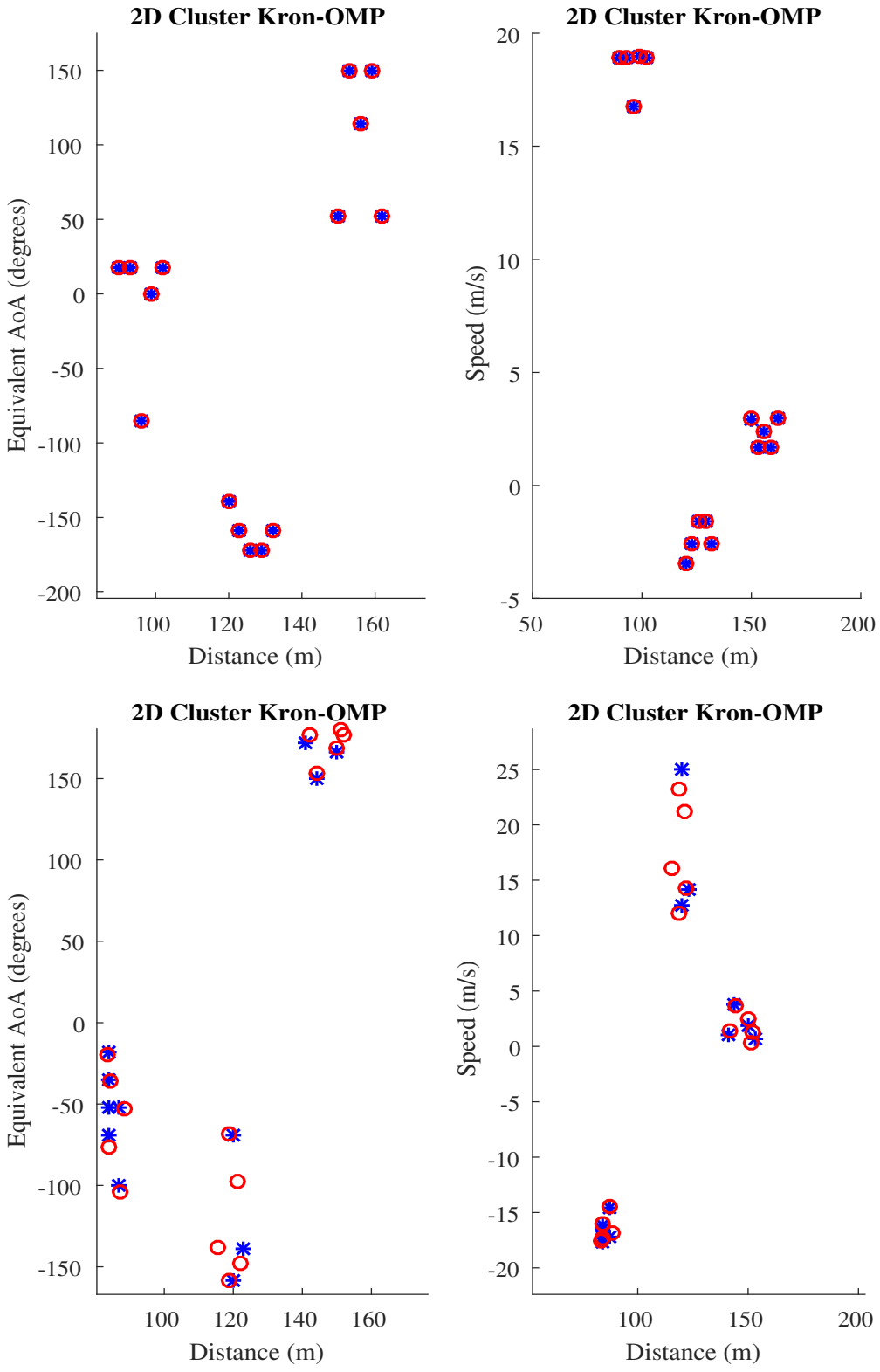

Figure 5.11: Two random realizations of downlink sensing using the proposed 2D cluster kron-OMP algorithm for quantized (top sub-figures) and non-quantized (bottom sub-figures) channel parameters.

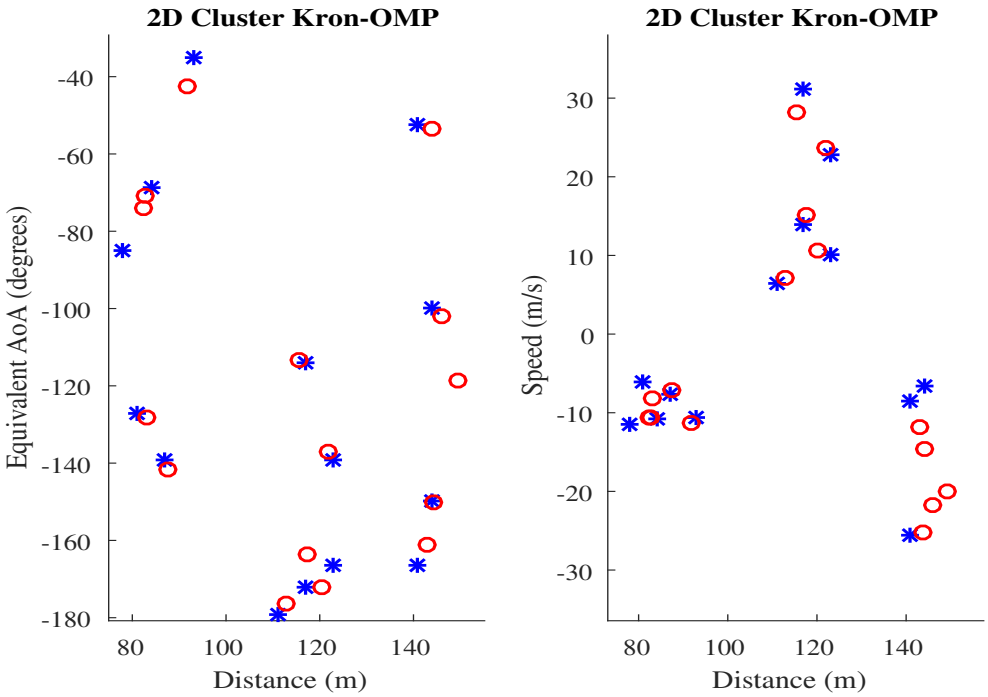

Figure 5.12: A random realization of uplink sensing using the proposed 2D cluster kron-OMP algorithm for non-quantized channel parameters.

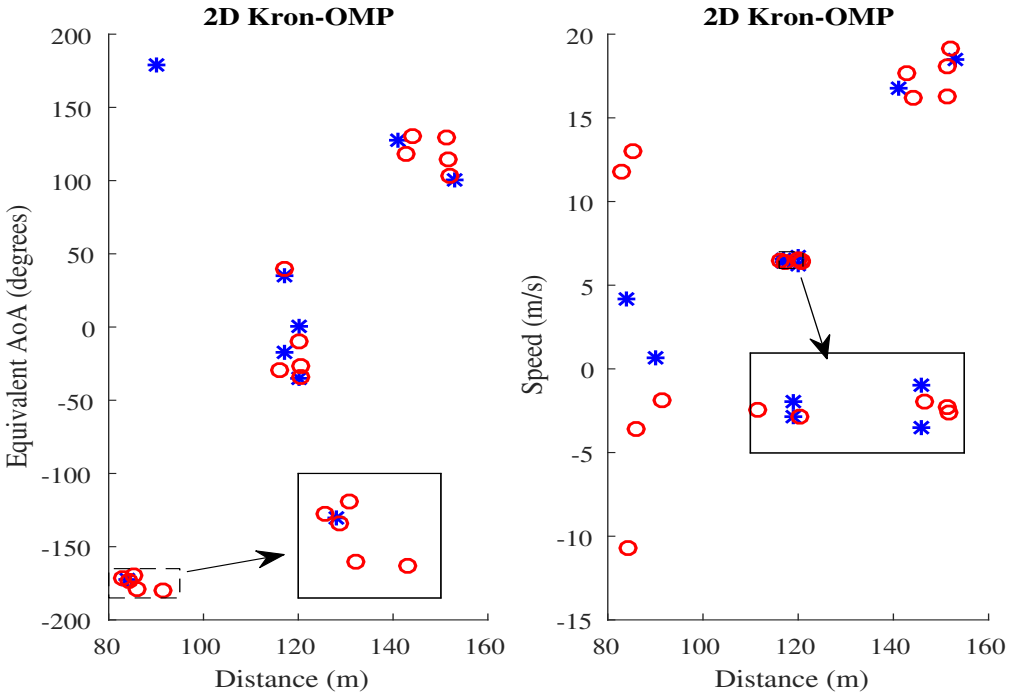

Figure 5.13: Uplink sensing using 2D kron-OMP for non-quantized channel parameters with $N_s = 28$ DMRS subcarriers (7 PRB). Black zoomed in boxes are for showing certain missed estimates incapability of preserving cluster pattern.

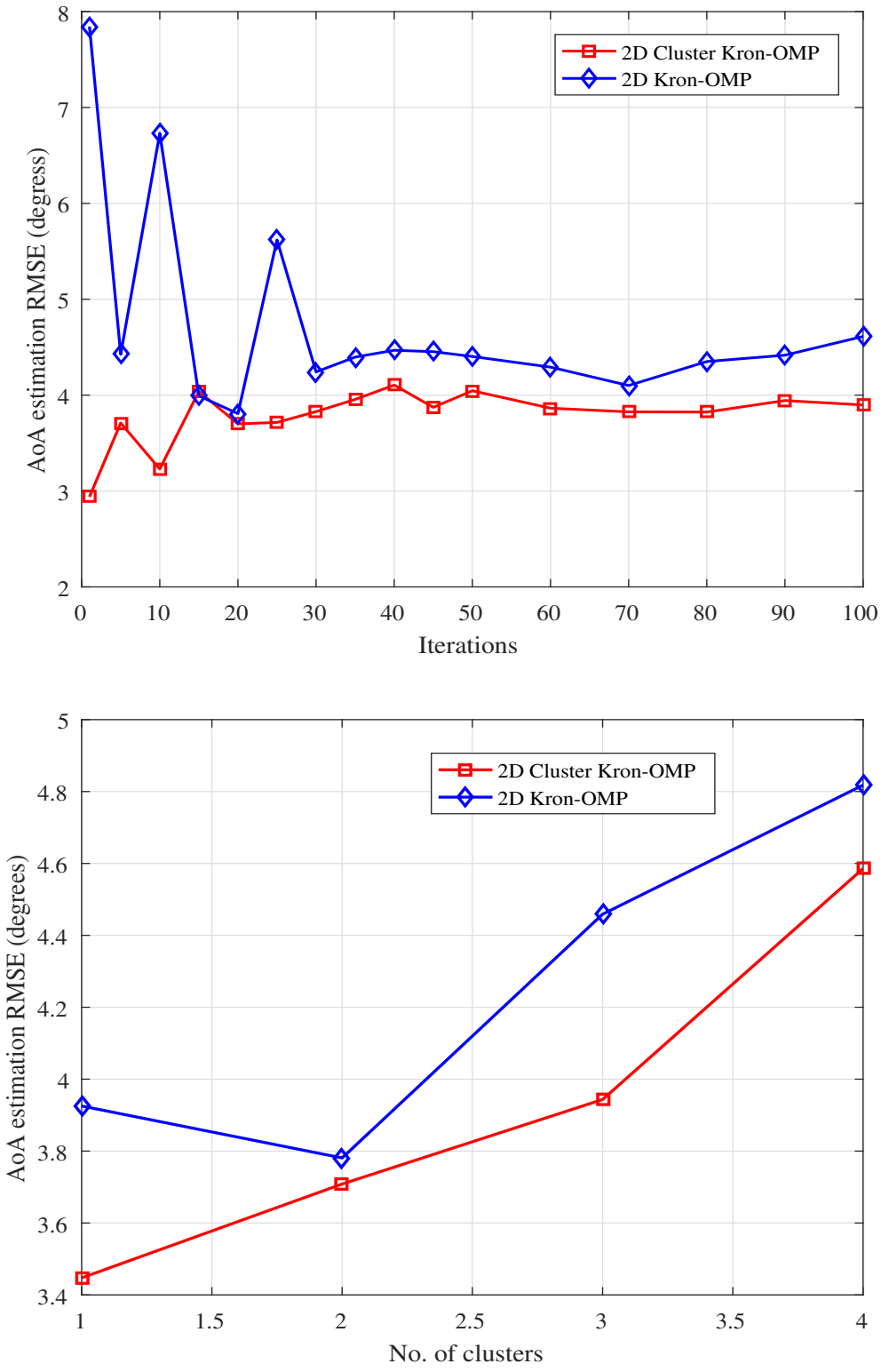

Figure 5.14: RMSE of the AoA estimates obtained by both methods with $N_s = 28$ for non-quantized channel parameters

Chapter 6

Conclusions and Future Work

6.1 Conclusions

This thesis has developed a framework for a perceptive mobile network that integrates radio communication and sensing into one system, transforming the current communication-only mobile network. The proposed framework presents a unified platform that enables both uplink and downlink sensing, using the uplink and downlink communication signals, respectively. There have been many studies on joint communication and radio sensing systems, as we have referenced in Chapter 2. However, the perceptive mobile network is the one that systematically studies how to apply JCAS to the large-scale cellular networks, by specifically considering the system architecture, signal and propagation models in cellular networks.

In Chapter 2, we compared our work to known works on existing JCAS systems, passive radar sensing and radar and communication coexisting systems. This thesis also presents the required system modifications to enable the integration of these systems. It is one of the major contributions of this thesis as discussed in the Introduction chapter. One major issue for the integration here is how to deal with the transmission signal leakage to the receiver for sensing, while communication systems do not naturally have the capability of suppressing such leakage signals. Hence we first state that such a problem does not exist in uplink sensing and therefore no significant changes are needed in uplink sensing. However, downlink sensing requires

hardware changes for JCAS operation. The full duplex technology is presented as one potential solution to enabling JCAS on the current communication-only platform. Due to its immaturity, we also presented two near-term alternative solutions in Chapter 2. After that the thesis formulated the mathematical model for sensing. We proposed both the direct and indirect schemes based on compressive sensing for estimating the sensing parameters.

In this thesis, the multipath is randomly generated following a cluster channel model with complex Gaussian distribution. The sensing algorithms are tested in the presence of AWGN for direct method in Chapter 3, and both AWGN and channel reconstruction error for the indirect method in Chapter 4. We further introduced the background subtraction method and the Gaussian mixture model for clutter suppression in Chapter 5. Our scheme is shown to work efficiently and is particularly suitable for the cases when sufficient measurements are only available in one domain.

This thesis illustrates three preliminary sensing algorithms using 1D, 2D and 3D compressive sensing algorithms, and provides simulation results, using channels generated from both our own cluster model and 5G QuaDRiGa channel model. These results indicate that reasonable sensing performance can be achieved, and demonstrate respective advantages and disadvantages of these algorithms. This thesis work also disclosed some interesting research problems to work on as future works, such as the ambiguity problem due to interleaved subcarriers and reduced resolution in 3D CS algorithms.

This thesis also proposes a 2D cluster Kronecker OMP algorithm for sensing parameter estimation in perceptive mobile networks, which can exploit the cluster structure in multipath channels. By introducing a cluster prior, our algorithm can efficiently detect the coarse locations of the clusters, leading to more accurate sparse reconstruction performance when block CS algorithms are applied. Simulation results demonstrate that our proposed algorithm can achieve better parameter estimation accuracy, for both on-grid and off-grid channel models, compared to the scheme without using prior knowledge.

The perceptive mobile network can potentially facilitate many new sensing applications in smart city, smart home and smart transportation, while providing communication services. Although there are significant challenges ahead to make the perceptive mobile network fully operational, this work here is a solid first step, demonstrating the feasibility and way forward.

6.2 Future Work

We have demonstrated in Chapter 3, Chapter 4 and Chapter 5 that using available compressive sensing techniques to DMRS signals, we can achieve acceptable sensing results with either a direct or indirect scheme in cluster channel with reduced clutter. However, there remain problems to be solved, and the sensing accuracy is expected to be further improved too. Some of these problems are:

- How to solve the ambiguity problem that may be present in all domains, but particularly for the delay?

  We discussed this issue in Section 4.2.3 and provide a few suggestions, such as, selection of the right estimate, for example, the magnitude, or integration of coarse and fine estimation methods for reducing the ambiguity in solutions.

- How to do sensing based on limited observations for uplink sensing when a user is only allocated with a small number of resource blocks?

  The uplink (DMRS) signals for one user may only occupy a very limited number of subcarriers. Therefore, we can only get a small number of observations for the delay estimation, which could be even less than the number of multipaths. In this case, it will be insufficient to estimate each multipath, and the output can contain large errors. We are looking at potential solutions for this problem, for example, by designing better dictionaries and using filtering techniques.

- Whether we can construct a better sensing dictionary to achieve a good balance

between interpreting physics and quantization error in on-grid compressing sensing? Will it be feasible to use off-grid sensing and how?

Most of the existing techniques, including our results presented in Chapter 3, 4 and 5, use the DFT dictionary or its variants for sensing. DFT dictionary is particularly suitable for the time-delay-line type of channel models, but they become less efficient for cluster channels, since each column in the dictionary can only represent one multipath. When the number of multipaths is large, which is typical for cluster multipath, this dictionary becomes ineffective. On the other hand, the cluster structure of multipath may be better modelled by other dictionaries such as the wavelet. We are currently investigating such cases which can allow us to represent the cluster multipath with lower sparsity. Moreover, theoretical analysis of the performances of the developed sensing techniques can also be a future research direction, for example, the Cramer-Rao lower bound derivation for the estimated sensing parameters.

Appendix A

DMRS Signals

A.1 Generation of DMRS Signals

The DMRS signal sequence $\chi(n)$ is generated as,

$$\chi(n) = \frac{1}{\sqrt{2}}(1 - 2 * c * (2 * n)) + j\frac{1}{\sqrt{2}}(1 - 2 * c * (2 * n + 1)). \tag{A.1}$$

Pseudo random sequence $c(i)$ is based on Gold sequence and $c(i)$ sequence generator initialized with,

$$c_{init} = (2^{17}(\mathbf{N}_{symb}^{slot} * \eta_{s.f}^{\mu} + \ell + 1)(2 * \mathbf{N}_{ID}^{\eta_{SCID}} + 1) + 2 * \mathbf{N}_{ID}^{\eta_{SCID}} + \eta_{SCID}) \text{mod } 2^{31}. \tag{A.2}$$

Here, ℓ is the OFDM symbol number within the slot, μ is subcarrier numerology, $\eta_{s.f}^{\mu}$ is the slot number within a frame, then η_{SCID} is given by the DMRS sequence initialization field, and $\mathbf{N}_{symb}^{slot}$ gives the number of symbols per slot, and finally $\mathbf{N}_{ID}^{\eta_{SCID}}$ is given by the DMRS configuration.

The generation of DMRS is defined relative to a three-dimensional resource element (RE) grid representing a 14-symbol slot for the full carrier (in the PDSCH or PUSCH numerology) across the layers/DMRS ports of the PDSCH. Each column of DMRS RE represents the grid locations for a separate layer/port (the third dimension of the grid). The complex values of DMRS sequence are also returned in

matrix, mainly the DMRS signal. DMRS signal values and indices both are known to the BS, and we can use these indices as a prior when obtaining sensing results from received signals.

In terms of frequency domain DMRS density, there are two different RRC prescribed configuration types. Configuration type 1 defines 6 subcarriers per PRB per antenna port, comprising alternating subcarriers. Configuration type 2 defines 4 subcarriers per PRB per antenna ports, consisting of 2 groups of 2 neighbouring subcarriers. Different shifts are applied to the sets of subcarriers used, dependent on the associated antenna port or code division multiplexing (CDM) group. For type 1, there are 2 possible CDM groups/shifts across up to 8 possible antenna ports (p=1000...1007), and, for type 2, there are 3 possible CDM groups/shifts across 12 ports (p=1000...1011). Please refer TS 38.211 Section 7.4.1.1 [87] for the full configuration details.

In terms of time-domain DMRS symbol positions, the PDSCH mapping type can be either slot-wise (type A) or non-slot-wise (type B). The mapping type specifies the relative locations of the associated DMRS. For slot-wise mapping type A, the first DMRS symbol is signalled by a field in the master information block (MIB) to be either 2 or 3. For the non-slot-wise mapping type B, the first DMRS symbol is always the first symbol of the PDSCH time allocation.

Fig. A.1 shows an example of DMRS subcarrier allocation with its indices. We showed indices for 1 RE for up to four layers. Both slot-wise and non-slot wise subcarrier indices for type 2 (grouped subcarrier) and type 1 (alternating subcarrier) can be seen in this figure.

A.2 DMRS Resources within One PRB

There are 12 subcarriers in one PRB and 14 OFDM symbol in one slot. NR DMRS supports massive MU-MIMO; it can be beamformed and supports up to 12 orthogonal layers. At the end, generated DMRS sequence is passed through resource mapper to finally obtain OFDM signal at the antenna ports for multiple users.

	A type slot wise				B type non slot wise			
Type 2	25	193	363	531	1	169	339	507
	26	194	364	532	2	170	340	508
	31	199	369	537	7	175	345	513
	32	200	370	538	8	176	346	514
Type 1	25	193	362	530	1	169	338	506
	27	195	364	532	3	171	340	508
	29	197	366	534	5	173	342	510
	31	199	368	536	7	175	344	512
	33	201	370	538	9	177	346	514
	35	203	372	540	11	179	348	516

Figure A.1: DMRS subcarrier indices within one PRB

According to 3GPP specifications, UE's are configured with two DMRS configuration in the front loaded case of PDSCH/PUSCH. In short, two types of DMRS configuration settings according to 3GPP are utilized for our sensing scheme. Configuration 1 supports up to 8 ports (single user-MIMO) and Fig. A.2 provides DMRS allocation in 1 PRB where one symbol defines 6 subcarriers (6 RE) per PRB per antenna port with subinterval=2, comprising alternating interleaved subcarriers. Slot-wise mapping type A provides position of DMRS symbol on 3rd symbol in slot.

On the other hand, configuration 2 supports up to 12 ports (MU-MIMO) and Fig. A.3 shows DMRS allocation in 1 PRB where one symbol defines 4 subcarriers per PRB per antenna port, consisting of 2 groups of 2 neighbouring grouped subcarriers. We used Type B DMRS subcarriers in the uplink sensing simulation. Non-slot wise mapping type provides position of DMRS symbol on 1st symbol in slot. In one PRB, we have 4-grouped subcarrier with subinterval value of 3.

Fig. A.4 indicates all 252 DMRS subcarriers generated from Type-B, where first symbol contains all the grouped subcarriers.

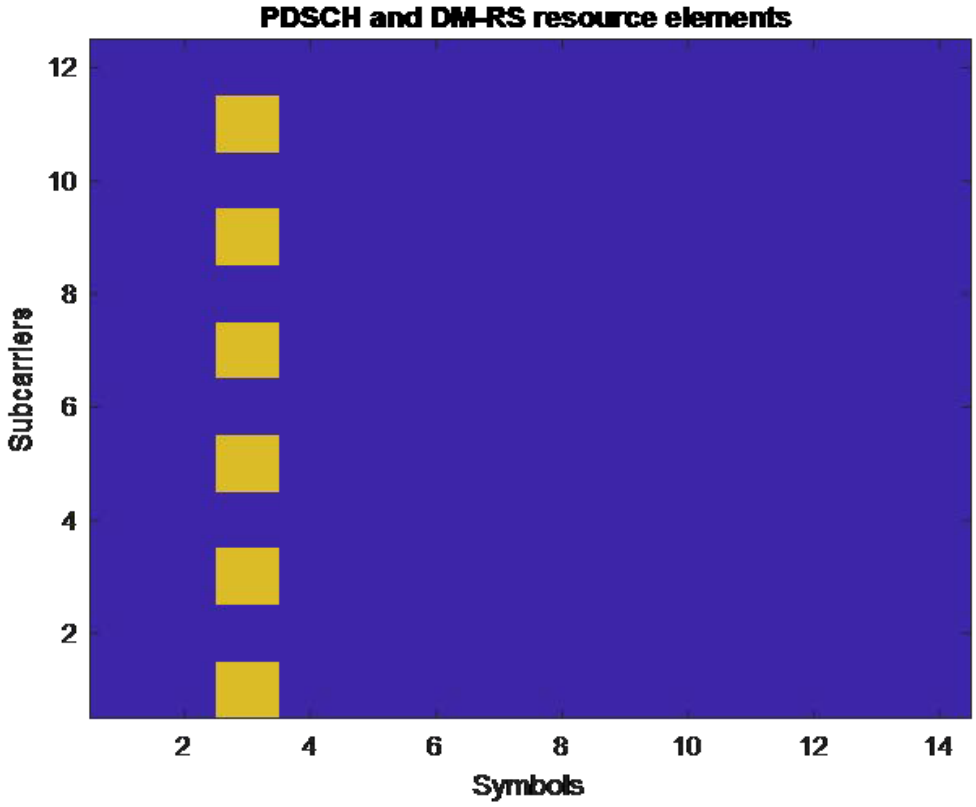

Figure A.2: DMRS subcarrier allocation within one PRB (alternating subcarriers)

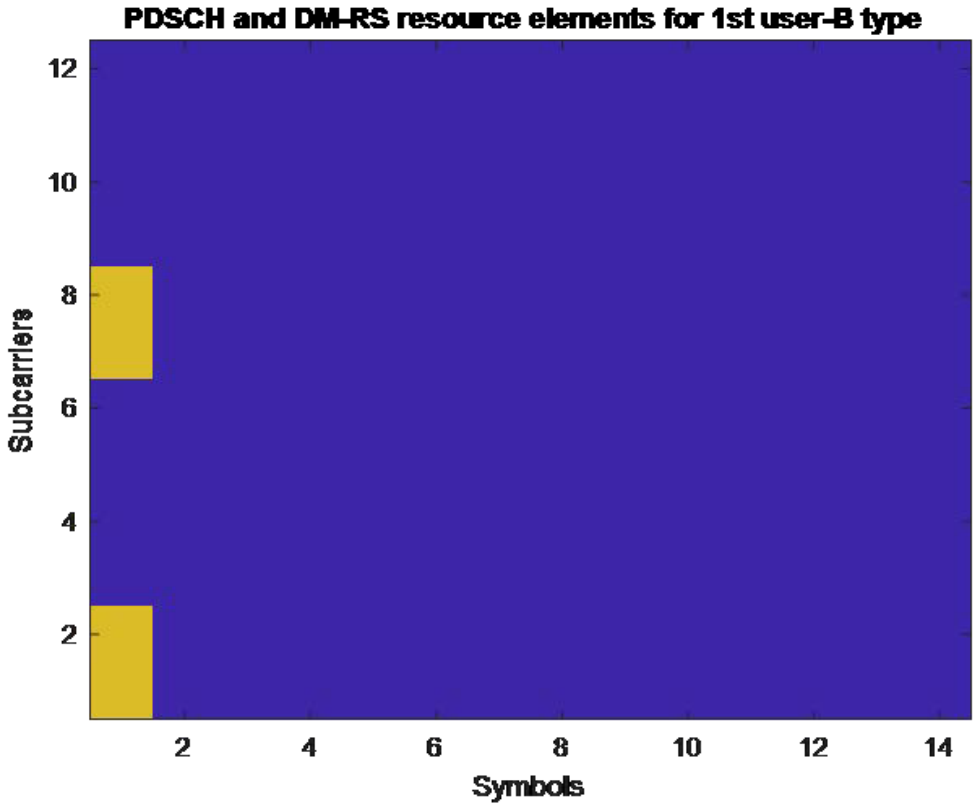

Figure A.3: DMRS subcarrier allocation within one PRB (grouped subcarriers)

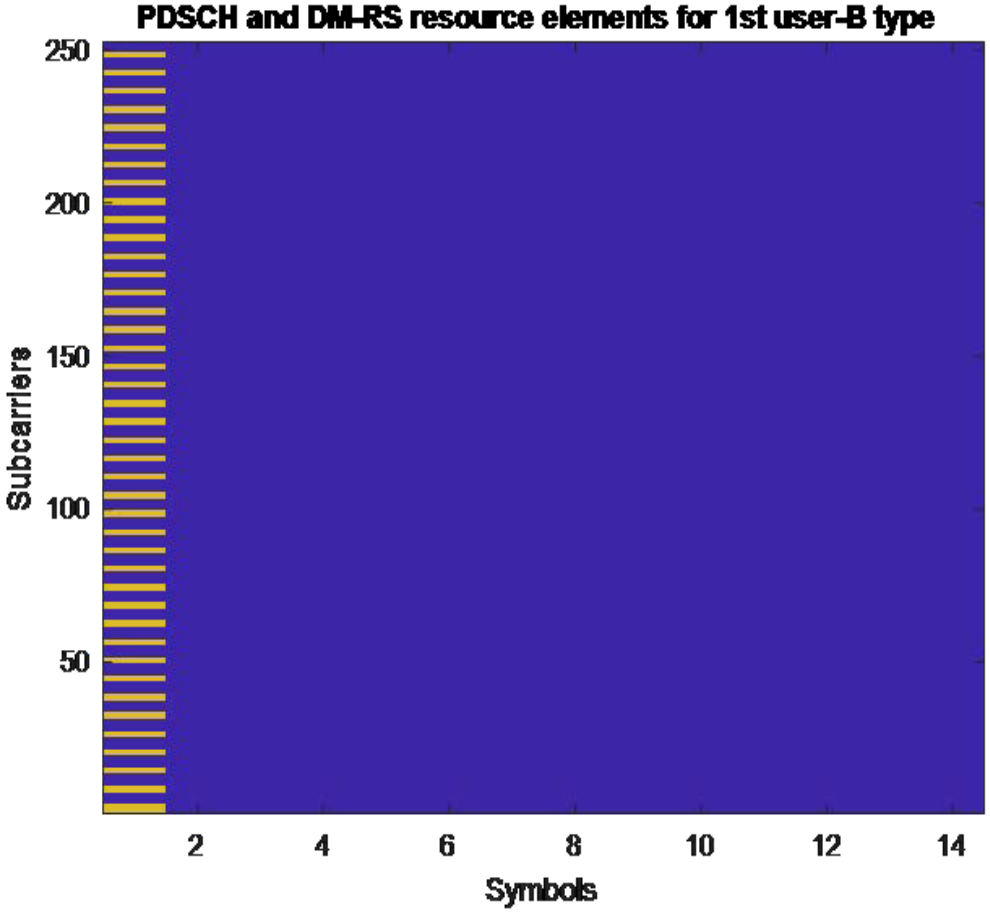

Figure A.4: DMRS subcarrier allocation within one PRB (252 Subcarriers)

Bibliography

[1] J. A. Zhang, A. Cantoni, X. Huang, Y. J. Guo, and R. W. Heath Jr, "Framework for an Innovative Perceptive Mobile Network Using Joint Communication and Sensing," in *2017 IEEE 85th Vehicular Technology Conference (VTC Spring)*. IEEE, June 2017, Conference Proceedings, pp. 1–5.

[2] J. A. Zhang, X. Huang, Y. J. Guo, and R. W. Heath Jr, "Joint Communications and Sensing Using Two Steerable Analog Antenna Arrays," in *2017 IEEE 85th Vehicular Technology Conference (VTC Spring)*, June 2017, Conference Proceedings, pp. 1–5.

[3] J. A. Zhang, X. Huang, Y. J. Guo, J. Yuan, and R. W. Heath Jr, "Multibeam for joint communication and radar sensing using steerable analog antenna arrays," *IEEE Transactions on Vehicular Technology*, vol. 68, no. 1, pp. 671–685, Jan 2019.

[4] C. W. Rossler, E. Ertin, and R. L. Moses, "A software defined radar system for joint communication and sensing," in *2011 IEEE Radar Conference (RADAR)*. IEEE, Conference Proceedings, pp. 1050–1055.

[5] A. R. Chiriyath, B. Paul, and D. W. Bliss, "Radar-Communications Convergence: Coexistence, Cooperation, and Co-Design," *IEEE Transactions on Cognitive Communications and Networking*, vol. 3, no. 1, pp. 1–12, 2017.

[6] C. Sturm and W. Wiesbeck, "Waveform Design and Signal Processing Aspects for Fusion of Wireless Communications and Radar Sensing," *Proceedings of the IEEE*, vol. 99, no. 7, pp. 1236–1259, 2011.

[7] Y. Zhang, Q. Li, L. Huang, Song, and J., "Waveform Design For Joint Radar-Communication System With Multi-User Based On MIMO Radar," in *2017 IEEE Radar Conference (RadarConf)*, Conference Proceedings, pp. 0415–0418.

[8] R. Harris, J.-K. Lam, and E. F. Burroughs, "The potential of cell phone radar as a tool for transport applications," Association for European Transport and contributors, Report, 2005.

[9] N. David, O. Sendik, H. Messer, and P. Alpert, "Cellular Network Infrastructure: The Future of Fog Monitoring?" *Bulletin of the American Meteorological Society*, vol. 96, no. 10, pp. 1687–1698, 2015.

[10] B. Paul, A. R. Chiriyath, and D. W. Bliss, "Survey of RF communications and sensing convergence research," *IEEE Access*, vol. 5, pp. 252–270, 2017.

[11] L. Han and K. Wu, "Joint wireless communication and radar sensing systems – state of the art and future prospects," *IET Microwaves, Antennas and Propagation*, vol. 7, no. 11, pp. 876–885, 2013.

[12] C. R. Berger, B. Demissie, J. Heckenbach, P. Willett, and S. Zhou, "Signal processing for passive radar using OFDM waveforms," *IEEE Journal of Selected Topics in Signal Processing*, vol. 4, no. 1, pp. 226–238, Feb 2010.

[13] K. Chetty, G. E. Smith, and K. Woodbridge, "Through-the-Wall Sensing of Personnel Using Passive Bistatic WiFi Radar at Standoff Distances," *IEEE Transactions on Geoscience and Remote Sensing*, vol. 50, no. 4, pp. 1218–1226, April 2012.

[14] P. Kumari, J. Choi, N. G. Prelcic, and R. W. Heath Jr, "IEEE 802.11ad-based Radar: An Approach to Joint Vehicular Communication-Radar System," *IEEE Transactions on Vehicular Technology*, vol. PP, no. 99, pp. 1–1, 2017.

[15] R. C. Daniels, E. R. Yeh, and R. W. Heath Jr, "Forward collision vehicular radar with IEEE 802.11: Feasibility demonstration through measurements," *IEEE Transactions on Vehicular Technology*, vol. 67, no. 2, pp. 1404–1416, Feb 2018.

[16] V. Petrov, G. Fodor, J. Kokkoniemi, D. Moltchanov, J. Lehtomaki, S. Andreev, Y. Koucheryavy, M. Juntti, and M. Valkama, "On unified vehicular communications and radar sensing in millimeter-wave and low terahertz bands," *IEEE Wireless Communications*, vol. 26, no. 3, pp. 146–153, June 2019.

[17] M. L. Rahman, J. A. Zhang, X. Huang, Y. J. Guo, and R. W. Heath Jr, "Framework for a perceptive mobile network using joint communication and radar sensing," *IEEE Transactions on Aerospace and Electronic Systems*, pp. 1–1, 2019.

[18] F. Liu, L. Zhou, C. Masouros, A. Li, W. Luo, and A. Petropulu, "Toward dual-functional radar-communication systems: Optimal waveform design," *IEEE Transactions on Signal Processing*, vol. 66, no. 16, pp. 4264–4279, Aug 2018.

[19] F. Liu, C. Masouros, A. Li, H. Sun, and L. Hanzo, "MU-MIMO communications with MIMO Radar: From co-existence to joint transmission," *IEEE Transactions on Wireless Communications*, vol. 17, no. 4, pp. 2755–2770, April 2018.

[20] A. Gameiro, D. Castanheira, J. Sanson, and P. Monteiro, "Research challenges, trends and applications for future joint radar communications systems," *Wireless Personal Communications*, vol. 100, no. 1, March 2018.

[21] E. Cianca, M. D. Sanctis, and S. D. Domenico, "Radios as sensors," *IEEE Internet of Things Journal*, vol. 4, no. 2, pp. 363–373, April 2017.

[22] J. Liu, H. Liu, Y. Chen, Y. Wang, and C. Wang, "Wireless sensing for human activity: A survey," *IEEE Communications Surveys Tutorials*, pp. 1–1, 2019.

[23] S. Wang and G. Zhou, "A review on radio based activity recognition," *Digital Communications and Networks*, vol. 9, 03 2015.

[24] X. Zhang. (2015) Millimeter-wave for 5G: Unifying Communication and Sensing. https://www.microsoft.com/en-us/research/wp-content/uploads/2015/03/Xinyu-Zhang_5GmmWave.pdf/. [Online; accessed 08-November-2017].

[25] M. Braun, "OFDM radar algorithms in mobile communication networks," *PhD thesis, Institut fur Nachrichtentechnik des Karlsruher Instituts fur Technologie, Karlsruhe*, 2014.

[26] A. Hassanien, M. G. Amin, E. Aboutanios, and B. Himed, "Dual-function radar communication systems: A solution to the spectrum congestion problem," *IEEE Signal Processing Magazine*, vol. 36, no. 5, pp. 115–126, 2019.

[27] F. Liu, C. Masouros, A. Petropulu, H. Griffiths, and L. Hanzo, "Joint radar and communication design: Applications, state-of-the-art, and the road ahead," *IEEE Transactions on Communications*, pp. 1–1, 2020.

[28] A. Hassanien, C. Sahin, J. Metcalf, and B. Himed, "Uplink signaling and receive beamforming for dual-function radar communications," in *2018 IEEE 19th International Workshop on Signal Processing Advances in Wireless Communications (SPAWC)*, 2018, pp. 1–5.

[29] E. BouDaher, A. Hassanien, E. Aboutanios, and M. G. Amin, "Towards a dual-function mimo radar-communication system," in *2016 IEEE Radar Conference (RadarConf)*, 2016, pp. 1–6.

[30] A. Ahmed, Y. D. Zhang, and B. Himed, "Distributed dual-function radar-communication mimo system with optimized resource allocation," in *2019 IEEE Radar Conference (RadarConf)*, 2019, pp. 1–5.

[31] L. Zheng, M. Lops, Y. C. Eldar, and X. Wang, "Radar and communication coexistence: An overview: A review of recent methods," *IEEE Signal Processing Magazine*, vol. 36, no. 5, pp. 85–99, Sep. 2019.

[32] A. F. Martone, K. A. Gallagher, and K. D. Sherbondy, "Joint radar and communication system optimization for spectrum sharing," in *2019 IEEE Radar Conference (RadarConf)*, April 2019, pp. 1–6.

[33] R. Saruthirathanaworakun, J. M. Peha, and L. M. Correia, "Opportunistic sharing between rotating radar and cellular," *IEEE Journal on Selected Areas in Communications*, vol. 30, no. 10, pp. 1900–1910, November 2012.

[34] M. Labib, V. Marojevic, A. F. Martone, J. H. Reed, and A. I. Zaghloui, "Coexistence between communications and radar systems: A survey," *URSI Radio Science Bulletin*, vol. 2017, no. 362, pp. 74–82, Sep. 2017.

[35] E. Yousif, F. Khan, T. Ratnarajah, and M. Sellathurai, "On the spectral coexistence of colocated MIMO radars and wireless communications systems," in *2016 IEEE 17th International Workshop on Signal Processing Advances in Wireless Communications (SPAWC)*, July 2016, pp. 1–5.

[36] F. Liu, C. Masouros, A. Li, and T. Ratnarajah, "Robust MIMO beamforming for cellular and radar coexistence," *IEEE Wireless Communications Letters*, vol. 6, no. 3, pp. 374–377, June 2017.

[37] F. Liu, L. Zhou, C. Masouros, A. Lit, W. Luo, and A. Petropulu, "Dual-functional cellular and radar transmission: Beyond coexistence," in *2018 IEEE 19th International Workshop on Signal Processing Advances in Wireless Communications (SPAWC)*, June 2018, pp. 1–5.

[38] A. Hassanien, B. Himed, and M. G. Amin, "Transmit/receive beamforming design for joint radar and communication systems," in *2018 IEEE Radar Conference (RadarConf18)*, April 2018, pp. 1481–1486.

[39] Z. Geng, R. Xu, H. Deng, and B. Himed, "Fusion of radar sensing and wireless communications by embedding communication signals into the radar transmit waveform," *IET Radar, Sonar Navigation*, vol. 12, no. 6, pp. 632–640, 2018.

[40] A. Hassanien, E. Aboutanios, M. Amin, and G. Fabrizio, "A dual-function mimo radar-communication system via waveform permutation," *Digital Signal Processing*, vol. 83, 08 2018.

[41] W. Baxter, E. Aboutanios, and A. Hassanien, "Dual-function mimo radar-communications via frequency-hopping code selection," in *2018 52nd Asilomar Conference on Signals, Systems, and Computers*, 2018, pp. 1126–1130.

[42] H. Lou, Q. Zhang, B. Liang, and Y. Chen, "Waveform design and analysis for radar and communication integration system," in *IET International Radar Conference 2015*, Oct 2015, pp. 1–6.

[43] C. Shahriar, A. Abdelhadi, and T. C. Clancy, "Overlapped-MIMO radar waveform design for coexistence with communication systems," in *2015 IEEE Wireless Communications and Networking Conference (WCNC)*, March 2015, pp. 223–228.

[44] B. Paul, "RF Convergence of Radar and Communications: Metrics, Bounds, and Systems," PhD Thesis, 2017.

[45] D. E. Hack, L. K. Patton, B. Himed, and M. A. Saville, "Detection in passive MIMO radar networks," *IEEE Transactions on Signal Processing*, vol. 62, no. 11, pp. 2999–3012, June 2014.

[46] S. Gogineni, M. Rangaswamy, B. D. Rigling, and A. Nehorai, "Cramér-Rao bounds for UMTS-based passive multistatic radar," *IEEE Transactions on Signal Processing*, vol. 62, no. 1, pp. 95–106, Jan 2014.

[47] R. S. A. R. Abdullah, A. A. Salah, A. Ismail, F. Hashim, N. E. A. Rashid, and N. H. A. Aziz, "LTE-based passive bistatic radar system for detection of ground-moving targets," *ETRI Journal*, vol. 38, no. 2, pp. 302–313, 2016.

[48] C. B. Barneto, L. Anttila, M. Fleischer, and M. Valkama, "OFDM radar with LTE waveform: Processing and performance," in *2019 IEEE Radio and Wireless Symposium (RWS)*, Jan 2019, pp. 1–4.

[49] J. Park and R. W. Heath, "Analysis of blockage sensing by radars in random cellular networks," *IEEE Signal Processing Letters*, vol. 25, no. 11, pp. 1620–1624, Nov 2018.

[50] Y. L. Sit, C. Sturm, and T. Zwick, "Doppler estimation in an ofdm joint radar and communication system," in *2011 German Microwave Conference*, March 2011, pp. 1–4.

[51] D. H. N. Nguyen and R. W. Heath, "Delay and doppler processing for multi-target detection with ieee 802.11 ofdm signaling," in *2017 IEEE International Conference on Acoustics, Speech and Signal Processing (ICASSP)*, March 2017, pp. 3414–3418.

[52] X. Wang, A. Hassanien, and M. G. Amin, "Dual-function MIMO radar communications system design via sparse array optimization," *IEEE Trans. Aerospace and Electronic Systems*, vol. 55, no. 3, pp. 1213–1226, 2019. [Online]. Available: https://doi.org/10.1109/TAES.2018.2866038

[53] X. Wang, A. Hassanien, and M. G. Amin, "Sparse transmit array design for dual-function radar communications by antenna selection," *Digital Signal Processing*, vol. 83, pp. 223–234, 2018.

[54] Y. Rong, A. R. Chiriyath, and D. W. Bliss, "Multiple-antenna multiple-access joint radar and communications systems performance bounds," in *2017 51st Asilomar Conference on Signals, Systems, and Computers*, Oct 2017, pp. 1296–1300.

[55] M. Bică and V. Koivunen, "Multicarrier radar-communications waveform design for rf convergence and coexistence," in *ICASSP 2019 - 2019 IEEE International Conference on Acoustics, Speech and Signal Processing (ICASSP)*, May 2019, pp. 7780–7784.

[56] Y. Liu, G. Liao, J. Xu, Z. Yang, and Y. Zhang, "Adaptive OFDM integrated radar and communications waveform design based on information theory," *IEEE Communications Letters*, vol. 21, no. 10, pp. 2174–2177, Oct 2017.

[57] Jun Li, Guisheng Liao, and H. Griffiths, "Range-dependent clutter cancellation method in bistatic MIMO-STAP radars," in *Proceedings of 2011 IEEE CIE International Conference on Radar*, vol. 1, Oct 2011, pp. 59–62.

[58] L. Qian, "Radar clutter suppression solution based on ICA," in *2013 Fourth International Conference on Intelligent Systems Design and Engineering Applications*, Nov 2013, pp. 429–432.

[59] Y. C. Eldar, R. Levi, and A. Cohen, "Clutter removal in sub-nyquist radar," *IEEE Signal Processing Letters*, vol. 22, no. 2, pp. 177–181, Feb 2015.

[60] A. R. Chiriyath, B. Paul, and D. W. Bliss, "Simultaneous radar detection and communications performance with clutter mitigation," in *2017 IEEE Radar Conference (RadarConf)*, May 2017, pp. 0279–0284.

[61] C. W. Lim and M. B. Wakin, "Recovery of periodic clustered sparse signals from compressive measurements," in *2014 IEEE Global Conference on Signal and Information Processing (GlobalSIP)*, Dec 2014, pp. 409–413.

[62] L. Yu, H. Sun, G. Zheng, and J. Pierre Barbot, "Model based bayesian compressive sensing via local beta process," *Signal Process.*, vol. 108, no. C, pp. 259–271, Mar. 2015. [Online]. Available: http://dx.doi.org/10.1016/j.sigpro.2014.09.018

[63] L. Yu, C. Wei, J. Jia, and H. Sun, "Compressive sensing for cluster structured sparse signals: variational bayes approach," *IET Signal Processing*, vol. 10, no. 7, pp. 770–779, 2016.

[64] Z. Zhang and B. D. Rao, "Recovery of block sparse signals using the framework of block sparse bayesian learning," in *2012 IEEE International Conference on*

Acoustics, Speech and Signal Processing (ICASSP), March 2012, pp. 3345–3348.

[65] C. Jiao, Z. Zhang, C. Zhong, and Z. Feng, "An indoor mmwave joint radar and communication system with active channel perception," in *2018 IEEE International Conference on Communications (ICC)*, May 2018, pp. 1–6.

[66] M. Alloulah and H. Huang, "Future millimeter-wave indoor systems: A blueprint for joint communication and sensing," *Computer*, vol. 52, no. 7, pp. 16–24, July 2019.

[67] F. Liu and C. Masouros, "Hybrid beamforming with sub-arrayed MIMO radar: Enabling joint sensing and communication at mmwave band," in *ICASSP 2019 - 2019 IEEE International Conference on Acoustics, Speech and Signal Processing (ICASSP)*, May 2019, pp. 7770–7774.

[68] K. V. Mishra, M. R. Bhavani Shankar, V. Koivunen, B. Ottersten, and S. A. Vorobyov, "Toward millimeter-wave joint radar communications: A signal processing perspective," *IEEE Signal Processing Magazine*, vol. 36, no. 5, pp. 100–114, Sep. 2019.

[69] P. Kumari, S. A. Vorobyov, and R. W. H. Jr, "Adaptive virtual waveform design for millimeter-wave joint communication-radar," 2019.

[70] S. H. Dokhanchi, B. S. Mysore, K. V. Mishra, and B. Ottersten, "A mmwave automotive joint radar-communications system," *IEEE Transactions on Aerospace and Electronic Systems*, vol. 55, no. 3, pp. 1241–1260, June 2019.

[71] S. Sur, X. Zhang, P. Ramanathan, and R. Chandra, "BeamSpy: Enabling Robust 60 GHz Links Under Blockage," in *NSDI'16 Proceedings of the 13th Usenix Conference on Networked Systems Design and Implementation*. USENIX Association Berkeley, CA, USA, Conference Proceedings, pp. 193–206.

[72] S. Sur, V. Venkateswaran, X. Zhang, and P. Ramanathan, "60 GHz Indoor Networking through Flexible Beams: A Link-Level Profiling," in *SIGMETRICS'15*. ACM, Conference Proceedings, pp. 71–84.

[73] J. Zhang, X. Zhang, P. Kulkarni, and P. Ramanathan, "OpenMili: A 60 GHz Software Radio Platform With a Reconfigurable Phased-Array Antenna," in *MobiCom'16*. ACM, Conference Proceedings, pp. 162–175.

[74] M. L. Rahman, P. Cui, J. A. Zhang, X. Huang, Y. J. Guo, and Z. Lu, "Joint communication and radar sensing in 5G mobile network by compressive sensing," in *2019 19th International Symposium on Communications and Information Technologies (ISCIT)*, Sep. 2019, pp. 599–604.

[75] M. L. Rahman, J. A. Zhang, X. Huang, and Y. J. Quo, "Analog antenna array based sensing in perceptive mobile networks," in *2017 IEEE-APS Topical Conference on Antennas and Propagation in Wireless Communications (APWC)*, Sep. 2017, pp. 199–202.

[76] J. A. Zhang, X. Huang, Y. J. G. and, and M. L. Rahman, "Signal Stripping Based Sensing Parameter Estimation in Perceptive Mobile Networks," in *2017 IEEE-APS Topical Conference on Antennas and Propagation in Wireless Communications (APWC)*. IEEE, Conference Proceedings, pp. 67–70.

[77] B. Friedlander, "Waveform design for MIMO radars," *IEEE Transactions on Aerospace and Electronic Systems*, vol. 43, no. 3, pp. 1227–1238, July 2007.

[78] A. M. Haimovich, R. S. Blum, and L. J. Cimini, "MIMO radar with widely separated antennas," *IEEE Signal Processing Magazine*, vol. 25, no. 1, pp. 116–129, 2008.

[79] J. Liang and Q. Liang, "Design and analysis of distributed radar sensor networks," *IEEE Transactions on Parallel and Distributed Systems*, vol. 22, no. 11, pp. 1926–1933, Nov 2011.

[80] L. Zheng and X. Wang, "Super-resolution delay-doppler estimation for OFDM passive radar," *IEEE Transactions on Signal Processing*, vol. 65, no. 9, pp. 2197–2210, May 2017.

[81] G. Marino, D. Tarchi, V. Kyovtorov, Sammartino, and P. F., "Ground based MIMO SAR and land clutter modelling: difficulties and guidelines," in *2015 Signal Processing Symposium (SPSympo)*, Conference Proceedings, pp. 1–5.

[82] V. F. Mecca, D. Ramakrishnan, and J. L. Krolik, "MIMO radar space-time adaptive processing for multipath clutter mitigation," in *Fourth IEEE Workshop on Sensor Array and Multichannel Processing, 2006.*, July 2006, pp. 249–253.

[83] C. Liu, C. Song, and Q. Lu, "Random noise de-noising and direct wave eliminating based on SVD method for ground penetrating radar signals," *Journal of Applied Geophysics*, vol. 144, pp. 125 – 133, 2017.

[84] P. K. Verma, A. N. Gaikwad, D. Singh, Nigam, and M. J., "Analysis of clutter reduction techniques for through wall imaging in UWB range," *Progress In Electromagnetics Research B*, vol. 17, pp. 29–48, 2009.

[85] F. Tivive, A. Bouzerdoum, and M. Amin, "A subspace projection approach for wall clutter mitigation in through-the-wall radar imaging," *IEEE Trans. Geosci. Remote Sens.*, vol. 53, no. 4, p. 2108–2122, 2015.

[86] 3GPP TR 38.913, "Study on scenarios and requirements for next generation access technologies," *V15.0.0*, June 2018.

[87] 3GPP TS 38.211, "Physical channels and modulation," *V15.2.0*, July 2018.

[88] Z. Zhang, X. Chai, K. Long, A. V. Vasilakos, and L. Hanzo, "Full duplex techniques for 5G networks: self-interference cancellation, protocol design, and relay selection," *IEEE Communications Magazine*, vol. 53, no. 5, pp. 128–137, May 2015.

[89] Y. Liu, Z. Tan, H. Hu, L. J. Cimini, and G. Y. Li, "Channel Estimation for OFDM," *IEEE Communications Surveys and Tutorials*, vol. 16, no. 4, pp. 1891–1908, 2014.

[90] G. L. Stuber, J. R. Barry, S. W. McLaughlin, L. Ye, M. A. Ingram, and T. G. Pratt, "Broadband MIMO-OFDM wireless communications," *Proceedings of the IEEE*, vol. 92, no. 2, pp. 271–294, 2004.

[91] T. Hwang, C. Yang, G. Wu, S. Li, Li, and G. Y., "OFDM and Its Wireless Applications: A Survey," *IEEE Transactions on Vehicular Technology*, vol. 58, no. 4, pp. 1673–1694, 2009.

[92] M. Jiang and L. Hanzo, "Multiuser MIMO-OFDM for Next-Generation Wireless Systems," *Proceedings of the IEEE*, vol. 95, no. 7, pp. 1430–1469, 2007.

[93] P. Cheng, Z. Chen, Y. Rui, Y. J. Guo, L. Gui, M. Tao, and Q. T. Zhang, "Channel Estimation for OFDM Systems over Doubly Selective Channels: A Distributed Compressive Sensing Based Approach," *IEEE Transactions on Communications*, vol. 61, no. 10, pp. 4173–4185, 2013.

[94] M. K. Ozdemir and H. Arslan, "Channel estimation for wireless OFDM systems," *IEEE Communications Surveys and Tutorials*, vol. 9, no. 2, pp. 18–48, 2007.

[95] Y. Li, N. Seshadri, and S. Ariyavisitakul, "Channel estimation for OFDM systems with transmitter diversity in mobile wireless channels," *IEEE Journal on Selected Areas in Communications*, vol. 17, no. 3, pp. 461–471, 1999.

[96] Y. G. Li, J. H. Winters, and N. R. Sollenberger, "MIMO-OFDM for wireless communications: signal detection with enhanced channel estimation," *IEEE Transactions on Communications*, vol. 50, no. 9, pp. 1471–1477, 2002.

[97] M. Biguesh and A. B. Gershman, "Training-based MIMO channel estimation: a study of estimator tradeoffs and optimal training signals," *IEEE Transactions on Signal Processing*, vol. 54, no. 3, pp. 884–893, 2006.

[98] J. Akhtman and L. Hanzo, "Decision Directed Channel Estimation Aided OFDM Employing Sample-Spaced and Fractionally-Spaced CIR Estimators," *IEEE Transactions on Wireless Communications*, vol. 6, no. 4, pp. 1171–1175, 2007.

[99] O. O. Oyerinde and S. H. Mneney, "Subspace Tracking-Based Decision Directed CIR Estimator and Adaptive CIR Prediction," *IEEE Transactions on Vehicular Technology*, vol. 61, no. 5, pp. 2097–2107, 2012.

[100] A. Paulraj and C. B. Papadias, *Array Processing for Mobile Communications*. CRC Press LLC, 2000.

[101] J. A. Zhang, W. Ni, P. Cheng, and Y. Lu, "Angle-of-Arrival Estimation Using Different Phase Shifts Across Subarrays in Localized Hybrid Arrays," *IEEE Communications Letters*, vol. 20, no. 11, pp. 2205–2208, 2016.

[102] J. A. Zhang, X. Huang, and V. Dyadyuk, "Massive hybrid antenna array for millimeter-wave cellular communications," *IEEE Wireless Communications*, vol. 22, no. 1, pp. 79–87, 2015.

[103] M. A. Toutounchian, "Beamforming for Multiuser MIMO systems," Thesis, 2014.

[104] W. U. Bajwa, J. Haupt, A. M. Sayeed, and R. Nowak, "Compressed Channel Sensing: A New Approach to Estimating Sparse Multipath Channels," *Proceedings of the IEEE*, vol. 98, no. 6, pp. 1058–1076, 2010.

[105] X. Cheng, M. Wang, and S. Li, "Compressive Sensing Based Beamforming for Millimeter-Wave OFDM Systems," *IEEE Transactions on Communications*, vol. 65, no. 1, pp. 371 – 386, 2017.

[106] M. A. Davenport., M. F. Duarte, Y. C. Eldar, and G. Kutyniok, *Introduction to compressed sensing*. New York: Cambridge University Press, 2012.

[107] W. U. Bajwa, A. Sayeed, Nowak, and Robert, "Sparse Multipath Channels: Modeling and Estimation," in *2009 IEEE 13th Digital Signal Processing Workshop and 5th IEEE Signal Processing Education Workshop*. IEEE, Conference Proceedings, pp. 320–325.

[108] X. Yang, "Research on compressed sensing and its applications in wireless communications," PhD Thesis, 2014.

[109] P. Zhang, L. Gan, S. Sun, Ling, and C., "Atomic norm denoising-based channel estimation for massive multiuser MIMO systems," in *2015 IEEE International Conference on Communications (ICC)*, Conference Proceedings, pp. 4564–4569.

[110] G. Tang, B. N. Bhaskar, P. Shah, and B. Recht, "Compressed Sensing Off the Grid," *IEEE Transactions on Information Theory*, vol. 59, no. 11, pp. 7465–7490, 2013.

[111] R. W. Heath Jr, N. Gonzalez-Prelcic, S. Rangan, W. Roh, and A. M. Sayeed, "An Overview of Signal Processing Techniques for Millimeter Wave MIMO Systems," *IEEE Journal of Selected Topics in Signal Processing*, vol. 10, no. 3, pp. 436–453, 2016.

[112] S. Yousefi, H. Narui, S. Dayal, S. Ermon, and S. Valaee, "A survey on behavior recognition using WiFi channel state information," *IEEE Communications Magazine*, vol. 55, no. 10, pp. 98–104, Oct 2017.

[113] M. A. Hadi, S. Alshebeili, K. Jamil, and F. E. A. El-Samie, "Compressive sensing applied to radar systems: an overview," *Signal, Image and Video Processing*, vol. 9, no. 1, pp. 25–39, Dec 2015. [Online]. Available: https://doi.org/10.1007/s11760-015-0824-y

[114] Ender and J. H. G., "On compressive sensing applied to radar," *Signal Process.*, vol. 90, no. 5, pp. 1402–1414, May 2010.

[115] Chun-Yang Chen and P. P. Vaidyanathan, "Compressed sensing in MIMO radar," in *2008 42nd Asilomar Conference on Signals, Systems and Computers*, Oct 2008, pp. 41–44.

[116] C. F. Caiafa and A. Cichocki, "Computing sparse representations of multidimensional signals using Kronecker bases," *Neural Computation*, vol. 25, no. 1, pp. 186–220, Jan 2013.

[117] A. Fannjiang and H.-C. Tseng, "Compressive radar with off-grid targets: a perturbation approach," *Inverse Problems*, vol. 29, no. 5, p. 054008, 2013. [Online]. Available: http://stacks.iop.org/0266-5611/29/i=5/a=054008

[118] B. Liu, Z. Zhang, G. Xu, H. Fan, and Q. Fu, "Energy efficient telemonitoring of physiological signals via compressed sensing: A fast algorithm and power consumption evaluation," *Biomedical Signal Processing and Control*, vol. 11, no. Supplement C, pp. 80 – 88, 2014.

[119] D. Wipf and B. Rao, "An empirical Bayesian strategy for solving the simultaneous sparse approximation problem," *Signal Processing, IEEE Transactions on*, vol. 55, no. 7, pp. 3704–3716, July 2007.

[120] J. A. Zhang, Z. Chen, P. Cheng, and X. Huang, "Multiple-measurement vector based implementation for single-measurement vector sparse Bayesian learning with reduced complexity," *Signal Processing*, vol. 118, pp. 153–158, 2016.

[121] S. Ji, Y. Xue, and L. Carin, "Bayesian compressive sensing," *IEEE Transactions on Signal Processing*, vol. 56, no. 6, pp. 2346–2356, June 2008.

[122] 3GPP TS 38.104, "5G NR base station (BS) radio transmission and reception," *V15.2.0 Release 15*, July 2018.

[123] 3GPP TS 38.101-1, "5G NR user equipment (UE) radio transmission and reception," *V15.2.0 Release 15*, July 2018.

[124] Q. Gu, *Receiver System Analysis and Design.* Boston, MA: Springer US, January 2005, pp. 229–310.

[125] E. Baransky, G. Itzhak, N. Wagner, I. Shmuel, E. Shoshan, and Y. Eldar, "Sub-nyquist radar prototype: Hardware and algorithm," *IEEE Transactions on Aerospace and Electronic Systems*, vol. 50, no. 2, pp. 809–822, April 2014.

[126] P. Cui, J. A. Zhang, W. Lu, Y. Guo, and H.-B. Zhu, "Statistical sparse channel modeling for measured and simulated wireless temporal channels," *IEEE Transactions on Wireless Communications*, vol. PP, pp. 1–1, 09 2019.

[127] S. Jaeckel, L. Raschkowski, K. Börner, and L. Thiele, "Quadriga: A 3-d multi-cell channel model with time evolution for enabling virtual field trials," *IEEE Transactions on Antennas and Propagation*, vol. 62, no. 6, pp. 3242–3256, 2014.

[128] D. Shutin, "Cluster analysis of wireless channel impulse responses," in *International Zurich Seminar on Communications, 2004*, Feb 2004, pp. 124–127.

[129] M. F. Duarte and R. G. Baraniuk, "Kronecker compressive sensing," *IEEE Transactions on Image Processing*, vol. 21, no. 2, pp. 494–504, Feb 2012.

[130] G. Hakobyan and B. Yang, "A novel OFDM-MIMO radar with non-equidistant subcarrier interleaving and compressed sensing," in *2016 17th International Radar Symposium (IRS)*, May 2016, pp. 1–5.

[131] S.-W. Chen, L. K. Wang, and J.-H. Lan, "Moving Object tracking Based on Background Subtraction Combined Temporal Difference," in *International Conference on Emerging Trends in Computer and Image Processing (ICETCIP'2011)*, Conference Proceedings, pp. 16–19.

[132] T. Wei and X. Zhang, "mTrack: High-Precision Passive Tracking Using Millimeter Wave Radios," in *MobiCom'15.* ACM, Conference Proceedings, pp. 117–129.

[133] A. Sobral and A. Vacavant, "A comprehensive review of background subtraction algorithms evaluated with synthetic and real videos," *Computer Vision and Image Understanding*, vol. 122, pp. 4 – 21, 2014.

[134] D. Povey, L. Burget, M. Agarwal, P. Akyazi, F. Kai, A. Ghoshal, O. Glembek, N. Goel, M. Karafiát, A. Rastrow, R. C. Rose, P. Schwarz, and S. Thomas, "The subspace gaussian mixture model—a structured model for speech recognition," *Computer Speech and Language*, vol. 25, no. 2, pp. 404 – 439, 2011.

[135] L. Haihan, Y. Li, S. Zhou, and W. Jing, "A novel method to obtain CSI based on gaussian mixture model and expectation maximization," in *2016 8th International Conference on Wireless Communications Signal Processing (WCSP)*, Oct 2016, pp. 1–5.

[136] B. Selim, O. Alhussein, S. Muhaidat, G. K. Karagiannidis, and J. Liang, "Modeling and analysis of wireless channels via the mixture of Gaussian distribution," *IEEE Transactions on Vehicular Technology*, vol. 65, no. 10, pp. 8309–8321, Oct 2016.

[137] C. S. Grant, T. K. Moon, J. H. Gunther, M. R. Stites, and G. P. Williams, "Detection of amorphously shaped objects using spatial information detection enhancement (SIDE)," *IEEE Journal of Selected Topics in Applied Earth Observations and Remote Sensing*, vol. 5, no. 2, pp. 478–487, April 2012.

[138] B. W. Bader and T. G. Kolda, "Efficient MATLAB computations with sparse and factored tensors," *SIAM Journal on Scientific Computing*, vol. 30, no. 1, pp. 205–231, December 2007.